Numerical analysis of unsteady compressible flow in the hose of Bubble Curtain Technology

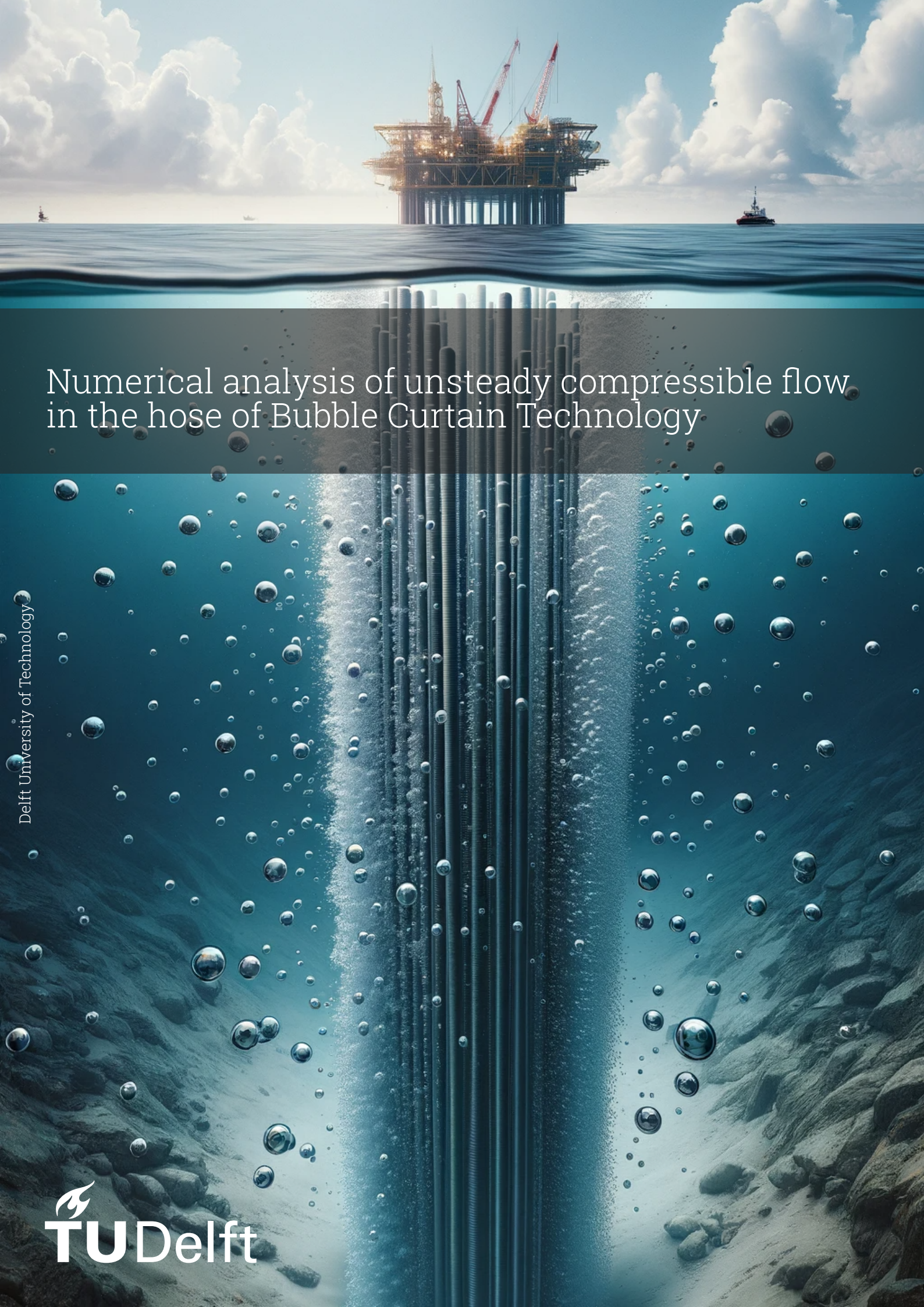

Delft University of Technology

TU Delft

Numerical analysis of unsteady compressible flow in the hose of Bubble Curtain Technology

by

Student Name: Dhirde Mayur Maruti

Master of Science in Offshore and Dredging Engineering

Student Number: 5633389
Project duration: March 2023–March 2024
Thesis committee: Dr.ir. A. Jarquin Laguna, TU Delft, Chairman
Dr.ir. G.H. Keetels, TU Delft
Ir. Yaxi Peng, TU Delft

TU Delft

"Dedicated to my family"

Abstract

Wind turbines are becoming larger, and with them, their foundations. Moreover, these turbines are increasingly being deployed in deeper offshore regions, demonstrating the growing frontier of renewable energy exploration. Impact piling is the most commonly used installation technique for monopiles. As a result, during the monopile installation process, impact pilings generate underwater noise levels that push the industry to its utmost. The aquatic environment may be adversely affected by the high-impulse noise emissions generated during this installation technique. Larger piles need more forceful hammer blows, which produce greater noise. The necessity for efficient underwater noise reduction solutions has grown following offshore wind farm's faster growth. The deployment of bubble curtain technology (BCT) has emerged as a potential solution. While the BCT operational concept has been demonstrated in practice, a detailed investigation related to fluid dynamics, geometric characteristics, and operational parameters has yet to be conducted. It's important to note that this need for investigation is specifically applicable to large BCT systems. The goal of this research is to better understand the dynamics of unsteady compressible flow inside BCT hoses as well as the impact of operational factors on the pneumatic aspects of the bubble curtain system along the hose length.

The fundamental aims of this thesis were meticulously structured. Initially, the goal was to create a 1D unsteady model of compressible flow in pipeline systems, which would serve as the framework for future research. The model was verified against existing research to ensure its robustness and dependability. The verified model indicated a 2-4% difference in flow rates and pressure responses compared to the existing research. Following that, the study expanded to include nozzle configurations, gradually incorporating nozzles into the verified pipeline model. The model was later developed to include configurations with one, three, and five nozzles. The introduction of nozzles had a substantial impact on flow dynamics, where larger diameters increased dampening on transient pressure fluctuations. Additionally, concerns related to numerical instability were addressed, and a comparison between the convective inertia term and its absence was carried out. The simulations became more precise and stable when the convective inertia element was eliminated for this research. As these developments progressed, the final model with five nozzles was used as the foundation for the scaled BCT model.

Further, a final scaled BCT model was developed, and sensitivity analysis was performed using parameters from existing research with arbitrary changes, as per the pneumatic model in this research. In particular, the sensitivity analysis indicated the importance of geometric components (hose diameter, nozzle diameter, hose length, and nozzle spacing) and operational parameters (discharge coefficient, water depth, and flow rate of supplied air (*Q_FAD*)) in BCT system operation. The sensitivity of the system to both steady-state and transient impacts resulting from time-varying boundary conditions was emphasized in this study. The key findings show that while smaller hose and nozzle diameters increase backflow, greater discharge coefficient and air flow rate values decrease the amount of reverse flow, which is caused by abrupt boundary conditions. Hose length and nozzle spacing adjustments reduced negative flow and controlled flow rate peaks. An additional sensitivity study of the flow rate via nozzles revealed that the only parameters that substantially impact the flow rate through the nozzle are the nozzle diameter and discharge coefficient (*C_d*), with a 2-3% increase above reference values found when these parameters were in the maximum value range. Other geometric and operational parameters in the tested ranges had a relatively lower influence on the nozzle flow rates or generated pressure variations.

The scaled BCT unsteady compressible flow dynamics model presented in this thesis is still in its early stages of development, but it can serve as a basis for the development of full-scale pneumatic models that can enhance BCT and lessen the environmental impact of offshore wind farm operations.

Acknowledgement

Before you lies the work that not only signifies the completion of my MSc in Offshore and Dredging Engineering but also encompasses the essence of my academic journey at TU Delft.

Foremost, I extend my deepest gratitude to my supervisor, Dr.ir.A.Jarquin Laguna. Your insight in finding this thesis topic and enabling me to pursue it has been invaluable. I am deeply grateful for your unwavering support, guidance from the very first day to the final review of my thesis, and your always-available stance for questions and clarifications related to our topic. Your patience when I struggled to understand concepts at the first attempt and your motivational spirit during our discussions have been foundational to my growth and success.

Finally, I would like to thank my parents. Their constant encouragement and support have been my foundation throughout this journey. Without them, none of this would have been achievable.

I have thoroughly enjoyed the process of conducting this project and writing this thesis. I hope that you find as much enjoyment and insight in reading it as I have in creating it.

Mayur Maruti Dhirde
Delft, March 2024

Contents

List of Figures

List of Tables

Nomenclature

Abbreviations

Abbreviation	Definition
BCT	Bubble Curtain Technology
BBC	Big Bubble Curtain
PDEs	Partial Differential Equations
ODEs	Ordinary Differential Equations
MOC	Method of Characteristics
FIFM	Fully Implicit Finite Difference Method
FAD	Free Air Delivery

Symbols

Symbol	Definition	Unit
v	Velocity of gas directed along the axis of pipe or hose	[m/s]
A	Cross-section area of pipe	[m^2]
C_p	Specific heat at constant pressure	[J/kgK]
D	Pipe diameter	[m]
g	Gravitational acceleration	[m/s^2]
f	Friction factor	[-]
h	Specific enthalpy	[J/kg]
m	Mass flow rate	[kg/m^2 s]
n	Time level	[-]
N	Number of node	[-]
P	Pressure of the gas	[Pa]
R	Specific gas constant	[J/kgK]
t	Time	[s]
T	Temperature	[K]
Z	Compressibility factor	[-]
W	Frictional force per unit length of pipe	[N/m]
ρ	Density	[kg/m^3]
ρ_r	Reduced density	[kg/m^3]
ϵ	Pipe roughness	[mm]

1 Introduction

Offshore wind is a rapidly developing industry with the potential to play an increasingly important role in electricity production in the near future. As the industry grows, wind farms are built further offshore, where the wind is less turbulent and there is more room to expand the size of the wind farms. Furthermore, the capacity and size of wind turbine generators are growing due to technical developments. As a result, to ensure stability and enough support for the generator, the foundation of the structure expands. In general, a monopile (a large-diameter steel cylinder) is the preferred foundation due to its economic benefits and relatively simple installation. For the installation of a monopile, a large amount of energy is applied by the impact of a hammer on top of the pile. Central to this challenge is the noise pollution generated during the installation of wind turbines, particularly from the impact of pile driving on monopile foundations. This noise, propagating through water and air, poses a significant threat to marine life, necessitating stringent noise regulations and effective mitigation strategies [1].

Among the different noise reduction strategies, the use of bubble curtain technology has emerged as a particularly potential approach. This approach involves the discharge of air bubbles from a perforated hose, which creates a barrier that absorbs or reflects sound waves, lowering noise and vibration levels. However, it is important to note that the understanding of the unsteady processes within the bubble curtain hoses is yet unknown. This study examines the complexities of gas flow within these hoses using numerical modeling techniques. The primary purpose is to determine how transient flow dynamics, as impacted by characteristics such as nozzle designs, flow rate, hose geometry, and water depth, affect the flow dynamics of bubble curtain systems. Despite considerable research on bubble curtains, the exact behavior of fluid flow within their distribution hoses, particularly under changing operational conditions, is mostly unknown.

This thesis is structured by starting with a thorough literature review to lay the foundational knowledge, followed by a detailed description of the research methodology. Subsequent chapters discuss model development, verification, challenges encountered, particularly concerning numerical stability, and the scaled representation of the BCT pneumatic model. The research comes to an end with a discussion that not only highlights the implications of the study but also suggests avenues for future research in this field. As the world increasingly leans towards environmentally conscious and sustainable technologies, the insights gained from this research are expected to contribute to understanding the flow dynamics along the length of the bubble curtain technology hose. By enhancing this understanding, the study may contribute to the full-scale pneumatic development of a model that takes into account transient flow phenomena that might occur due to changes in operation along the length of the Bubble Curtain Technology (BCT). This contribution aims to support the protection of marine environments and promote the sustainable growth of the offshore wind industry. This contribution aims to support the protection of marine environments and promote the sustainable growth of the offshore wind industry. A schematic cross-section of an air supply hose resting on the seabed is depicted in Figure 1.1a. The air injection into the water causes bubbles to develop above the perforated hole. The installation vessel is positioned in the middle of Figure 1.1b, which depicts an aerial view of the application of a double Big Bubble Curtain (BBC). The two rings are the rising bubbles that reach the water's surface.

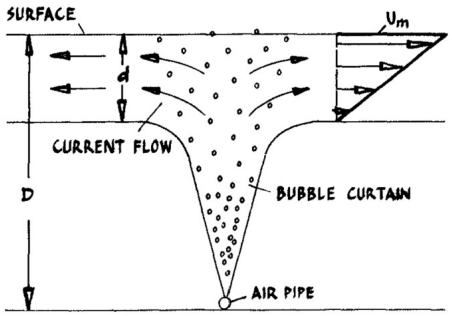

(a) Schematic representation of the bubble curtain [2]

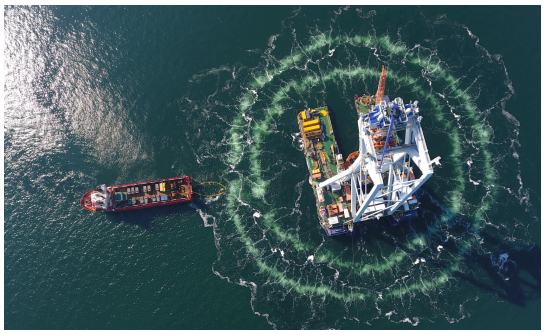

(b) An aerial view of the BBC setup in use [3]

Figure 1.1: Schematic representation and aerial view of the BBC

1.0.1. Background and Significance

The Rise of Offshore Wind Energy

The development of the offshore wind sector has been greatly aided by the global transition to renewable energy sources [4]. Offshore wind farms have stronger and more reliable wind patterns than their onshore equivalents, which results in increased energy efficiency. But this trend toward offshore places is not without its difficulties. The development of wind farms in maritime settings poses intricate environmental and engineering issues, particularly when installing wind turbine generators on monopile foundations [5].

Environmental Challenges: Focus on Noise Pollution

Underwater noise pollution is a significant environmental concern linked to the installation of offshore wind farms [6]. The installation process, which often involves using heavy hammers to drive steel monopiles into the seafloor, generates noise. When this noise travels through the water, it severely harms marine life by interfering with aquatic animal's ability to communicate, navigate, and breed behaviors of various aquatic species, which is explained in this article by T. Aran Mooney [7]. The growing awareness of these environmental impacts has led to stricter regulations and a pressing need for effective noise mitigation strategies.

Bubble Curtain Technology: An effective way to reduce Underwater noise

In response to these challenges, the application of bubble curtain technology has become recognized as a potential approach for reducing the impact of underwater noise produced by offshore projects [8]. While existing models primarily focus on the acoustic aspects of the system [9], the flow dynamics within the hose have received less attention. This overlook may result in issues with flow stability, pressure fluctuations, and bubble dispersion. Despite thorough research on bubble formation, size, and dispersion having been done, the potential implications of unsteady compressible flow dynamics on the system's operation characteristics have not been thoroughly addressed. This master's thesis aims to carry out a numerical analysis of the unsteady compressible flow in the bubble curtain hose. This research intends to fill the knowledge gap and offer helpful insights regarding the transient flow dynamics that might occur due to changes in the operations of the system by looking at variables including flow stability, pressure variations, and other pertinent characteristics. Finally, this research aims to enhance the understanding of unsteady compressible flow inside BCT hoses and examine the impact of operational parameters on the pneumatic aspects of the bubble curtain system along the hose length.

Motivation

The efficiency and uniformity of the bubble curtain technology are greatly influenced by the compressed air flowing inside the hose. The flow dynamics inside the hose haven't been thoroughly studied, even though they may influence system performance. To obtain the ideal size, distribution, and velocity of air bubbles traveling through the nozzle, it is crucial to comprehend and regulate the compressible air

flow within the hose. Flow velocity, geometry, and nozzle spacing are all parameters that can impact the rate and degree of air compression within the hose. Inadequate regulation of these elements might result in the generation of uneven bubbles and non-uniform flow, lowering the overall efficiency of the bubble curtain system. Non-uniform flow can cause unwanted pressure drops and system defects, jeopardizing the system's functioning. Moreover, while dealing with high flow rates, it is critical to examine the hose's designed pressure range. Excessive pressure might cause the hose to bulge or fail, which can result in operational difficulties. Furthermore, the spacing between nozzles must be carefully considered to eliminate gaps that would reduce the system's overall efficiency. Additionally, the depth of the water column can have a big influence on how much compressed air flows through the hose. As the water depth grows, so does the hydrostatic pressure at the bottom of the water column, necessitating more pressure to overcome. As a result of the increased pressure, the flow rate of compressed air inside the hose may rise. This research intends to give significant insights by conducting an examination of the unsteady compressible flow dynamics within the hose of bubble curtain technology. Further, this information can be used to develop a comprehensive full-scale pneumatic model, which may be used to optimize compressor usage, increasing system efficiency and effectiveness. Overall, by studying the flow dynamics of unsteady compressible flow along the hose length, this research might contribute to the improvement of bubble curtain technology.

1.0.2. Objectives of the Study

The primary objectives of this study are to further our understanding of the unsteady compressible flow through the BCT along the hose length. To do this, the study concentrates on the following two objectives:

- **Understand how the unsteady flow of compressed air along the hose length influences the dynamic of bubble curtain technology.**
- **Examine how various operational parameters, including air flow rate, pressure, water depth, and hose geometry, influence the pneumatic aspects of the bubble curtain system along the hose length.**

The choice to begin this research with a 1D model is based on the motivation to pursue a manageable level of complexity, considering the existing gaps in the understanding of unsteady processes in the hose of bubble curtain technology. The elongated shape of the hose and the predominance of axial fluctuations in flow characteristics emphasize the need for a balanced approach. Consequently, the 1D model can offer an efficient yet simple representation of the essential dynamics, making it possible to identify and examine the basic flow properties under various operating circumstances. Moreover, the selection of the 1D method is guided by its capacity to balance accuracy and computational time, making it especially suitable for capturing key characteristics of transient flow phenomena in bubble curtain systems. Before getting into the dynamic and time-dependent aspects of compressible flow in bubble curtain technology hoses, an understanding of steady-state characteristics is important. These steady-state conditions serve as a baseline for assessing system stability, detecting abnormalities, and verifying models. This fundamental knowledge provides a vital starting point for a more in-depth exploration of the dynamic behavior of compressible flow and its responses to diverse operating conditions in bubble curtain technology.

Overall, the choice of a 1D approach was made to fulfill the requirement for a computationally efficient yet acceptable model, establishing a foundation for investigating the flow dynamics in bubble curtain technology under various operational circumstances. It sets the basis for future studies, which may include higher-dimensional models or experimental settings.

Research questions:
With hydrodynamics as the main focus and the effect of operating parameters on bubble curtain technology, this thesis addresses two topics concurrently. Research questions, both main and secondary, were identified for each of the two subjects.

1D Unsteady state model of compressible flow in the hose of bubble curtain technology.

- How can a 1D unsteady state model be developed and utilized to analyze the behavior of flow in the hose of a bubble curtain, considering the impacts of different operating conditions and design parameters on the flow characteristics?
- In the context of the unsteady state model, how can variations in air pressure and flow rate affect the dynamics of the bubble curtain system?
- What insights can be derived from such modelling to guide future investigations, especially those incorporating higher-dimensional models?

To analyze the hose-nozzle system's geometric properties and the impact of operational parameters.

- How do variations in operating variables, such as pressure and flow rate, influence the bubble curtain in a submerged environment under unsteady conditions?
- In the hose-nozzle system, how do the size and spacing of the nozzles influence the bubble curtain at various water depths, especially in unsteady flow scenarios?

1.0.3. Scope and Limitations

Scope
In order to understand the flow dynamics of compressed air inside the hose, it requires an understanding of hydrodynamics inside the hose and the parameters that influence the bubble curtain technology. Primarily, a literature study was conducted to gain an understanding of the parameters that play a role in the dynamics of compressible flow. In this study, a 1D model is proposed, and numerical analysis has been performed using that model as the foundation. This study's scope includes the following areas: operational parameters, nozzle design, and water depth.

Limitations
While this study aims to provide comprehensive insights into the dynamics of bubble curtain technology, it is important to acknowledge several limitations. The specificity of the 1D unsteady state model and the utilization of a scaled model are significant constraints that may necessitate further explanation or justification in other sections, such as the discussion or future work. These aspects can be revisited to provide a more detailed understanding of the research findings.

- Model Specificity: The use of a 1D unsteady model allows a more focused investigation of the axial dynamics of bubble curtain systems. However, this reduction may not adequately capture the intricacies of a three-dimensional environment in which lateral and vertical flow dynamics play an important role. This limitation can be discussed or justified at a later stage.
- Scaled model: This study uses a scaled model to simulate transient compressible flow via a pipeline, which represents the hose in bubble curtain technology. While scaling reduces computation demands and simplifies analysis, it may result in inconsistencies between model predictions and full-scale operational behaviors, particularly in terms of flow dynamics.
- Isothermal Conditions: Assuming isothermal conditions simplifies thermal dynamics in flows. This assumption, however, ignores the possible effects of temperature fluctuations on flow dynamics, which may affect the impact of bubble curtains in real-world circumstances.
- Operational Parameter Range: The study concentrates on a range of operational parameters that are most commonly encountered in bubble curtain technology (BCT). This focus may restrict the application of our findings to settings outside of this predetermined range, perhaps missing the system's response in severe or abnormal operational scenarios.
- Environmental Factors: This study does not fully analyze external factors, including sea conditions, temperature, and salinity. These factors may have a considerable impact on the flow dynamics of bubble curtains in situ.
- Lack of Experimental Validation: A critical limitation of this study is the absence of experimental data to validate the numerical model. There is still inconsistency about the model's capacity to correctly forecast real-world events in the absence of empirical validation. This gap emphasizes the need for more study to improve the model's applicability and reliability by combining numerical simulations with experimental or field data.

1.0.4. Thesis Structure

This thesis is structured into ten main chapters, each focusing on a specific aspect of the numerical analysis of unsteady compressible flow within bubble curtain technology hoses. Below is an outline of each chapter:

- Chapter 2: Literature Review
  The chapter on literature review gives an in-depth review of pipeline research as a reference for flow in the hose. It discusses the significance of numerical analysis in fluid dynamics and defines the present research within the larger framework of the subject.
- Chapter 3: Methodology
  The research model and technique are detailed in this chapter. It offers a full explanation of the pneumatic model used in this work, as well as the verification technique and approach to nozzle implementation inside the model.
- Chapter 4: Model Development and Initial Verification
  This chapter outlines the development of the transient gas flow model as the starting point for this research. Furthermore, it represents the verification process, establishing the foundation for further model refinement and analysis.
- Chapter 5:Nozzle Implementation
  This chapter outlines the step-wise introduction of nozzles into the model, with a focus on the scaled BCT model. It begins with a single nozzle, continues to three, and concludes with a five-nozzle system as the final model.
- Chapter 6: Analysis of Numerical Instability
  The sixth chapter focuses on identifying and analyzing numerical instability concerns within the model. The influence of the convective inertia term and the discretization approach utilized, as well as the simulation adjustments taken to resolve these instabilities, are discussed.
- Chapter 7: Comparative Analysis and Stability Improvement
  This section of the thesis investigates how to improve the stability of the model and compares simulations that include and do not include the convective inertia term. It evaluates the stability and offers information about the models with 1, 3, and 5 nozzles.
- Chapter 8: Model Evolution from Pipeline to Scaled BCT Representation
  The model's progression from a transient pipeline representation to a scaled bubble curtain technology model is described in this chapter.
- Chapter 9: Discussion
  This chapter focuses on two major topics. First, it investigates the hydrodynamics of flow within the hose with a scaled 1D model of unsteady compressible flow. Second, it investigates the effect of the hose-nozzle system on operational parameters in bubble curtain technology.
- Chapter 10: Conclusion
  This last chapter summarizes major findings while emphasizing the research question and objectives. The study improves the understanding of bubble curtain technology by delving into unsteady compressible flow and the influence of operating circumstances.

2
Literature Review

This literature review intends to cover a variety of subjects connected to the overview of BCT and illustrate how pipeline flow dynamics are similar to hose flow dynamics, making both studies good sources of information. As a reference for flow in the hose of bubble curtain technology, this comprehensive literature review addresses the numerical analysis of unsteady compressible flow, especially in the context of pipeline studies. Moreover, the issue has been better understood by focusing on the behavior of transient compressible flow in pipeline systems as a basis for studying flow dynamics within bubble curtain hoses. Additionally, important elements were also studied, such as bubble curtain technology, compressed air flowing through nozzles, numerical equations for unsteady flow, pipeline studies as instances of hose flow, and other numerical techniques utilized in this field. As mentioned in the introduction, bubble curtain technology has emerged as a potential solution for various issues, such as offshore construction, environmental preservation, and noise reduction. The efficiency of bubble curtains in reducing noise transmission and producing effective barrier effects may depend on controlling the flow dynamics within the hose. It is crucial to have an understanding of the flow dynamics along the hose length of bubble curtains.

2.0.1. Overview of Bubble Curtain Technology

Theoretical description
Bubble curtain technology has evolved as a potential solution for underwater noise reduction in various offshore construction operations [10]. The use of a bubble curtain during the building of foundations, undersea structures, or other maritime infrastructure helps to reduce the impact of noise created during these operations. The device efficiently inhibits the transmission of sound through water by generating a barrier of air bubbles surrounding the noise source, considerably decreasing the noise levels perceived by marine life and neighboring environments [11].

One of the most common and generally recognized applications of bubble curtain technology is in pile-driving operations [12]. This method alters the speed of sound through water by forming a sheet or wall of air bubbles around the area where pile driving occurs, slowing noise transmission from the noise source to the surrounding environment. Compressed air is released via tiny holes in PVC rings or hoses, resulting in a constant stream of bubbles [13]. These bubbles can either rise freely in the water or be enclosed within an additional casing to counteract the impact of currents and maintain a closed shield of bubbles. To implement a bubble curtain system, air compressors are typically positioned on the construction vessel or a nearby platform, supplying the required air to the bubble generating mechanism. The compressed air is then forced through the designated openings, leading to the formation of the bubble curtain. The system's design takes into consideration various factors, such as the depth of the water, water currents, and the specific noise reduction requirements of the project. A pile is surrounded by a confined bubble curtain in figure 2.1a, while the schematic cross-section of an air supply line resting on the seafloor is shown in figure 2.1b.

Application of BCT
Bubble curtains exist in multiple configurations, including single-layer and double-layer arrangements, and are placed in various combinations as well. As mentioned earlier, the effectiveness of this technology is highly dependent on the local conditions (especially currents, depth, and flow dynamics inside the hose). In deep water locations, strong currents can pull the rising air bubbles to the side

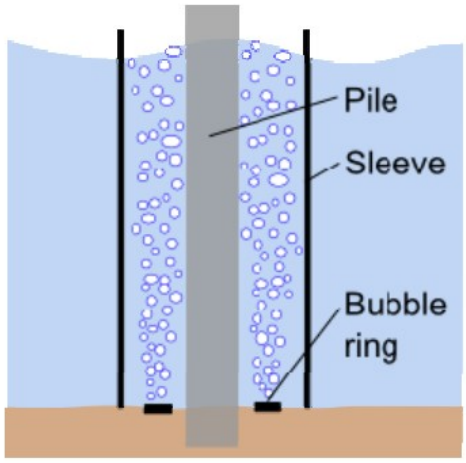

(a) Pile surrounded by bubble curtain
[2]

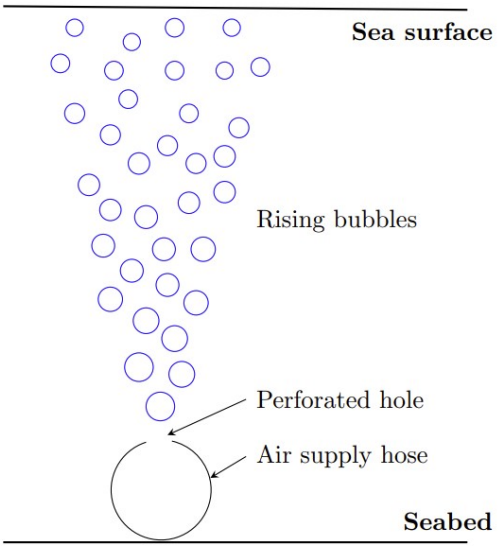

(b) An air supply hose's schematic cross-section resting on the sea bed
[2]

Figure 2.1: A bubble curtain surrounds a pile of air supply hoses laying on the seabed

instead of straight up, resulting in a highly dispersed bubble curtain that is less effective. Since sound in deeper waters is transmitted at a greater distance, a more extensive bubble curtain is required (Royal Haskoning DHV [14]. When a higher level of noise reduction is required (for example, for big monopiles), a double bubble curtain provides an even greater reduction potential. The BCT setup in figure 2.2 shows the pile-driving operation. The application of a bubble curtain system also usually requires a separate vessel in addition to the installation vessel for the storage of power packs, air pumps, and compressors. However, the application of these devices on board a ship may be limited by the wave height. According to Koschinski and Lüdemann [14], in the case of large movements of the ship, problems may occur with the suction process of the oil, and the devices could be automatically shut down. This may cause time delays in the monopile installation procedure [15].

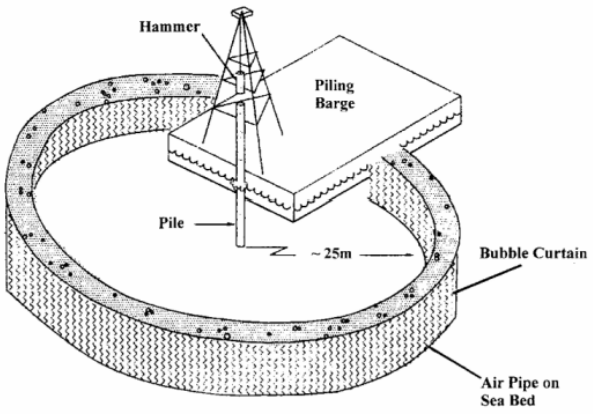

Figure 2.2: Bubble curtain setup
[8]

Compressed air flowing through Nozzle
The amount of compressed air that passes through the nozzle is a crucial factor in bubble curtain technology since it directly influences the generation of bubbles and dispersion. The essential parameters of compressed air, such as mass flow rate and velocity, have a significant influence on the functioning of the bubble curtain. The mass flow rate is critical because it represents the quantity of compressed air that flows through the nozzle per unit of time. It has a direct effect on the volume and intensity of bubble formation, influencing the effectiveness of the bubble curtain in achieving its intended aims, such as noise reduction under underwater conditions. Moreover, the nozzle's design and shape influence flow properties such as velocity, pressure, and discharge profiles. Furthermore, determining the behavior of compressed air passing through the nozzle is critical for enhancing the bubble curtain system, as it has a substantial influence on bubble size, distribution, and overall bubble curtain effectiveness. Chapter 5 will provide a more detailed description of compressed air progressing through the nozzle and its algebraic numerical equation.

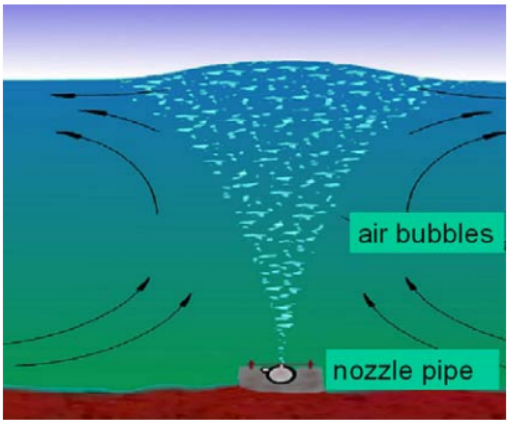

(a) Air flowing through nozzle
[16]

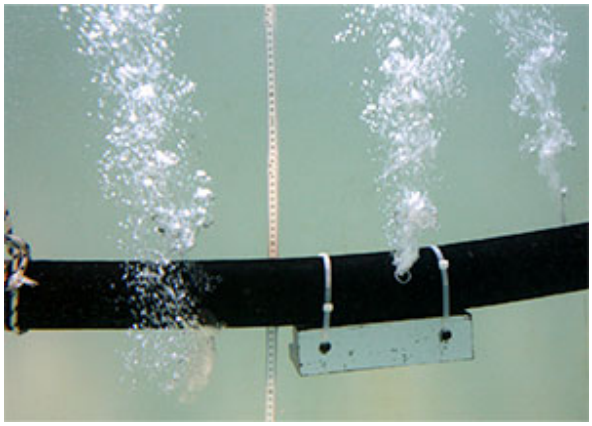

(b) Compressed air flowing through hose nozzle system
[17]

Figure 2.3: Flow of air through nozzle

2.0.2. Previous Studies on Unsteady Compressible Flow

Transient flow studies in pipelines have been extensively researched and can serve as a reference to examine flow in BCT hoses. A.R.D. Thorley and C.H. Tiley's study "Unsteady and Transient Flow of Compressible Fluids in Pipeline: A Review of Theoretical and Some Experimental Studies" [18] is a key paper that shows the usefulness of pipeline studies for assessing flow in hose. The hose used in bubble curtain technology can be thought of as a smaller version of a pipeline, with compressed air moving through it in the same way that a compressible fluid does in a pipeline. As a result, the concept of transient flow in pipelines may be applied to flow analysis in hoses. Transient flow in pipelines and hoses shares some similarities, such as abrupt variations in flow rate, wall friction, and fluid-structure interaction. As long as the proper boundary conditions and fluid properties are taken into account, mathematical models that are used to analyze transient flow in pipelines can also be used to analyze transient flow in hoses.

The analysis of the flow in the bubble curtain technology's hose might be performed using knowledge of transient flow in pipes. A transient flow simulation of a gas pipeline, which was based on transfer function models and the finite volume approach for slow and rapid transients, is one pertinent research study on this subject [19]. The results were verified with experimental data from a pipeline network; nonetheless, the difference between the simulation result and the actual result was 1.15 %. Similarly, [20], [21] research was conducted on the simulation of transient flow using a fully implicit finite volume model. By assuming that the flow is isothermal, it is assumed that temperature changes in the fluid are slow enough to be canceled by heat conduction and the surrounding environment. As a result, the energy equation is ignored, and the system is now governed by the continuity equation and momentum equation. This paper's findings were compared to two existing models: a FIFM approach and a MOC.

In simulations of slow and rapid transients, both models achieved efficient outcomes. Additionally, the paper Transient flow in gas networks: traveling waves [22] looks at how pressure waves propagate in gas networks under transient flow conditions. The paper presents a numerical model for gas flow in networks that accounts for gas compressibility and pipe flow resistance. The paper presents numerical simulations to investigate the propagation of pressure waves and derives a set of partial differential equations that describe the transient behavior of the gas flow in the network. The findings show that Pressure waves in gas networks can have a significant impact on network flow and pressure behavior, particularly when flow rates change abruptly or valves close quickly.

For the implicit operation of a bubble curtain system, it is essential to comprehend and regulate transient flow in the hose. The transient flow has an impact on system dynamics, wall friction, pressure pulsations, bubble formation and dispersal, and flow stability. Since the primary focus of this research is on flow system dynamics, the generation of bubbles is outside the scope of our current BCT study. Along with transient flow, this literature investigated another key component of BCT, namely the mass flow rate through nozzles. To appropriately describe fluid flow in unsteady or time-varying conditions, incorporate the nozzle equation into the governing equations. The nozzle equation describes the flow behavior associated with the nozzle shape and establishes a relationship between flow rate via a hose, flow rate through the nozzle, and pressure. The algebraic equation for mass flow rate has been found in the literature and will be utilized in the BCT model.

However, a thorough grasp of the numerical analysis of unsteady compressible flow within the framework of bubble curtain technology has been given by this review of the literature. The utilization of pipeline studies as references for flow in the hose illustrates the need to comprehend transient flow phenomena. Under academic requirements, a thorough literature study of this thesis was also completed and submitted.

3 Methodology

3.0.1. Overview of Research Design

The approach adopted in this research is designed to systematically investigate the numerical analysis of unsteady compressible flow in the hoses used in bubble curtain technology. The study design is specifically created to meet the stated goals and respond to the research questions presented in the chapter 1. An outline of the study strategy, including the conceptual framework, the computational techniques used, and the justification for the selected techniques, is given in this part. Additionally, this study's research strategy includes several crucial elements. First, to get important background knowledge on unsteady compressible flow inside the bubble curtain technology, comprehensive literature research has been carried out in Chapter 2. To comprehend flow dynamics in the hose, it will be necessary to assess pertinent research on unsteady compressible flow in pipes. After the literature has been reviewed, a thorough analysis of flow dynamics will be conducted to gain an understanding of the behavior of compressed air flow within the hose. The major focus will be on the pressure distribution, flow rate through the nozzle, and general flow characteristics. The goal of this study is to further the comprehension of how modifications to operational parameters affect the pneumatic aspects of the bubble curtain system along the hose length.

To further understand the flow dynamics, a 1D numerical model has been developed, and simulations with various operational parameters will be conducted. This means looking at hose design adjustments, nozzle spacing adjustments, and accounting for the impact of water depth. Through an examination of these parameter changes, important information about how they affect flow dynamics in the pneumatic aspects of the bubble curtain system along the hose length will be obtained. Ultimately, analysis and interpretation of the numerical simulation output data, including pressure distribution, flow rate, and other relevant factors, will be undertaken. In addition to offering valuable insights to enhance our understanding of BCT during transient flow, this study will advance our knowledge of the flow dynamics inside the hose. A deeper knowledge of unsteady compressible flow inside the hose of bubble curtain technology is sought through this study technique. The study's findings might be used to develop a full-scale pneumatic model that takes into account transient flow phenomena occurring along the length of the BCT. The flow chart below 3.1 gives an overview of the study design approach.

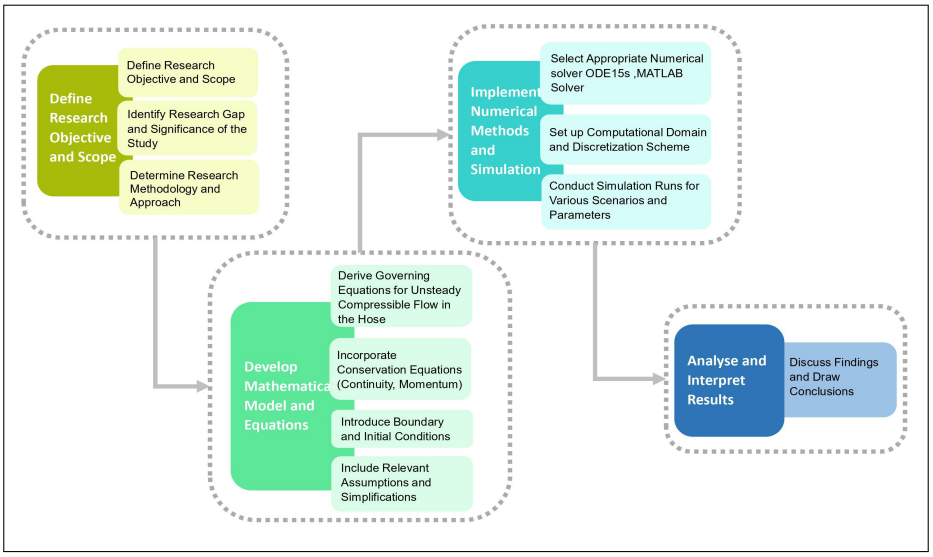

Figure 3.1: Overview of Research Design Flowchart

3.0.2. Basic Theory of Fluid Dynamics

Fluid dynamics is a field of fluid mechanics that studies the movement of liquids and gases [22]. The study of fluid dynamics provides a systematic structure that supports these practical disciplines, including empirical and semi-empirical laws obtained from flow measurement and applied to practical applications. A fluid dynamics issue is often solved by calculating different fluid parameters such as flow velocity, pressure, density, and temperature as functions of time and space. The classical theory of incompressible fluid mechanics [23] is concerned with flows in which temperature and density change owing to pressure and kinetic energy fluctuations are small, i.e., density is nearly independent of pressure [24]. This is a common occurrence while evaluating liquid fluid movement. Compressible flow, on the other hand, occurs when pressure fluctuations greatly impact the density and temperature of a gas. Flow analysis in such instances must account for differences in fluid thermodynamic parameters [25]. A transient flow model, on the other hand, is more suitable to account for wall friction, as these variables might impact the flow's time-dependent behavior.

Unsteady flow denotes a dynamic state in which flow rates fluctuate continuously throughout time. This variability might result from fluctuations in gas or liquid flow rates, pressure distributions, or changes in flow patterns inside the hose, and is specifically connected to the dynamic properties of flow rates within the framework of the BCT. Conversely, transient flow characterizes the whole condition of the flow system, including variations in other important parameters like density, temperature, and pressure across time in addition to flow rate changes. Transient flow, as used in the BCT, represents how the flow regime is dynamic and ever-changing. It illustrates the fluctuating effects of pressure waves and changes in flow patterns on the system, emphasizing the necessity of observing and understanding these factors to preserve the consistency and efficiency of the BCT within its operational environment.

The transient behavior inside the BCT and the unsteady compressible flow are bound together. The appearance of transient conditions in the hose can be attributed to the intrinsic compressibility effects and dynamic variations in flow rates that occur during unsteady flow. As an example, BCT processes that cause variations in gas or liquid flow rates also cause pressure fluctuations and density changes, which ultimately result in the transient state inside the hose. This correlation highlights the interdependence and ensuing influence of dynamic flow behavior on the overall transient state of the system by highlighting how the particular mechanisms producing unsteady compressible flow patterns within the BCT dictate and influence the transient flow condition.

"Depending on the specific goals and requirements of the analysis, in this study, unsteady compressible flow is studied, which contributes to the transient condition in a hose of BCT".

Governing Equation

To explain the fluid motion within the hose of the Bubble Curtain Technology (BCT), two important governing equations are used: continuity equation and momentum conservation. Since an existing research model on transient flow in pipelines is utilized as the fundamental model for this research study, which is further developed into the scaled BCT model and will be explained briefly in Chapter 8, the equation from this research article [26], "An implicit method for transient gas flows in pipe networks, as proposed by kiuchi 1994," is considered the starting point. Before delving into the mathematical formulation of this equation, the following assumptions are made for this study, which align with those utilized in the existing research model [26].

Assumption

- 1-D isothermal compressible flow: A compressible fluid (such as a gas) moving under circumstances where the temperature stays constant is referred to as isothermal compressible flow. The flow is particularly regarded as one dimension in a 1-D isothermal compressible flow, which means that variations occur only in one direction. The complex structure of the gas movement within the pipeline is made simpler by the 1-D isothermal assumption. It is assumed that the thermal dynamics of the flow are constant and consistent throughout the pipeline. In terms of physical perspective, the fluid (e.g., a gas moving through water) can successfully achieve and sustain thermal equilibrium with its environment based on the stability of its thermal conductivity and its gradual adjustments. Throughout the long-distance transmission process, this equilibrium keeps the water's temperature largely steady and constant. Therefore, in these kinds of situations, it is considered appropriate to assume isothermal compressible flow. However, existing research primarily focuses on isothermal conditions, neglecting the conservation of the energy equation. In this study, the energy equation was similarly neglected, aligning with the approach taken in the existing research used for model verification [27].
- Steady-state friction: Since there are currently no friction factors established for transient gas flows, it is usual practice to utilize steady flow formulations [18]. Assuming steady-state friction indicates that the friction factor, which influences head loss due to friction, does not change over time, even when the flow is unsteady. To simplify and facilitate the study of transient gas flows in pipe networks, the assumption of steady-state friction is frequently used. Section 3.0.2 provides a thorough discussion of steady-state friction.
- Negligible expansion of pipe wall due to pressure changes: It is assumed that the expansion of the pipe wall resulting from pressure changes is low, meaning that any deformation or enlargement of the wall in response to changes in internal pressure is negligible. This assumption states that when internal pressure varies, the pipe wall stays constant and doesn't vary much in size. This is predicated on the material used to construct the pipeline having a high modulus of elasticity. Due to the high modulus of elasticity, any radial expansion of the pipe wall is guaranteed to be minimal when compared to the pipe's total diameter. In summary, this assumption simplifies the analysis by assuming the pipe wall is completely stationary, with any radial expansion regarded as insignificant due to the material's high modulus of elasticity with the pipe's diameter.

Each assumption is intended to improve the model by focusing on the important dynamics and assuming that some variables remain constant or have minimal effect. In the present research, the analysis focuses on mass conservation and momentum dynamics, which are crucial for understanding and modeling the fluid behavior within the BCT hose under isothermal conditions.

Convection Form: Continuity and Momentum equations

Continuity Equation:

$$\frac{\partial P}{\partial t} + c^2 \frac{\partial m}{\partial x} = 0 \tag{1}$$

where P is the pressure of the gas flowing through the pipe, $\frac{\partial P}{\partial t}$ is the term that represents the time rate of change of pressure within the fluid, c is the sound speed in an isothermal condition, m is the mass flow rate, and the $\frac{\partial m}{\partial x}$ term denotes the spatial rate of change of the mass flow rate along the pipeline.

Momentum Equation:

$$\frac{\partial m}{\partial t} + \frac{\partial \left(\frac{m^2 c^2}{P}\right)}{\partial x} + \frac{\partial P}{\partial x} + \frac{fm|m|c^2}{2PD} = 0 \tag{2}$$

where $\frac{\partial m}{\partial t}$ represents the time rate of change of the mass flow rate and $\frac{m^2 c^2}{P}$ represents the momentum flux. The term $\frac{\partial P}{\partial x}$ denotes the spatial rate of change of pressure along the flow direction, f denotes the Darcy-Weisbach friction factor, a dimensionless number describing the pipe's resistance due to friction, and D represents the diameter of the pipe. Further, the friction factor f is given as a function of the Reynolds number and the internal roughness of the hose material (ε). Under the assumption of isothermal flow, the speed of sound $c = \sqrt{zRT}$. The compressibility factor z is calculated in the present method by the simple equation (see Reet and Skogman 1987)[28], which is a function of pressure and temperature in reasonable ranges. The first and second terms in Equation 2 are inertia terms.
Applying the u/v differentiation formula to the second convective inertia term in the equation 2 can further simplify the momentum equation.

$$\frac{\partial m}{\partial t} + \left(\frac{2mc^2}{P}\right)\frac{\partial m}{\partial x} + \left(\frac{m^2 c^2}{P^2}\right)\frac{\partial P}{\partial x} \quad + \frac{\partial P}{\partial x} + \frac{fm|m|c^2}{2PD} = 0 \tag{3}$$

Friction
The friction term, represented by W in the fundamental equations, can be described as the frictional force per unit length of pipe resisting the flow. Assuming that the minor losses are small compared with the distributed losses, the frictional force W for a gas may be written as:

$$W = \frac{A}{d}\rho f \frac{u|u|}{2} \tag{4}$$

where f is the Darcy friction factor, A is the cross-sectional area of the pipe, d is the diameter of the pipe, and u is the velocity of the gas.
Since, at present, there have been no friction factors defined for transient gas flows, it is common practice to use the steady flow definitions, which are explained briefly in the research of A. R. D. Thorley [18]. The friction factor is strongly dependent on the liquid volume fraction, and different calculation techniques give substantially different results. There are two main options for obtaining a value for the friction:

- Modify the Reynolds number and roughness terms of the Colebrook equation.
- Include in the expression for friction a multiplier that is determined empirically.

According to Thorley, modifying the Reynolds number and roughness factors is better suited for unsteady and steady flow analysis. In this study, as previously mentioned, the focus is on transient flow. The Colebrook-White equation was used to compute the Darcy friction factor [22].

.

$$\frac{1}{\sqrt{f}} = -2\log\left(\frac{1}{3.7}\frac{\varepsilon}{D_\mathrm{p}} + \frac{2.51}{\mathrm{Re}\sqrt{f}}\right) \tag{5}$$

where f is the Darcy friction factor, D_p is diameter of pipe, and ε/D_p denotes pipeline relative roughness and Re is Reynolds number.

$$Re = \frac{\rho v D}{\mu} \tag{6}$$

where ρ is the density of air, v is the velocity, D is the diameter of the pipe, and μ is the dynamic viscosity of the fluid, remains unchanged under isothermal conditions.

State Equation of an Ideal Gas
When investigating the dynamics of unsteady compressible flow inside bubble curtain technology, the ideal gas state equations were used. This equation defines the relationship between a gas's pressure, density, and temperature, allowing for a better understanding of its behavior under various conditions. Specifically, under isothermal conditions where the temperature stays constant despite pressure and density fluctuations, the state equation simplifies the analysis by eliminating the need to consider heat transmission between the gas and its surroundings [29].

$$P = \rho RT \tag{7}$$

where P represents the pressure, ρ the density, R the specific gas constant, and T the constant temperature. However, this formulation does not explicitly account for the compressibility factor, which is crucial in determining the speed of sound in a gas. The compressibility and temperature of an ideal gas affect the speed of sound, which indicates how pressure fluctuations travel through the gas. For an ideal gas, the speed of sound is given by $c = \sqrt{\gamma RT}$. This equation highlights the dependence of sound speed on the gas's thermal properties, which are inherently considered through the adiabatic constant γ. While the first discussion centered on the isothermal condition as a simplification for evaluating gas flow dynamics, it is important to recognize the impact of compressibility, particularly in terms of sound speed. The compressibility factor Z, which is often near one for an ideal gas under standard conditions, can depart from unity under different pressure and temperature settings, influencing the gas's behavior and the accuracy of the ideal gas law. While the ideal gas law provides a simple model for gas behavior, actual gases exhibit deviations, particularly under high-pressure or extreme temperature conditions, which may be explained by incorporating the compressibility factor Z into the state equation $P = Z\rho RT$. This study used the ideal gas law $P = \rho RT$ to describe the unsteady compressible flow of air in bubble curtain technology. The purpose was to strike a balance between analytical simplicity and capturing essential gas characteristics under isothermal conditions.

3.0.3. Description of the pneumatic Model

The basic partial differential equations (PDEs) governing unsteady compressible flow in the setting of fluid dynamics were established in the section before. The continuity and momentum equations, which are essential components of the mathematical framework required to simulate the intricate flow behavior within bubble curtain technology hoses, are included in these PDEs. To transform these theoretical notions into an actual computational model, it is necessary to convert partial differential equations (PDEs) into a form that can be solved through numerical solutions. In order to do this, the PDEs must be transformed into ordinary differential equations (ODEs), which can subsequently be solved numerically. The conversion procedure is essential because it immediately lowers the difficulty of solving PDEs and aligns the problem with an established method of numerical analysis. The pneumatic model described in this section utilizes the Method of Lines (MOL), an approach for numerically solving PDEs.

Method of Lines
Note that equations 1 and 2 have two independent variables, x and t, which is why they are classified as PDEs. The fundamental idea behind the MOL is to use algebraic approximations in place of the spatial derivatives in the PDEs. The spatial derivatives are no longer explicitly expressed in terms of the spatial independent variables after this completion. Essentially, the only variable that remains is the initial-value variable, which in a physical problem is usually time. In other words, the equations represent an approximation system of ODEs that approximates the original PDEs with just one independent variable remaining. The challenge, then, is to formulate the approximating system of ODEs. Once this is done, they can apply any integration algorithm for initial-value ODEs to compute an approximate numerical solution to the PDEs. Thus, one of the salient features of the MOL is the use of existing and generally well-established numerical methods for ODEs [30].

First, the need is to replace the spatial derivatives $\frac{\partial m}{\partial x}$ and $\frac{\partial P}{\partial x}$ from the PDEs of equations 1 and 2 with an algebraic approximation or discretization scheme. To do this, a numerical method is used, which is called finite differences. In the present study, three different discretization schemes have been used, starting with central discretization, followed by backward and forward discretization, which will be explained in detail further.

Central discretization
In the following research, the central discretization approach is used to ensure high accuracy in the numerical simulations, especially in the spatial discretization approach of MOL. The balanced method of central discretization, which uses information from points on both sides of each spatial node, makes it stand out. A second-order correct representation of the spatial derivatives is made possible by this method, which is essential for encapsulating the complex behavior of unsteady compressible flow.

The second order is the level of accuracy that the central discretization approach achieves while approximating the spatial derivatives. The approximation error reduces quadratically with decreasing node distance Δx . The error term for a second-order approximation is proportional to Δx^2, showing that it decreases significantly as the grid is refined. In contrast to a first-order approximation, where the error is directly proportional to Δx, grid refinement has a slower rate of error reduction. Second-order accuracy is especially crucial for capturing the complex behavior of unsteady compressible flow because it assures that the numerical solution converges faster to the true solution as the mesh becomes finer. This greater level of precision is required to resolve the complicated spatial variations and transient phenomena associated with unsteady flows without significantly increasing computational time. In summary, the central discretization method, which uses a balanced approach and achieves second-order accuracy, was chosen for its capacity to produce a more accurate representation of spatial derivatives, which is required for the complex modeling of intricate unsteady compressible flow dynamics.
From the figure 3.2 the central discretization can be written as follows.

$$u_x \approx \frac{u_{i+1} - u_{i-1}}{2\Delta x} + O\left(\Delta x^2\right)$$

where i is an index designating a position along a grid in x and Δx is the spacing in x along the grid. Further, this will be substituted in the continuity and momentum equations.

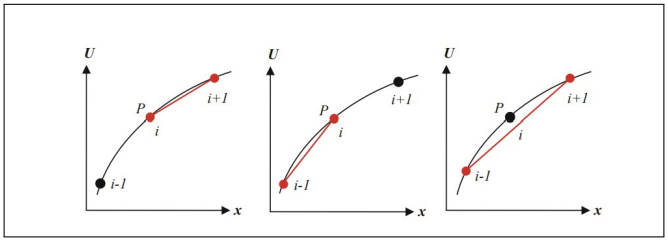

Figure 3.2: Forward, backward and central spatial difference
[31]

Central discretization of continuity equation

$$\frac{dP}{dt} = -c^2 \frac{m_{i+1} - m_{i-1}}{2\Delta x} = 0 \tag{8}$$

Central discretization of Momentum equation

$$\frac{dm}{dt} = -\left(\frac{2m_i}{P_i}\right)\frac{m_{i+1} - m_{i-1}}{2\Delta x} + \left(\frac{m_i^2}{P_i^2}\right)\frac{P_{i+1} - P_{i-1}}{2\Delta x} - \frac{P_{i+1} - P_{i-1}}{2\Delta x} - f\frac{m_i|m_i|c^2}{2P_i D} \tag{9}$$

where dP/dt is the ordinary derivative of pressure with respect to time, dm/dt is the ordinary derivative of mass flow rate with respect to time, f is Darcy-Weisbach friction factor, D is the diameter of the pipe, c is the sound speed in an isothermal condition, i represents the spatial index at a particular location, $i+1$ and $i-1$ represent neighboring spatial locations, and Δx is spatial grid spacing.

Discretization at boundary condition
For the left-end value of x, $i=1$, and for the right-end value of x, $i=M$; that is, the grid in x has M points. Then the MOL approximation at $i=M$,

$$\frac{dP}{dt} = -c^2 \frac{m_{M+1} - m_{M-1}}{2\Delta x} = 0 \tag{10}$$

$$\frac{dm}{dt} = -\left(\frac{2m_M}{P_M}\right)\frac{m_{M+1} - m_{M-1}}{2\Delta x} + \left(\frac{m_M^2}{P_M^2}\right)\frac{P_{M+1} - P_{M-1}}{2\Delta x} - \frac{P_{M+1} - P_{M-1}}{2\Delta x} - f\frac{m_M|m_M|c^2}{2P_M D} \tag{11}$$

Note that m_{M+1} and P_{M+1} are outside the grid in x; that is, $M+1$ is a fictitious point. To deal with this, the second-order backward discretization method is applied at the boundary $x=M$ for equation 8 in order to eliminate this ghost point. Additionally, in this study on equation 9 the last grid point has a boundary condition; the details of this boundary condition are covered in the section that follows the verification strategy.

Backward discretization

$$\frac{dP}{dt} = -c^2 \frac{3m_M - 4m_{M-1} + m_{M-2}}{2\Delta x} \tag{12}$$

At i=1,

$$\frac{dP}{dt} = -c^2 \frac{m_2 - m_0}{2\Delta x} = 0 \tag{13}$$

$$\frac{dm}{dt} = -\left(\frac{2m_1}{P_1}\right)\frac{m_2 - m_0}{2\Delta x} + \left(\frac{m_1^2}{P_1^2}\right)\frac{P_2 - P_0}{2\Delta x} - \frac{P_2 - P_0}{2\Delta x} - f\frac{m_1|m_1|c^2}{2P_1 D} \tag{14}$$

The node points m_0 and P_0 are outside the grid in x; that is, 0 is a fictitious point. To deal with this, the second-order forward discretization method is applied at the boundary $x=1$ for equation 9 in order to eliminate this ghost point. Additionally, in this study on equation 8 the first grid point has a boundary condition; the details of this boundary condition are covered in the next section.

Forward discretization

$$\frac{dm}{dt} = -\left(\frac{2m_1}{P_1}\right)\frac{-3m_1 + 4m_2 - m_3}{2\Delta x} + \left(\frac{m_1^2}{P_1^2}\right)\frac{-3P_1 + 4P_2 - P_3}{2\Delta x} - \frac{-3P_1 + 4P_2 - P_3}{2\Delta x} - f\frac{m_1|m_1|c^2}{2P_1 D} \tag{15}$$

This transformation of PDEs, into ODEs the equations 8 and 9 illustrates the essence of the MOL, namely, the replacement of the spatial derivatives, in this case x, so that a system of ODEs approximates the original PDEs. Then, to compute the PDEs solution, they solve the approximating system of ODEs. However, before they can solve this integration in t, the PDE problem must be fully specified. Since both the central discretized ODEs are first-order in t and first-order in x, they require two initial conditions and two boundary conditions. These prerequisites are crucial because they provide a well-posed problem and ground the simulation in a real-world situation. The next section goes into detail about those conditions.

Next, the solutions are obtained for the system of ordinary differential equations (ODEs) that results after establishing initial and boundary conditions. The robust ode15s solver in MATLAB [32] is used as a numerical integrator that is suitable for stiff systems of ODEs, which are frequently seen in fluid dynamics applications that involve unsteady compressible flows. The solver efficiently and reliably integrates the equations across time, producing the temporal evolution of the system under different circumstances, by utilizing adaptive time-stepping and sophisticated numerical methods.

3.0.4. Verification Strategy

Verification is a crucial step that comes after developing the pneumatic model for unsteady compressible flow and discretizing the relevant governing equations. In this study, the model is verified against the "Kiuchi model" from the research paper by Tatsuhiko Kiuchi titled "An implicit method for transient gas

flows in pipe networks" (Kiuchi, 1994) [26]. A fully implicit finite-difference technique for estimating the unsteady gas flow in pipeline networks is presented in this existing research. Because of its computational efficiency and stability, it serves as a baseline for these research objectives. Based on a set of assumptions that reduce the physical issue to a one-dimensional isothermal compressible flow with steady-state friction and negligible pipe wall expansion owing to pressure variations, the model uses the Newton-Raphson technique for solving finite-difference equations.

Model Parameters

A straight pipe of 50 km in length with a 500 mm internal diameter is shown in figure 3.3 was used for this case study, holding a gas of molecular weight 18.0 at a pressure of 5 MPa. Further, the outlet valve opens, and the outflow steps up from zero to 300,000 (m^3/hr) while the inlet pressure is maintained at 5 MPa. After maintaining this condition for 20 minutes, the outlet valve closes. The friction factor f is assumed to be 0.008 for the calculation and number of discretization sections: 50, ground temperature T_{amb} = 25°C,

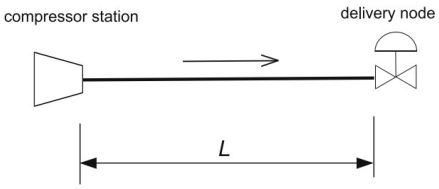

Figure 3.3: Pipeline information [33]

Initial and Boundary Conditions for the Kiuchi Model

Applying the initial and boundary conditions in their original form is crucial for verifying our numerical model against the Kiuchi model. These prerequisites are necessary to guarantee the comparability of the simulations and the significance of the results. The initial pressure within the pipeline is assumed to be uniform and is set to P=5 MPa and the flow rate Q_n = 0 m^3/hr. In the study of fluid dynamics, particularly when applied to bubble curtain technology, it is critical to distinguish between normal, Free Air Delivery (FAD), and real conditions, since each has a substantial influence on system performance interpretation. Normal circumstances are usually defined by a standard set of environmental characteristics, which frequently include a temperature of 20 °C, and atmospheric pressure at sea level (101.325 kPa). These standardized measurements provide a uniform baseline for comparing system performance across several research and applications.

In the case of bubble curtain technology, FAD conditions are very important. Although FAD conditions have generally been connected with air compressors, in the case of bubble curtains, they might be understood to represent the volume of air delivered by the system to construct the curtain under the same environmental circumstances as the intake. This measure is critical for determining the actual durability of the bubble curtain in its operating context since it accounts for the air volume available to construct the barrier without the influence of the compression process. In contrast, real conditions include the actual operating settings under which the bubble curtain technology operates. These can comprise a wide range of situational variables such as water temperature, depth pressure, site-specific salinity, current flows, and other environmental elements. In our simulation, we start with a uniform pipeline pressure of 5 MPa, which accurately represents the high-pressure environment faced by bubble curtains. To simulate a realistic startup scenario, the initial flow rate Q_n is set to 0 m^3/hr. As the simulation progresses, the boundary conditions $P(x=0,t)$=5 MPa and $Qn(x=L,t)=f\_2(t)$ are used to simulate the system's behavior over time. The constant high pressure at the pipeline's start and the changing flow rate at the output, which varies according to the function $f\_2(t)$, are intended to simulate the fluctuating circumstances that a bubble curtain system may encounter in a real-world scenario. Additionally, the boundary conditions used in this study were taken from the Kiuchi model. Kiuchi's original model measures the flow rate in cubic meters per hour (m^3/hr). To align with the SI unit system used in this research, the flow rate is further transformed from m^3/hr to m^3/sec.

Existing research Kiuchi Model: The boundary conditions of kiuchi's from the figure 3.4.

- $P(x = 0, t) = 5\,\text{MPa}$,
- $Q\_n(x = L, t) = f\_2(t)$.

$$f\_2(t) = \begin{cases} 0\,\mathrm{m}^3/\mathrm{hr}, & \text{if } 0 \le t < 10\,\mathrm{min} \\ 3\times10^5\,\mathrm{m}^3/\mathrm{hr}, & \text{if } 10 \le t < 30\,\mathrm{min} \\ 0\,\mathrm{m}^3/\mathrm{hr}, & \text{if } 30 \le t < 60\,\mathrm{min} \end{cases}$$

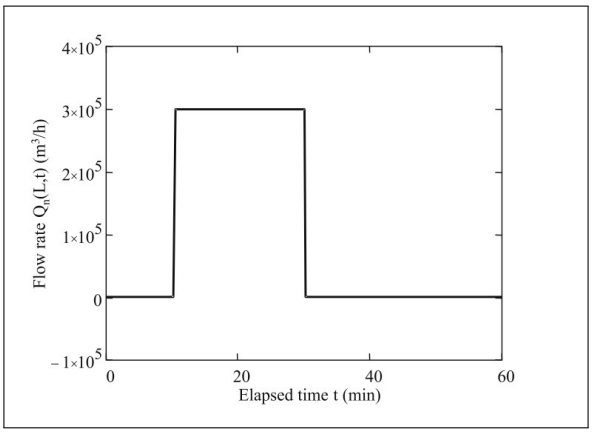

Figure 3.4: Change of flow rate at $x = L$ for case study ($f\_2(t)$).
[33]

Incorporating Kiuchi's model Results

The second term in equation 2 is called the convective inertia term. In the Kiuchi study, the second term of convective inertia was neglected due to the assumption of low flow velocity with respect to wave speed. The flow rate change at Node 1 with respect to time is depicted in figure 3.5a. Additionally, Kiuchi compared his method with the Guys, Lax–Wendroff, Crank–Nicolson, and method of characteristics methods. An unstable solution was obtained via the Crank-Nicolson approach when dealing with long-time steps. When pipes are separated into suitably tiny sections for both rapid and slow transient events, the Lax–Wendroff technique and the method of characteristics employ the explicit approach and provide an accurate result, but they require a large amount of computing time. Kiuchi further shows that the Guys approach, which applies the implicit method, has significantly damped oscillation and strong stability for small time steps.

Further, the model was updated with the convective inertia term by Mohammad Abbaspour in his research [34]. The figure 3.5b. Moreover, several researchers have used the Kiuchi model, both with and without the convective inertia element, to examine transient flow in pipelines. Convective inertia in the Kiuchi model, where the fully implicit finite difference method was applied with large time steps, does not exhibit variation in the result; however, if the time steps were small, the convective inertia term has demonstrated variation in the results to capture high accuracy, as author K. S. Chapman [35] in his research explains in more detail. A trade-off between computing time and accuracy determined the use of the convective inertia term in their study. In detail, the next part explains the physical importance of the convective inertia term. The figure 3.5c shows the pressure changes at all nodes when the inertia term is included. Since the boundary condition *P(1)*=5 MPa, node 1 displays a straight line that entirely follows the boundary condition. Furthermore, when the flow rate starts rising at 10 minutes, the pressure lowers and enters a steady state condition, and when the flow rate drops to zero at 30 minutes, the pressure rises and reaches a new equilibrium condition that follows the trend of the flow rate boundary condition in expression 3.0.4.

Convective vs Non-convective inertia

When a valve is opened and closed to control flow, it is discovered that the inertia term is essential because the flow rate exhibits an up-and-down time step. The flow rate in the Kiuchi model, both with and without inertia, is controlled by a valve as indicated by the boundary condition 3.0.4. The computed flow behaves differently at different time steps until the flow reaches its steady-state conditions. For a large time in figure 3.5a, some of the governing equation terms, such as the convection inertia term, may not be affected by small disturbances during the sudden closing or opening of valves, and the calculation may not capture the fluid flow physics. In this case, the existence of the convection inertia term in momentum equations has no significant effect on the flow. On the other hand, for the small-time step, the effect of this term is significantly important and plays an important role in the fluctuation amplitude and damping before reaching the flow to its steady-state condition, as shown in figure 3.5b. In the present research, governing equations with convective inertia terms are used, and the findings are discussed in the next chapter.

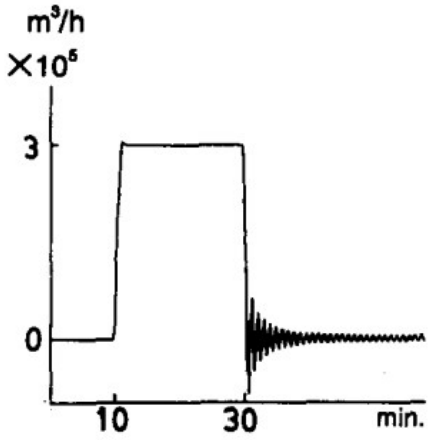

(a) Flow at isothermal condition without convective inertia

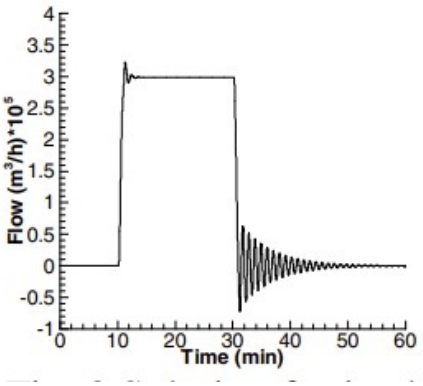

(b) Flow at isothermal condition with convective inertia

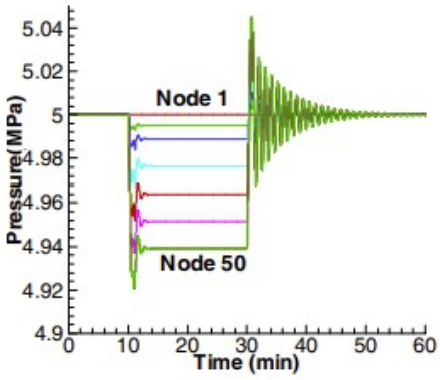

(c) Pressure at isothermal condition

Figure 3.5: Existing research: Kiuchi's solution for an isothermal model by considering inertia term with and without [34]

4

Model Development and Initial Verification

4.0.1. The Pneumatic Model of Transient Gas Flow

After outlining the framework for the simulation in the previous chapter, the focus now will be on modeling the transient gas flow model in MATLAB. Furthermore, this chapter will cover the actual implementation of the existing research model parameters, updated boundary conditions, and initial conditions used in the present research. While the model is based on the ideas presented by the Kiuchi model, it is important to understand that modifications are made that require changes to the boundary conditions to comply with the momentum-specific focus on pressure and mass flow rate based on continuity equations.

Utilization of Existing Research Model Parameters and Initial Conditions
The parameters from Kiuchi's study have been thoughtfully included in this model. These are essential for an accurate modeling of the transient gas flow and comprise the geometric dimensions of the pipe, the physical characteristics of the gas, and the operational parameters. By utilizing these parameters, the model ensures that the base state is reflective of a verification scenario. Additionally, there is no flow, and the pipe is initially in a uniform pressure condition. These initial conditions allow us to observe and analyze the system's response to the changes introduced by the boundary conditions. The previous chapter 3 provides a detailed explanation of the parameters as well as the initial state.

Present study-Adapted Boundary Conditions
For the boundary conditions, the constant inlet pressure stated in Kiuchi's model is the same in this model. However, in the current work, the flow rate condition is transformed into the mass flow rate condition to coincide with the mass conservation component of the governing equations. By including the gas's density, ρ, the volumetric flow rate Q can be mathematically transformed to the mass flux m, where $m = \rho \cdot Q$. The Kiuchi model was the starting point for this research, in which they used 50 nodes. To ensure consistency and facilitate a direct comparison with the Kiuchi model, the numerical analysis in this research employs the same node count. Despite trying with additional nodes, no significant differences in outcomes were observed; however, there was a considerable increase in computing time. Consequently, a decision was made to retain 50 nodes for the sake of comparison with the Kiuchi model, which served as the starting point for this research.

From Figure 3.4,the flow rate Q is obtained as $3 \times 10^5\,\mathrm{m}^3/\mathrm{hr}$. Further, it is converted to $83.34\,\mathrm{m}^3/\mathrm{s}$. Under FAD conditions, the density of air, ρ_{air}, is given as $1.2\,\mathrm{kg}/\mathrm{m}^3$, and the area of the pipe is calculated using $A_{\mathrm{pipe}} = \frac{\pi}{4} \times Dia^2$ where the diameter of the pipe is 500 mm.
The mass flow rate m can be calculated as $m = \frac{Q \times \rho_{\mathrm{air}}}{A_{\mathrm{pipe}}}$, resulting in $m = 509.3\,\mathrm{kg/s \cdot m^2}$.
The present model's modified boundary conditions are as follows:

- $P(x = 0, t) = 5.0\,\mathrm{MPa}$,
- $m(x = L, t) = f\_2(t)$.

$$f\_2(t) = \begin{cases} 0\,\mathrm{kg/s \cdot m^2} & \text{if } 0 \le t < 600\,\mathrm{sec} \\ 509.3\,\mathrm{kg/s \cdot m^2} & \text{if } 600 \le t < 1800\,\mathrm{sec} \\ 0\,\mathrm{kg/s \cdot m^2} & \text{if } 1800 \le t < 3600\,\mathrm{sec} \end{cases}$$

Result of the Present study

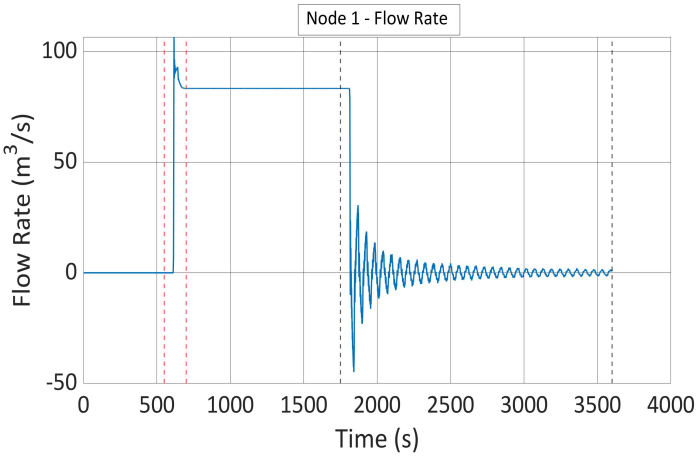

Figure 4.1: Present study flow rate at Node 1

The flow rate changes at Node 1 are illustrated in the figure 4.1. The first noticeable rise in flow rate occurs at around 600 seconds and is indicated by two vertical red lines. This change is caused by a boundary condition where the mass flow rate at the final node, *m(Nx)*, goes from 0 to 509.28 $kg/s \cdot m^2$. The flow rate at Node 1 stays comparatively constant until around 1800 seconds after the initial jump. This plateau points to a stable condition in which the system's outflow and inflow are equal.

The mass flow rate *m(Nx)* at the last node is reset to zero at 1800 seconds, which again matches the boundary condition, and there is a sharp decrease to zero. There is a considerable oscillation period just after the decrease. This oscillation is caused by the transient effect of a sudden change in the boundary condition. Additionally, the oscillation gradually damps to zero in about 3600 seconds. The oscillation in the flow rate is also found to be symmetrical about the steady-state value. The maximum value during the oscillation is 30.57 m^3/s, while the minimum value is about -44.77 m^3/s. Eventually, this oscillation damps out due to the conservation of mass and momentum.

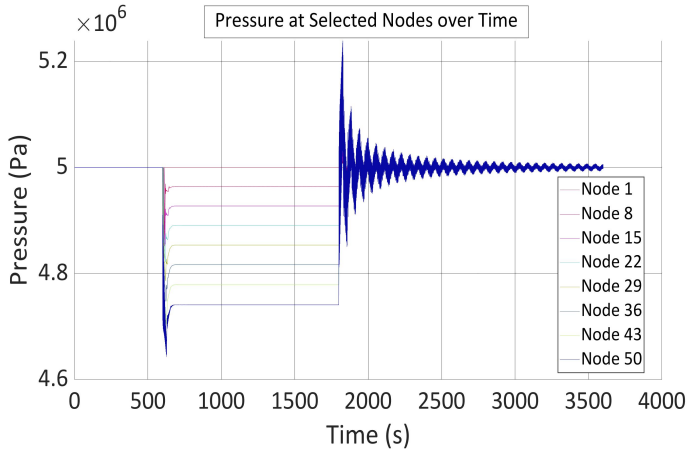

Figure 4.2: Present study pressure at selected node

The figure 4.2 begins at a pressure of around 5 MPa, which is consistent with the initial condition. Furthermore, when the flow starts (after 600 seconds), a pressure reduction occurs at the lower-numbered nodes nearest to the intake, and this decrease progressively spreads to the higher-numbered nodes. The minimum noticeable pressure drop was around 4.64 Pa. Moreover, Similar to the flow rate, pressure starts to fluctuate around 1800 seconds, which corresponds to the flow stopping. This is mostly

characteristic of a transient flow brought on by a sudden reduction in the mass flow rate. Every node exhibits oscillations, although those located further away from higher-numbered nodes are more evident and last longer. The maximum oscillation of pressure was found to be 5.23 Pa. The oscillations grow less noticeable with time, and it appears that the system is approaching a new equilibrium state.

4.0.2. Comparative Analysis with Existing Research

Flowrate at Node 1

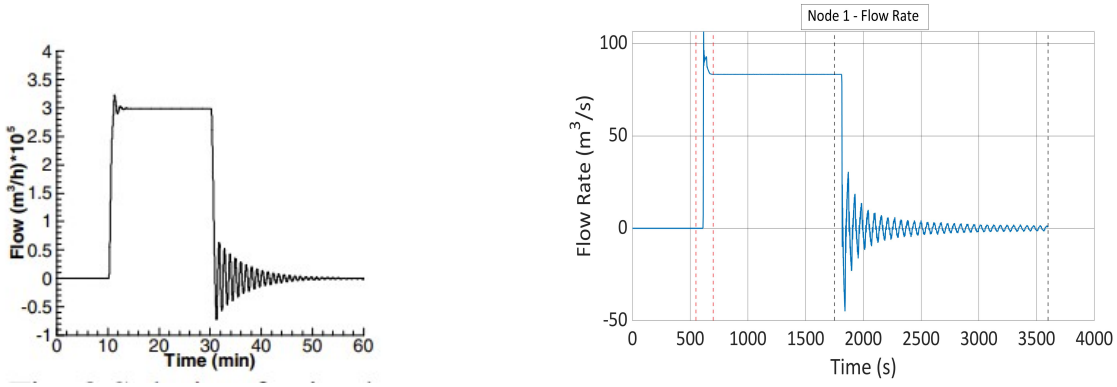

(a) Kuchi result: flow rate at Node 1

(b) Present study: flow rate at Node 1

Figure 4.3: Comparison between the present study's flow rate and Kiuchi's

Pressure at selected Nodes

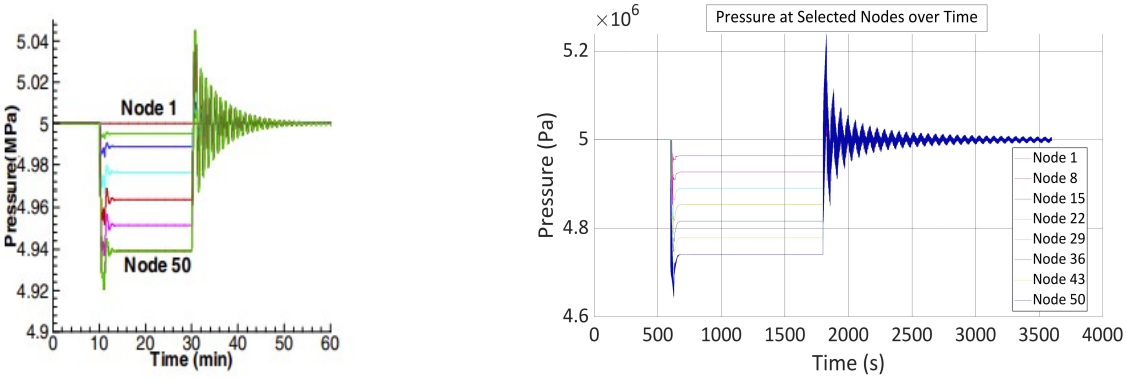

(a) Kuchi result: Pressure

(b) Present study: Pressure

Figure 4.4: Comparison between the present study's pressure and Kiuchi's

The figure 4.3 shows the comparison of the Present study with the kiuchi Model considering the convective inertia term.

- Response Time and Rise Time: The flow rate reaction to a boundary condition change in the Kiuchi model, with rising at 10 minutes. This reaction shows a system that responds to changes quickly and without apparent delay. The present model demonstrates a similar immediate reaction, with the flow rate rapidly rising. However, this occurs approximately 600 seconds, or 10 minutes into the simulation, which corresponds to the time of the Kiuchi model.
- Magnitude of Change: According to the Kiuchi model, the flow rate reaches a peak around 3.4×10^5 m^3/hr and then stabilizes until the boundary condition changes at the 30-minute point. In the current model, the flow rate peaks at around 103 m^3/s and remains constant until the boundary condition changes at 1800 seconds. When comparing units, it is critical to verify that they are consistent; for example, if we convert m^3/s to m^3/hr, the peak in the current model corresponds to 3.7×10^5 m^3/hr, which is equivalent to the Kiuchi model.

- Response to Boundary Condition: After 30 minutes, Kiuchi's model indicates a drop-down to zero flow rate, followed by a series of damped oscillations. The current model likewise predicts a drop in flow rate at the same period, followed by oscillations.
- Settling Time to Steady State: After around 60 minutes, the flow rate in the Kiuchi model stabilizes close to zero. The current model shows oscillations dampening down and achieving a steady state in 4000 seconds (about 67 minutes), which is a slightly longer settling time than the Kiuchi model.

The figure 4.4 illustrates the comparison between the pressure at the present study and Kuchi's model.

- Response to Flow Initiation: In Kiuchi's model, when flow begins, there is an instantaneous pressure decrease at Node 1, which progressively propagates to Node 50. Node 50's initial pressure drop is approximately 4.92 Pa. The present study demonstrates a comparable instantaneous pressure reduction across the nodes at the beginning of the flow, demonstrating a quick system reaction to changes in boundary conditions. Node 50's initial pressure drop is approximately 4.62 Pa. Kuchi's initial pressure drop is somewhat higher than the current model.
- Oscillations and Damping: Following the flow stop at 30 minutes, Kiuchi's model exhibits significant oscillations that begin at Node 8 and reduce faster than those at Node 50. The present study likewise shows oscillations after flow stoppage, with the oscillations being more apparent at Node 8. The oscillations damp out, similar to Kiuchi's results, but with slight differences in amplitudes and damping rates.
- Steady-State: After the oscillations damp down throughout the 60-minute time frame, Kiuchi's model recovers to a steady-state pressure level. The current study suggests that the system achieves a new equilibrium state once the oscillations subside, which occurs within the period of the graph, which is around 4000 seconds or 67 minutes.

4.0.3. Verification Outcomes

When the current study was compared to the existing research by Kiuchi, 2% to 4% differences in flow rates and pressure responses were observed. Differences in the magnitudes of flow rate changes as well as the frequency and amplitude of pressure oscillations after boundary condition changes were observed.

The Kiuchi model used a fully implicit finite difference technique to solve the system's Ordinary Differential Equations (ODEs). This approach used center and backward discretization for spatial and temporal components, respectively, which improved stability, especially for stiff difficulties commonly found in fluid dynamics simulations. In contrast, in the current research, MATLAB's ode15s solver, which is a numerical integrator designed for stiff systems of ODEs and differential algebraic equations (DAEs) is used. The time element of the equations is handled by this solution, while the spatial components were explicitly discretized using the central difference approach. The ode15s solver uses advanced algorithms that adjust the step size and method order based on the stiffness of the issue and the desired accuracy.

The differences between the two investigations show that spatial discretization combined with an adaptive time-stepping solution can result in distinct simulated dynamics. While the ode15s solver is robust and capable of handling complicated stiff systems, it may interpret the system's stiffness differently than Kiuchi's implicit technique, resulting in variations in the calculated solutions.

5
Nozzle Implementation

Building on the verification of the transient flow model in pipes (as described in Chapter 4, the next focus is on the nozzle, which is a key component of Bubble Curtain Technology (BCT). An important step in simulating the full scale of BCT systems is the incorporation of nozzle dynamics into the model. Since air bubbles are the main method of reducing noise in underwater situations, nozzles are essential to these systems. This chapter covers the process of adding nozzles to the verified pneumatic model and looks at how adding nozzles changes the flow properties of the hose, particularly the pressure and flow rate through the nozzles.
Furthermore, the investigation will proceed with the impact of nozzle installation on the transient flow inside the pipe using numerical modeling. This stage is crucial for both understanding the system's behavior and developing the model into a more complete representation of a BCT system. By the end of this chapter, the research will have generated an updated model that approximates the behavior of BCT in real life and provides important information regarding the flow dynamics of such systems.

5.0.1. Introduction of a Single Nozzle

Mass flow rate across the nozzles
In order to enhance the understanding of BCT systems with unsteady compressible inflow, the original step is to integrate nozzle characteristics into a validated pipeline model. This approach allows for the precise investigation of the nozzle's effect on inflow characteristics. The air mass inflow rate via the nozzle, which is an important factor in bubble conformation and dispersion, can frequently be calculated using classical gas dynamics.

Ideal mass flow rate
The mass flow rate of air exiting a nozzle could be calculated using isentropic and adiabatic compressible flow theory in conjunction with the state equation of the ideal gas law provided by:

$$P = \rho RT \tag{16}$$

Where P is the pressure, ρ is the air density, T is the temperature, and R is the specific gas constant (for air, it has a value of 287 J/kg/K). The Mach number M is defined as the ratio between the velocity of the gas across the nozzle U, and the local velocity of sound in the medium. For isentropic flow conditions, the speed of sound is $c^2 = \gamma RT$, where γ is the adiabatic constant.

$$M = \frac{U}{c} = \frac{U}{\sqrt{\gamma RT}} \tag{17}$$

The adiabatic constant is defined as the ratio of the specific heat evaluated at constant volume and pressure $\gamma = cp/cv$. The relations of temperature, pressure, and density T, P, ρ for the conditions inside the reservoir T_0, p_0 and ρ_0 are given by compressible flow theory [36]. The following equations assume that the velocity and fluid properties are constant across sections normal to the flow (i.e., there are no radial gradients). The air that enters and exits the nozzle has just an axial component to its velocity, as shown in the below figure 5.1.

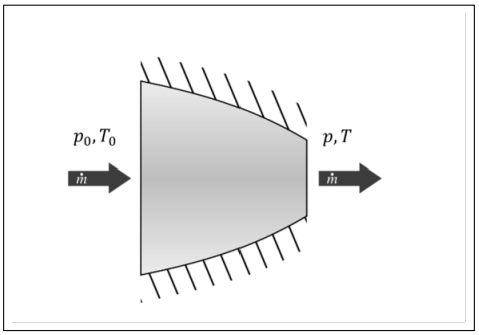

Figure 5.1: Schematic representation of an ideal nozzle

$$\frac{T_0}{T} = 1 + \left(\frac{\gamma - 1}{2}\right) M^2 \tag{18}$$

$$\frac{p_0}{p} = \left(1 + \left(\frac{\gamma - 1}{2}\right) M^2\right)^{\frac{\gamma}{\gamma - 1}} \tag{19}$$

$$\frac{\rho_0}{\rho} = \left(1 + \left(\frac{\gamma - 1}{2}\right) M^2\right)^{\frac{1}{\gamma - 1}} \tag{20}$$

It's important to notice from the above pressure rate equation that when the Mach number reaches the value of one, critical ratios are attained. Steady-state choked flow occurs when the downstream pressure falls below this critical value. From the mass inflow rate expression, the velocity is expressed in terms of the Mach number. Using the ideal gas state equation to express the density in terms of pressure and temperature, the specific mass flow rate is attained in the steady-state condition. [36]. Let's consider that m_v represents the specific mass flow rate, which is the mass flow rate per unit area of an ideal nozzle.

$$m_v = \rho U = \rho \sqrt{\gamma R T} M \tag{21}$$

$$m_v{}^2 = p_0^2 \left(\frac{p}{p_0}\right)^2 \frac{\gamma}{R T_0} \left(\frac{T_0}{T}\right) M^2 \tag{22}$$

The last formula can be used to represent the Mach number and temperature ratio as functions of the pressure ratio and gas adiabatic constant. Furthermore, the outlet pressure corresponds to the hydrostatic pressure determined by the water depth, and the reservoir conditions are comparable to those inside the pipeline. Additionally, for convenience of variable notation, m_v is replaced by m_{nz} which is again the mass flow rate per unit area of the nozzle.

$$\left(\frac{p_0}{p}\right) = \left(\frac{p_1}{p_{hst}}\right) \tag{23}$$

$$m_{nz}^2 = \frac{2\gamma}{\gamma - 1} p_i \rho_i \left[1 - \left(\frac{p_{hst}}{p_i}\right)^{\frac{\gamma - 1}{\gamma}}\right] \left(\frac{p_{hst}}{p_i}\right)^{\frac{2}{\gamma}} \tag{24}$$

Discharge coefficient

A discharge coefficient C_d is included to account for irrecoverable losses such as 0.5, 0.7, and 1 in the calculations. A dimensionless constant known as the discharge coefficient measures how well a nozzle transforms a fluid's pressure energy into kinetic energy. It is defined as the ratio of the fluid's actual mass flow rate through the nozzle to the mass flow rate that, in theory, would be expected for a fluid going through the same nozzle at the same pressure and temperature.

$$C\_d = \frac{m_{\text{actual}}}{m_{\text{theory}}} \tag{25}$$

In other words, it measures the nozzle's ability to transform the fluid's potential energy into kinetic energy. The discharge coefficient can be influenced by the form and size of the nozzle, the flow rate, and the fluid characteristics. Numerous computational and experimental investigations have been conducted to investigate air discharge coefficients via small-diameter orifices [37], [38]. Based on this investigation, the discharge coefficient $C\_d = 1$ was chosen for the pipeline model. Including the discharge coefficient, the mass flow rate between the nozzles is therefore given by:

$$m_{nz}{}^2 = C\_d \left(\frac{2\gamma}{\gamma - 1} p_i \rho_i \left[1 - \left(\frac{p_{hst}}{p_i} \right)^{\frac{\gamma-1}{\gamma}} \right] \left(\frac{p_{hst}}{p_i} \right)^{\frac{2}{\gamma}} \right) \tag{26}$$

Conservation of mass between segments

To incorporate the nozzle in the governing equation, conservation of mass is applied to the control volume of each segment. Equation 26 was utilized to calculate the mass flow rate of m_{nz} algebraically. The conservation of mass in this context shows how the mass flow rates through the nozzles and along the pipeline segments are interconnected.

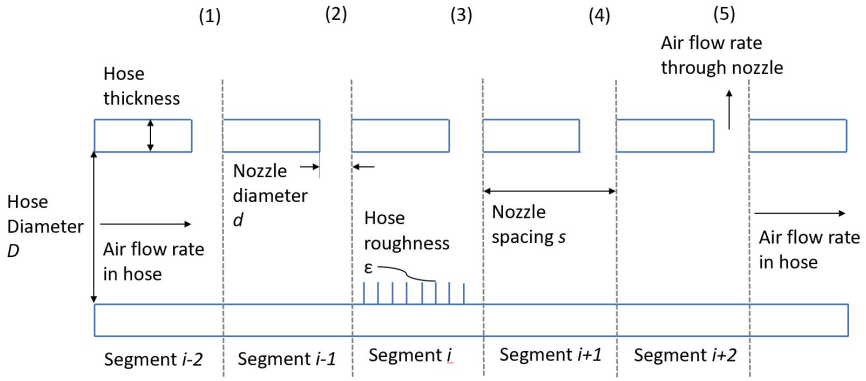

(a) Schematic representation of hose-nozzle system

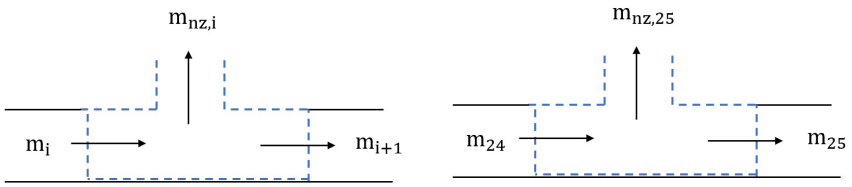

(b) Schematic representation of conservation of mass between segment

Figure 5.2: Schematic representation of the model with air transport inside the hose-nozzle system

According to the figure 5.2b, for any given node i mass balance equation would be:

$$m_i = m_{nz,i} + m_{i+1} \tag{27}$$

Where m_i represents the total mass flow rate into the segment at node i before any of it enters through the nozzle, m_{nz}, i represents the mass flow rate that enters the system through the nozzle at node i, m_{i+1} represents the mass flow rate that continues downstream to the next segment of the pipeline.
The hose model with the five nozzle implementation at the node point is shown in 5.2a, the same model was used for the pipeline. Let's concentrate on the implementation of the first nozzle. The nozzle was placed at node 25, and it is determined using algebraic equations; it does not take into consideration any space at node 25, so the mass flow rate of the nozzle was included as an intermediate calculation at node 25 using conservation of mass between nodes 24 and 25, as shown in the above figure 5.2b.

$$m_{24} = m_{nz} + m_{25}$$

Where m_{24} is the mass flow rate approaching node 25 from the upstream segment, in this case, the segment before node 25, m_{nz} is the mass flow rate through the nozzle, and m_{25} is the mass flow rate leaving node 25 and heading towards the downstream segment, in this case, the segment after node 25. Additionally, the same logic was applied when each node's nozzle count increased from one to three and then five. The next section will show the nozzle implemented in a numerical model with a modification in discretization based on the required model.

Modification in numerical model to implement nozzle

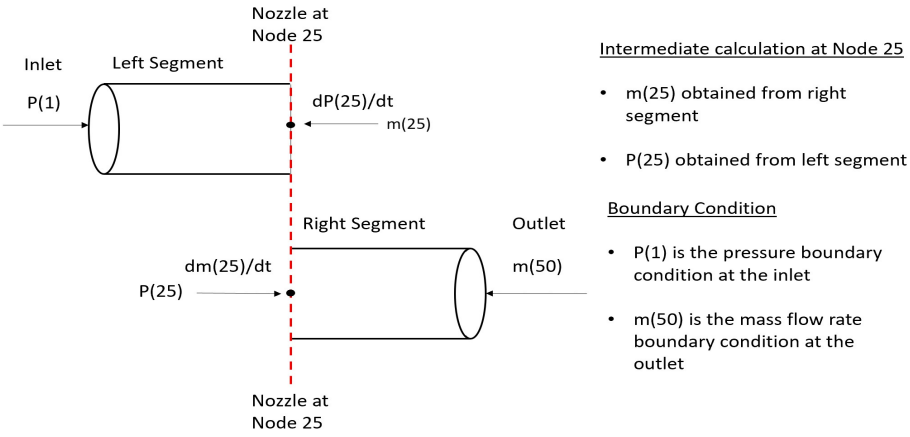

Figure 5.3: Diagram showing a section of the nozzle implementation in numerical model

Figure 5.3 depicts the schematic representation of the numerical model, including the usage of boundary conditions, a discretization method, and the nozzle's mass flow rate. Before getting into more depth, the governing equation 1, 2 has two unknown terms: mass flow rate and pressure. The ODEs reveal two independent variables with respect to t those are $\frac{dm}{dt}$ and $\frac{dP}{dt}$, which must be solved at each grid point.

The model uses two fundamental boundary conditions: *P(1)* at the first nodal point and m_{Nx} at the last grid point, as shown in the above figure. It is separated into 50 nodal points using the finite difference approach. Since in this numerical model, two equations are solved simultaneously, the model makes use of the "P-M model", which means the pressure is used as a boundary condition at one end and mass flow rate is present at the other end. At the first node point left of the model, pressure is present as a known variable based on boundary conditions, but the mass flow rate is an unknown variable at that point and needs to be calculated. The same situation is present at the last node, where the mass flow rate is known from the boundary condition and the pressure is unknown. To deal with this situation, the first grid point requires an equation to compute *dm(1)/dt* using forward discretization, whereas the last grid point requires an equation for *dP(50)/dt* using backward discretization.

Node 25 is modified to include a nozzle: The intermediate calculations are performed at Node 25, where the nozzle is located. The pipeline is divided into two segments: the left and right segments. The *dm(25)/dt* is calculated using forward discretization, which means using the right segment of the pipe. Next, after calculating *dm(25)/dt*, the second calculation remaining is *dP(25)/dt* at Node 25. The mass flow rate of the nozzle is computed using the algebraic equation 26. In the calculation of *dP(25)/dt* for the left segment, m_{25} is used, which contains the mass flow rate of the nozzle and the mass flow rate of the pipe. This strategy is also used when the model is expanded to include three and five nozzles along the pipe length.

Results

- Case I: The size of the nozzle is equivalent to the size of the pipe, which is considered to be an extreme condition[$D_{pipe} = D_{nozzle} = 500\,\text{mm}$].

Flowrate at Node 1

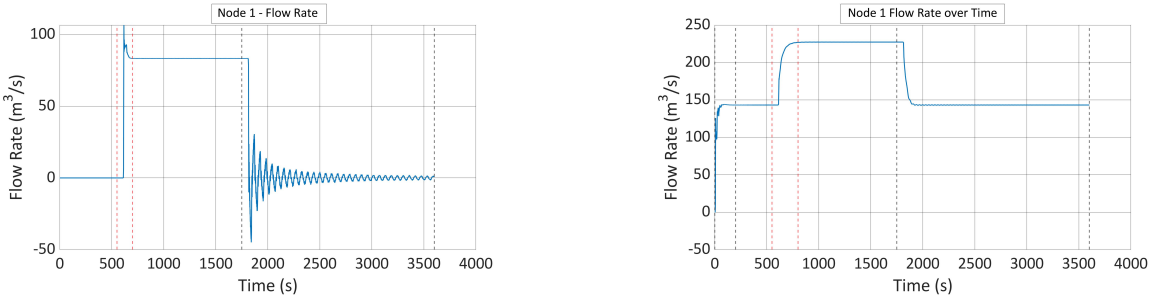

(a) Present study: Flow rate at node 1 without nozzle

(b) Present study: Flow rate at node 1 with single nozzle

Figure 5.4: The flow rate at node 1 without and with a $D_{nz} = 500\,\text{mm}$ nozzle

The graph above shows the flow rate at Node 1 over time after implementing a nozzle with the same diameter as the pipe. This is an extreme scenario where the nozzle diameter D_nozzle is equal to the pipe diameter pipe D_pipe at 500mm. Upon the system's beginning, Node 1 experiences an instantaneous surge in flow rate, consistent with the initial condition changing from a static state. The system's ability to quickly adapt to changes in flow conditions is demonstrated by the quick increase to a greater flow rate, which implies a rapid reaction to the imposed boundary conditions. After the peak, the flow rate quickly returns to a high constant value, indicating that steady-state flow has been established within the specified boundary constraints. Having equal diameters for the pipe and nozzle indicates that the system has adapted to the input conditions. The flow rate decreases noticeably around 1800 seconds, which is in line with the change in the boundary condition when the mass flow rate at the node m_{Nx} is reset to zero. The flow rate at Node 1 drops suddenly as a result of this modification, which signifies the stoppage of flow input into the system. Following this sudden drop, Node 1's flow rate reaches a lower plateau and stabilizes once more, but at a reduced rate. With the flow rate changing to reflect the system's new equilibrium, this new steady-state condition indicates that the system has achieved equilibrium under the revised boundary conditions.

Comparison of updated model with nozzle and present study without nozzle:
The flow rate without a nozzle is shown in Figure 5.4a, and the flow rate with a nozzle present is shown in Figure 5.4b. There is an initial surge in flow rate during the system, starting in both the modified and original models. The abrupt increase is indicative of the system's change from a static state to dynamic circumstances enforced by the boundary. Compared to the original model, the revised model, including the nozzle, seems to achieve a higher flow rate plateau for stability following the surge. This is because a nozzle's existence allows for a higher volume of flow through the system, which has resulted in the insertion of more flow. A damping impact on oscillations is seen in the modified model with the nozzle following the boundary condition modification at 1800 seconds. The nozzle's existence adds more resistance and ability to absorb the pressure wave energy, which gets rid of the oscillations. The original model without the nozzle shows more noticeable oscillations, indicating that the system is more susceptible to fluctuations in reaction to variations in flow conditions in the absence of the nozzle's damping effect.

The modified model with the nozzle has a more controlled reaction at Node 1, with a less pronounced drop in flow rate when the mass flow is terminated at 1800 seconds. This suggests that the nozzle is affecting the dynamics of the system, either by altering the flow direction and characteristics or by producing a stabilizing effect. On the other hand, when the mass flow stops, the original model without the nozzle exhibits a greater drop in flow rate, suggesting a more direct translation of the boundary condition changes across the system. The modified model with the nozzle settles into a lower plateau faster following the flow rate drop caused by the boundary condition adjustment, suggesting a quicker return to a new steady state. Without the nozzle, the original model exhibits continuous oscillations

until achieving a new steady-state flow rate, which represents the system's slow adaptation to the changed circumstances.

Check: The steady-state value reached in the updated model with a nozzle should be a difference between the flow rate of the present study without a nozzle and the excess flow rate of the updated model.
The steady-state value of the original model without the nozzle is 83.33 m^3/s and the steady-state value of the updated model with nozzle is 227.29 m^3/s from figure 5.4

Calculating the excess flow rate

$$\begin{aligned}\text{Excess flow rate} &= \text{Flow rate with nozzle} - \text{Flow rate without nozzle}\\ &= 227.29 - 83.33\\ &= 143.96\,m^3/s\end{aligned}$$

The result of this calculation verifies that the existence of the nozzle increases the steady-state flow rate by 143.96 m^3/s in the modified model.

Pressure at selected Nodes

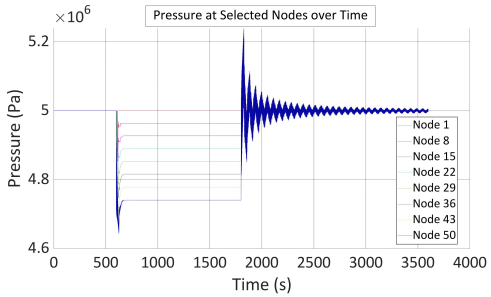

(a) Present study: Pressure without nozzle

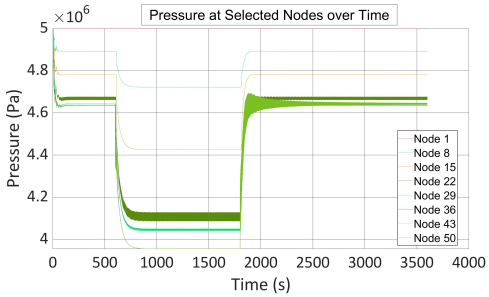

(b) Present study: Pressure with single nozzle

Figure 5.5: Pressure without and with a $D_{nz} = 500\,mm$ nozzle

The figure 5.5b shows the change in the pressure after implementing the nozzle. When the flow begins, there is a pressure reduction at the nodes with lower numbers. The pressure drop is particularly visible at Node 25, most likely due to the fluid's acceleration produced by the nozzle's functioning. Furthermore, after the first transient, the pressure at each node stabilizes at a level lower than the original circumstances. When the boundary condition changes at 1800 seconds, there is another transient pressure fall across all nodes, with Node 25 seeing the largest drop due to the stoppage of mass input. After the second transient, the pressures gradually recover and approach a new steady-state distribution.

Comparison of updated model with nozzle and present study without nozzle:
When the mass flow rate is reduced to zero in the original study without a nozzle, a pressure decrease occurs across all nodes after 1800 seconds, resulting in the typical compressible fluid transient. As observed in the pressure plot, this causes pressure waves and oscillations due to the abrupt stopping of flow. The reaction is different in the modified model with the nozzle at Node 25. When the flow has been stopped, there is still a transitory pressure decrease across all nodes, but the amplitude of the pressure oscillations is considerably reduced, particularly at Node 25. This implies that the nozzle functions as a damping element, absorbing part of the energy from the pressure waves and lowering the total dynamic responsiveness of the system. In the original model, after the second transient, the pressure gradually stabilizes, but with noticeable oscillations, showing that the system is seeking a new equilibrium. The modified model with the nozzle, on the other hand, demonstrates more rapid stabilization and a faster return to a new steady-state pressure distribution once the boundary condition changes. This result shows that the nozzle not only dampens pressure transients but also assists in the system's post-disturbance stability.

The original model illustrates how the compressible fluid transient effect, which takes time to dampen out, causes the system to oscillate significantly in the absence of the nozzle. The nozzle appears to have a stabilizing impact on the system based on the modified model's decreased oscillations and faster stability after flow stops. The nozzle's existence changes the local flow velocity and the fluid flow channel and adds resistance, all of which contribute to the damping effect that is being observed.

Flow rate through nozzle

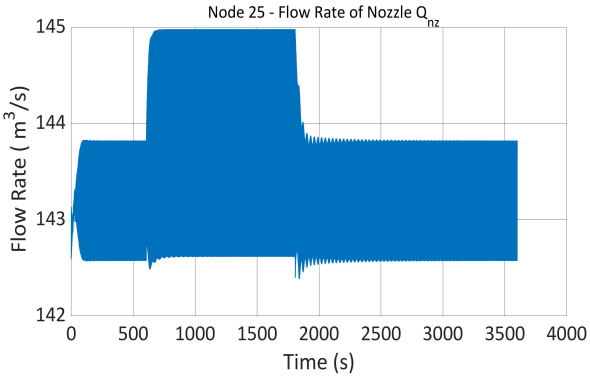

Figure 5.6: Present study: Flow rate of the nozzle

The nozzle's flow rate increases quickly when the system starts and boundary conditions are applied, which is similar to what Node 1 5.4b observed. The nozzle flow rate noticeably, rather than significantly, increases at 600 seconds into the simulation. The system's sensitivity to boundary changes and their direct influence on the flow rate through the nozzle are indicated by the correlation with a change in the boundary condition at m_{Nx}. The algebraic equation used for calculating the nozzle mass flow rate exhibits changes even when the majority of the parameters remain constant. These are attributed to fluctuations in the dynamic pressure at Node 25, or $P(25)$, which is utilized to compute the mass flow rate.

The flow rate through the nozzle stabilizes after the early variations and is mostly steady until the boundary conditions shift at 1800 seconds. Given the system characteristics, it seems that a steady-state flow through the nozzle is obtained based on the stability of the flow rate over this period. After 1800 seconds, when the flow rate drops to zero due to a change in boundary conditions, it has an impact on the entire system, including the nozzle. The flow rate through the nozzle decreases and stabilizes at 143.96 m^3/s, following the trend of the new boundary conditions. This consistency suggests that (perhaps related to the system setup or the existence of additional regulating elements at Node 25), the flow rate through the nozzle is dependent on the terminal boundary conditions.

Numerical instability in graph

The flow rate through the nozzle graph shown above exhibits graph instability. Since the system is supposed to be in a steady state with no flow at the beginning of the flow rate graph, the existence of numerical instabilities does signal a deviation from predicted behavior. Two potential causes were found: the first is the mass flow rate's initial state, which is zero; the second is a change in the discretization scheme at Node 25, which implements the nozzle in the system by using both backward and forward discretization. In this current research, the attempt to address the first issue involved adjusting the initial condition to a non-zero value; however, instability persists. Chapter 6 will provide a detailed analysis of this phenomenon and how it affects the stability of the system.

- Case II: The nozzle's size is changed to D_{nozzle} = 200 mm and D_{nozzle} = 150 mm to observe the change in flow rate and pressure

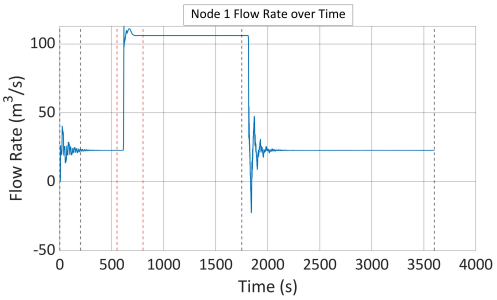

(a) Present study: Flow rate at Node 1 with D_{nz} = 200 mm

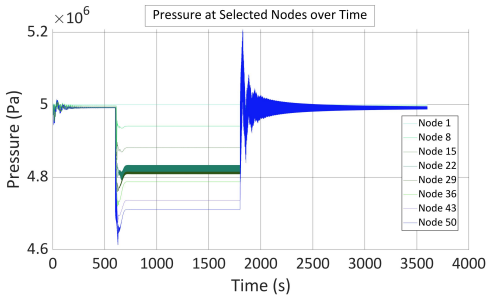

(b) Present study: Pressure at selected Nodes

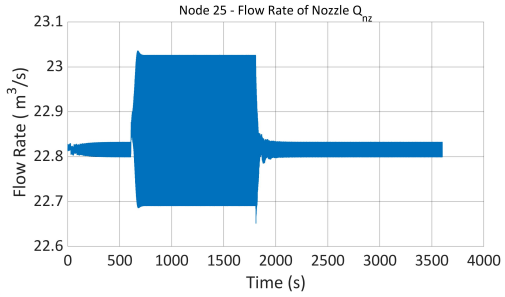

(c) Present study: Flow rate of nozzle at D_{nz} = 200 mm

Figure 5.7: Node 1 flow rate, pressure, and Nozzle flow rate at D_{nz} = 200 mm nozzle

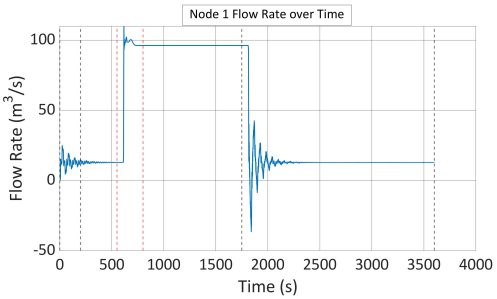

(a) Present study: Flow rate at Node 1 with D_{nz} = 150 mm

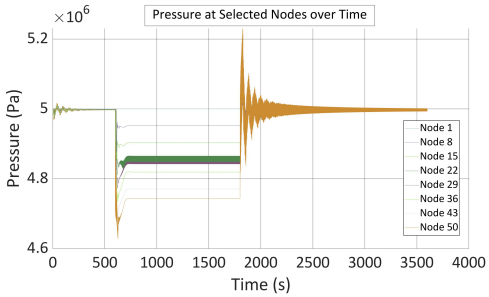

(b) Present study: Pressure at selected Nodes

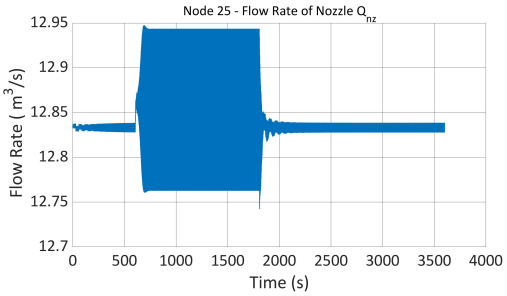

(c) Present study: Flow rate of nozzle at D_{nz} = 150 mm

Figure 5.8: Node 1 flow rate, pressure, and Nozzle flow rate at D_{nz} = 150 mm nozzle

Overall Analysis

There is more flow resistance at Node 1 when the nozzle diameter is lowered, which lowers the flow rate there. When the boundary condition changes at approximately 600 seconds, the magnitude of the flow rate at Node 1 to attain a steady state at a diameter of 200 mm is around 103 m^3/s, and when the further

diameter is lowered to 150 mm, it is around 98 m^3/s. This is because there is a restriction on the amount of fluid that can travel through in a given amount of time due to the nozzle's reduced cross-section. Given that the system can adapt to the decreased flow capacity more rapidly, it would also be predicted that the flow rate at Node 1 would eventually achieve a lower steady-state value. It is evident from the figure that at a diameter of 200 mm, the maximum value during the oscillation is 50 m^3/s. A larger nozzle diameter does have a greater capacity to dampen oscillations because it can allow more fluid to pass through, which can absorb and dissipate the energy from pressure waves. On the other hand, a 150 mm diameter narrower nozzle inhibits flow and may cause an increase in pressure upstream. As a result, when the fluid tries to flow through the confined space, it may produce larger and perhaps more frequent pressure waves, which might result in less efficient damping of oscillations; the highest value during the oscillation is 42 m^3/s.

With a narrower nozzle, the fluid accelerates to pass through the smaller area, resulting in a pressure decrease at startup, which is likely to be more noticeable. Because of the reduced nozzle size, there is a sharper and more noticeable transient pressure response at 1800 seconds when the boundary condition changes. A greater reaction may result from a more rapid upstream pressure spike due to limited flow when the flow rate is changed. As the nozzle diameter is lowered to 200 mm, the flow rate through the nozzle at Node 25 will be considerably less than it was at 500 mm which was observed in this figure 5.6. The decrease is directly proportional to the nozzle's cross-sectional area, which varies with the square of the diameter of a circular nozzle.

5.0.2. Expansion to Three Nozzles

In the original model, the system becomes much more intricate when nozzles with diameters ranging from 290 mm to 500 mm are added at Nodes 15, 25, and 35. There are more sites of pressure drop in the system when there are more nozzles. Fluid mechanics dictate that each nozzle serves as a constriction point, speeding up the flow and lowering the pressure in the process. The interaction between pressure waves originating from individual nozzles might result in increasingly complex wave interactions due to these pressure decreases. This may result in phenomena like wave superposition, where waves vary the system's pressure profile by adding constructively or destructively.

Sharp pressure and flow gradients caused by many nozzles can be difficult for numerical solvers to control. In this instance, the forward and backward discretization at the nozzles impacts the solver's task of handling abrupt changes between distinct flow regimes. Numerical instability may arise from the solver's ability to appropriately represent the steep gradients that characterize these transitions. Central discretization is used between grid points, which might cause fluctuation behavior when interacting with the forward and backward schemes at the nozzles, even if it offers a higher-order approximation. This might increase the solver's difficulties, especially when dealing with unsteady flows.

Results

- Case I: The size of the nozzle is equivalent to $D_{nozzle} = 280\,\text{mm}$ which is considered to be an extreme condition.

Flowrate at Node 1

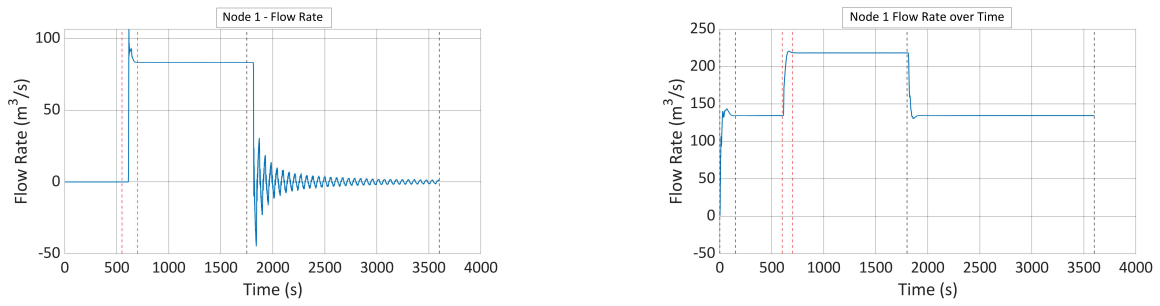

(a) Present study: Flow rate at node 1 without nozzle

(b) Present study: Flow rate at node 1 with three nozzles

Figure 5.9: The flow rate at node 1 without and with a $D_{nz} = 280\,\text{mm}$ nozzle

The system's first increase in flow rate, shown by the two vertical black lines, has resulted from the system changing from a static to a dynamic state. This is a typical phenomenon in fluid systems and can be amplified by problems with numerical instability, which were covered before in relation to discretization techniques. A shift in the boundary conditions corresponds with the sudden decrease in flow rate at 1800 seconds. This may indicate that the three nozzles functioning as sites of resistance have a combined effect that makes the system extremely sensitive to variations in mass flow input. The placing of three nozzles, each of which impacts flow, is predicted to have a cumulative damping effect on flow oscillations. Because each nozzle absorbs some of the flow's energy, pressure pulses can be less intense, and the flow rate can recover more rapidly after disturbances. With three nozzles, the system's dynamic response is probably more complicated since each nozzle contributes a unique property to the total flow behavior. This may result in a more regulated and gradual approach to attaining a new steady state by allowing for a more dispersed and subtle response to changes in flow conditions. In the system, each of the three nozzles acts as a point of energy dissipation. Each time the flow meets a nozzle, the energy from pressure waves and flow oscillations is absorbed, which can help lessen the impact of the transient unsteady effect.

Comparison of updated model with nozzle and present study without nozzle:
The initial flow rate surge at Node 1 occurs around 600 seconds after system startup in both the modified and original model without a nozzle. The system's intended behavior during the changeover from a no-flow to a flow situation is in line with this. The modified model's flow rate stabilizes similarly to the original model, suggesting that even with the nozzles added, the beginning circumstances and system startup procedure are identical. The change in boundary conditions at 1800 seconds causes an abrupt decrease in the flow rate at Node 1 in both models. The oscillations that follow this fall are, however, quickly diminished in the updated model with three nozzles, resulting in a faster stabilization of the flow rate. By absorbing the kinetic energy from the flow, multiple nozzles serve as a sequence of energy dissipation sites, lowering the oscillation amplitude and duration. As a result, the system becomes more stable and can attain a new steady-state condition faster.

The maximum steady-state flow rate at Node 1 without nozzles is estimated to be around 83.33 m^3/s. The modified model has three nozzles, which results in a considerable increase in the maximum steady-state flow rate at Node 1, reaching around 230 m^3/s. It may seem logical that adding nozzles could substantially increase the steady-state flow rate because doing so would usually introduce excess flow that has been introduced as a result of the nozzle's presence.

Pressure at selected Nodes

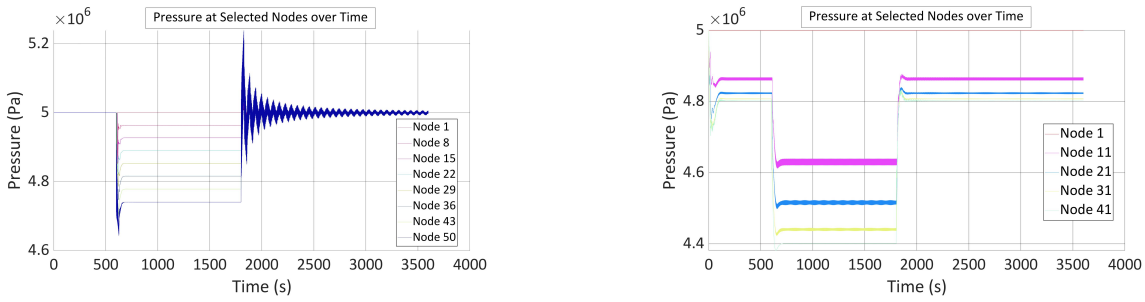

(a) Present study: Pressure without nozzle

(b) Present study: Pressure with three nozzles

Figure 5.10: Pressure without and with a D_{nz} = 280 mm nozzles

Around 600 seconds after the system starts up, there is an initial pressure decrease at every node on the graph, which is mostly caused by damping. When the system first starts up, there is a pressure decrease at every node on the graph. This is a typical feature of fluid systems when the flow begins and the pressure changes to overcome the system's initial resistance and inertia. Around 600 seconds later, a change in the boundary condition causes the mass flow rate to rapidly rise, which lowers the pressure at every node. All nodes experience an instantaneous stabilization of pressure after the initial transient. This quick transition to a steady state indicates that the system is well-behaved and finds equilibrium quickly, even with the additional complexity of several nozzles.

The lack of pressure oscillations after 1800 seconds indicates that the system's pressure waves have been dampened. There are several reasons for this:

- Modifications to Local Flow Velocity: The existence of nozzles modifies the local flow velocity, which may affect the properties of the pressure wave.
- Fluid Flow Channel Resistance: The nozzles increase the system's resistance, which causes more energy to be lost during flow and aids in damping.
- Nozzle-induced Damping: By releasing energy from pressure waves and aiding in system stabilization following disruptions, each nozzle has the potential to function as a damping device.

Comparison of updated model with nozzle and present study without nozzle:
As the system moves from static to dynamic circumstances, the pressure at all selected nodes exhibits an initial drop, suggesting that the flow is starting to establish itself. After the first decrease, the pressures settle reasonably rapidly, suggesting that the system is successfully attaining a steady state despite the initial transient. A significant transient reaction is noticed at 1800 seconds, which is demonstrated by a sharp decrease in pressure in every node. This is the point at which the mass flow input stops, causing the boundary conditions to alter. Nozzles provide extra pressure drops at each nozzle site, which can cause the system to react complexly as it adapts to the altered flow circumstances.

The pressures at the nodes exhibit a recovery towards a new steady state that is slightly lower than the initial steady-state levels following the transient reaction. This indicates that the system is adjusting to its new boundary condition. Following the fluctuating incident at 1800 seconds, there seem to be suppressed pressure fluctuations. This is probably because the nozzles increase resistance to the flow, which helps to disperse flow energy and diminish the amplitude of pressure oscillations. The system's noticeable dampening effect is partly due to the nozzles. They contribute to the smoothing out of pressure variations and faster system stabilization following disturbances by increasing resistance and varying the local flow velocities.

Flow rate through nozzles

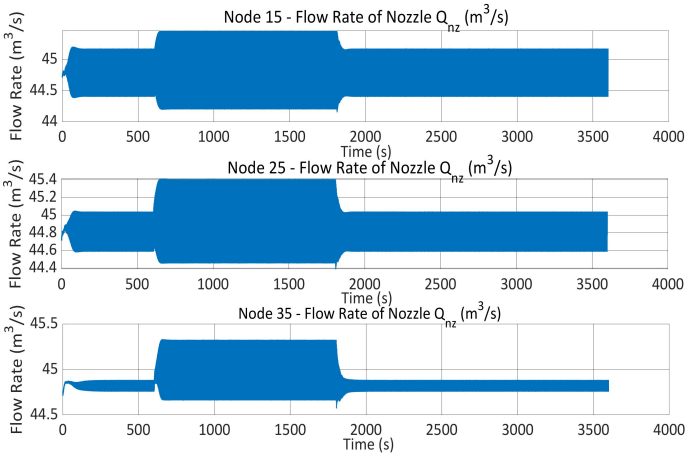

Figure 5.11: Present study: Flow rate of the three nozzles

Three nozzle's flow rate graphs at Nodes 15, 25, and 35 show an early rise in flow rate when the system first starts. This illustrates the nozzle's fast response to pressure conditions at their respective nodes and is consistent with changes in boundary conditions. The flow rates via the nozzles level out after the first surge. This implies that the nozzle sites' pressures stabilize, enabling a steady mass flow rate via every nozzle. Hence, the system moves into a quasi-steady state in which the flow is predictable and stable. The notable variation in flow rate seen at about 1800 seconds is consistent with a change in boundary conditions, most likely resulting from the cessation of mass flow input near the domain's end.

The system's quick reaction to this change is shown by the abrupt drop in flow rate through the nozzles. The flow rates through the nozzles exhibit a recovery following the transitory reaction to the boundary

condition change, and then they settle into a new, lower steady state. This shows that the nozzles are now functioning under a different set of pressures and flows, indicating that the system has adjusted to the new flow circumstances. The numerical instability in graphs has risen, which indicates the bulge in graphs, owing mostly to the discretization scheme, which will be discussed in further depth in Chapter 6.

- Case II: The nozzle's size is changed to $D_{nozzle} = 200\,\text{mm}$ and $D_{nozzle} = 150\,\text{mm}$ to observe the change in flow rate and pressure

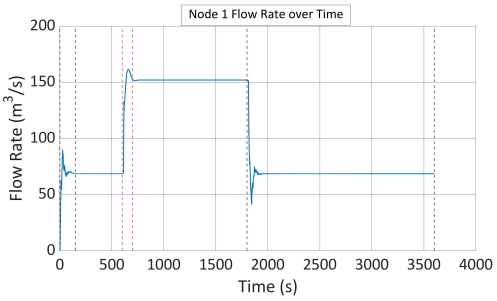

(a) Present study: Flow rate at Node 1 with $D_{nz} = 200\,\text{mm}$

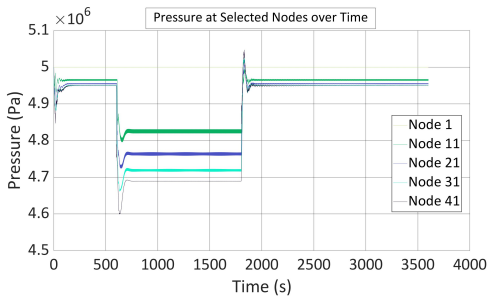

(b) Present study: Pressure at selected Nodes

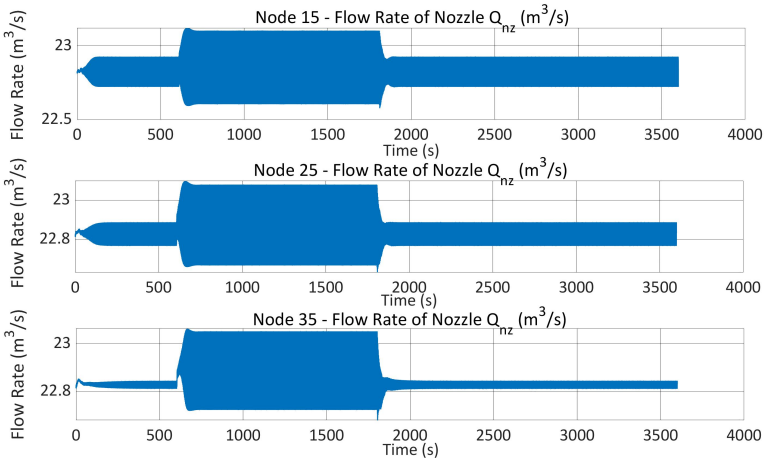

(c) Present study: Flow rate of nozzle at $D_{nz} = 200\,\text{mm}$

Figure 5.12: Node 1 flow rate, pressure, and Nozzle flow rate at $D_{nz} = 200\,\text{mm}$ for three nozzles

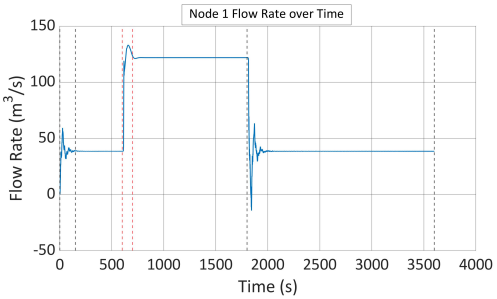

(a) Present study: Flow rate at Node 1 with $D_{nz} = 150\,\text{mm}$

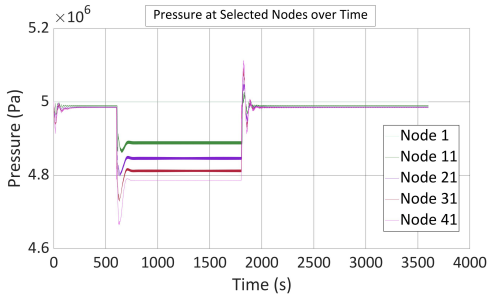

(b) Present study: Pressure at selected Nodes

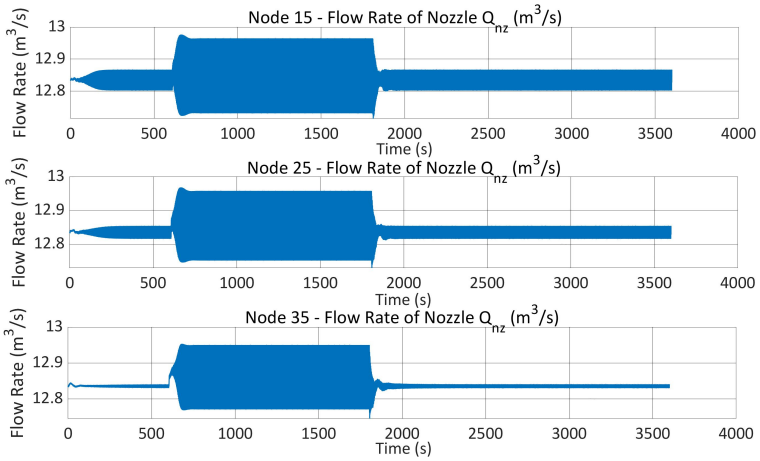

(c) Present study: Flow rate of nozzle at $D_{nz} = 150\,\text{mm}$

Figure 5.13: Node 1 flow rate, pressure, and Nozzle flow rate at $D_{nz} = 150\,\text{mm}$ for three nozzles

Overall Analysis

The presence of three nozzles of varying sizes has a significant impact on both the flow rate through each nozzle and the overall pressure dynamics of the system. When the nozzle diameter is reduced, there is higher flow resistance at Node 1, which reduces the flow rate there. When the boundary condition changes at roughly 600 seconds, the magnitude of the flow rate at Node 1 to achieve a steady state at a diameter of 200 mm is around 160 m^3/s, and it is around 130 m^3/s when the diameter is reduced to 150 mm. This is due to the nozzle's smaller cross-section, which limits the volume of fluid that can pass through in a given length of time. Since the system can adjust to decreasing flow capacity more quickly, the flow rate at Node 1 is expected to eventually reach a lower steady-state value. The figure shows that the greatest value during the oscillation is 80 m^3/s for a diameter of 200 mm and roughly 62 m^3/s for a diameter of 150 mm. A wider nozzle diameter helps dampen oscillations more efficiently because it allows more fluid to flow through, which can absorb and disperse the energy from pressure waves.

The greatest pressure decrease of around 600 seconds for nozzles with diameters of 200 mm is approximately 4.6 Pa, and for diameters of 150 mm, it is around 4.65 Pa, indicating that a change in diameter has no major influence on total system pressure. Additionally, the flow rate through the nozzles at Nodes 15, 25, and 35 decreases due to the reduced area in comparison to the flow rates observed when the diameter was 280 mm.

5.0.3. Final Model with Five Nozzles

After analyzing the addition of three nozzles to the updated model and assessing the system's flow rate and pressure, the model is further updated to include five nozzles. The nozzles are added at nodes 5, 15, 25, 35, and 45 in this final pneumatic model. This model's addition of five nozzles leads to a major increase in the complexity of the system. The addition of more nozzles increases the contact

between the flow and the system's boundaries, leading to a more intricate flow pattern. Each nozzle serves as a point of interaction for the flow. The challenges of dealing with the numerical solution arise as the number of nozzles in the system rises. There are more pressure drop locations when there are more nozzles. This may cause the flow dynamics downstream of each nozzle to change significantly. Modifying the nozzle's diameter can significantly affect the system. Reduced diameters will make the flow more difficult to move through, which might result in greater upstream pressures and reduced flow rates through each nozzle. On the other hand, greater diameters will enable higher flow rates but could make the system less effective at attenuating oscillations. Additionally, it is important to monitor the effects of nozzle diameter variations on steady-state flow rates and pressure distribution, as well as the system's response to transient events such as boundary condition changes.

Results

- Case I: The size of the nozzle is equivalent to $D_{nozzle} = 210\,\text{mm}$ which is considered to be an extreme condition.

Flowrate at Node 1

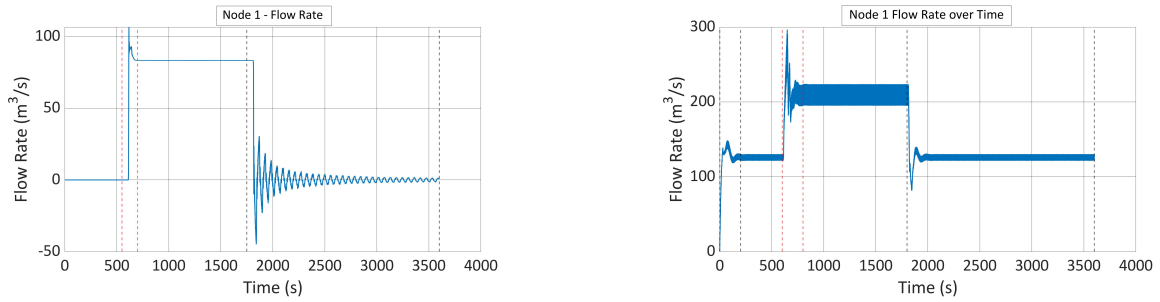

(a) Present study: Flow rate at node 1 without nozzle

(b) Present study: Flow rate at node 1 with five nozzles

Figure 5.14: The flow rate at node 1 without and with a $D_{nz} = 210\,\text{mm}$ at five nozzles

When the system first starts up, there is a substantial initial rise in flow rate. This implies a quick reaction to the system being pressurized and the flow channel via the nozzles being opened. Following the first spike, the flow rate levels off to a plateau. This suggests that the system approaches a quasi-steady state in which the input conditions of the system and the flow through the nozzles are balanced. The abrupt drop in flow rate at about 1800 seconds is suggestive of a shift in the boundary conditions, meaning that the mass flow input at the end of the system is being terminated. As a result, the flow rate of the system adapts to the changing boundary circumstances. The flow rate at Node 1 decreases once the boundary condition changes and then rises to a lower steady-state value. The system appears to have adjusted to the new operating circumstances and found a new balance between the input and the flow through the nozzles based on this recovery to a new plateau. The system is likely to have a damping effect when it has more nozzles than when it has fewer or none at all. This dampens oscillations caused by pressure waves and transient reactions, which can be seen in figure 5.14b after 1800 seconds.

Comparison of updated model with nozzle and present study without nozzle:
The flow channel is impacted by the addition of nozzles, which has an impact on the system's pressure and flow rate. Due to the surplus flow introduced by each nozzle, the model with five nozzles has a maximum peak flow rate of about 290 m^3/s at 600 seconds, whereas the model without nozzles has a maximum peak flow rate of around 103 m^3/s. Additionally, the model with a nozzle has a maximum steady state condition of around 230 m^3/ss, whereas the model without a nozzle has a maximum steady state condition of about 83.33 m^3/s.

A slight transitory behavior is shown that suggests the impact of the rapid shift in boundary condition, and after 1800 seconds, the model with the nozzle drops down to adopt the new boundary condition, ending the flow rate. Nozzles act as damping mechanisms to absorb pressure waves resulting from abrupt changes, leading to reduced oscillation in the flow rate when compared to the model without nozzles.

Pressure at selected Nodes

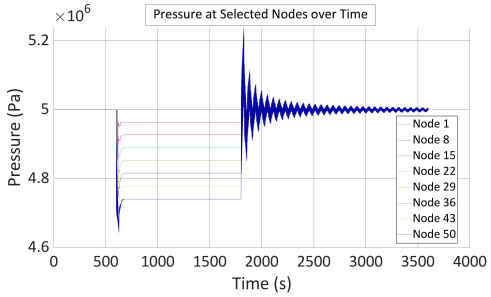

(a) Present study: Pressure without nozzle

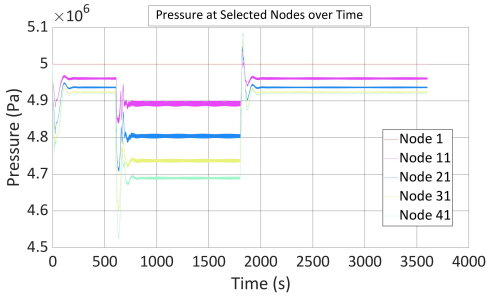

(b) Present study: Pressure with three nozzles

Figure 5.15: Pressure without and with a D_{nz} = 210 mm five nozzles

A pressure-time graph for a system with five 210 mm diameter nozzles at certain nodes is shown in the above figure. As the system starts, there is an initial pressure decrease at every node, which is a normal reaction to the start of the flow. Pressure at all nodes seems to stabilize immediately as a result of the system's apparent swift response to the start-up conditions. Each node's pressure seems to settle after the first transient, suggesting that the system has reached a steady state. The flat lines imply that the pressure drop across the nozzles has reached equilibrium and that the flow through them is now consistent. All nodes see a noticeable pressure drop at 1800 seconds, which is the system's reaction to a change in boundary conditions, most likely a stop in mass flow input. As a result, there is a transient condition while the pressure changes to fit the new flow pattern. Every node's pressure rises after the drop and seems to be getting closer to a new steady state, although at a slightly lower pressure level. This may indicate that the system is adjusting to the lower flow circumstances. Five nozzles offer several locations for pressure dissipation, which aids in reducing pressure oscillations and surges in the system. It appears that the nozzles are having an expected effect on the system based on the uniform behavior observed at all nodes.

After 1800 seconds, the graph shows no noticeable oscillations, which means that the nozzles are functioning as damping. At the beginning of the system, approximately 100 seconds after boundary condition adjustments, it seems that the system with five nozzles can quickly reach a steady state based on its pressure response.

Comparison of updated model with nozzle and present study without nozzle:
Since the system is starting up from a static state, there is an initial pressure drop that lasts for around 50 seconds at all nodes. The fluid accelerates to fill the pipe system and overcome initial inertia, causing an instantaneous reduction in pressure when the flow starts. When fluid systems go from rest to dynamic flow conditions, this is a typical occurrence. Additionally, at 600 seconds, the operating conditions change due to a boundary condition that increases the flow rate. This results in a pressure drop in both the nozzle-equipped and without-nozzle models, but the nozzle-equipped model experiences a greater drop in pressure as the flow accelerates through the nozzle's restricted diameter. Pressure upstream builds up at 1800 seconds as the flow rate drops and then stabilizes at a new steady-state situation. A temporary rise in pressure is seen in the graph as a result of the mass flow input being interrupted, the fluid slowing down, and the energy being transformed back into pressure energy.

The model without a nozzle has a maximum oscillation magnitude of around 5.25 Pa and gradually decreases after a while, whereas the model with a nozzle has a maximum oscillation magnitude of about 5.1 Pa and decreases after the initial spike. Because nozzles can dampen system oscillations, they can potentially reduce the magnitude of any oscillatory behaviors produced by transients.

Flow rate through nozzles

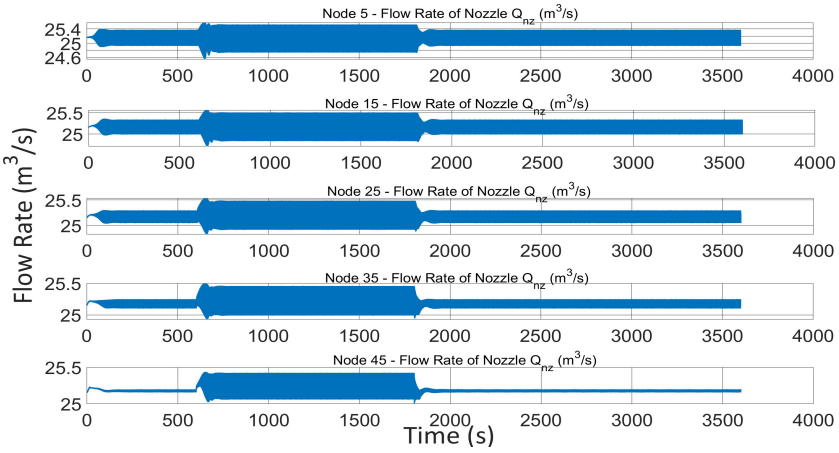

Figure 5.16: Present study: Flow rate of the five nozzles

There is a sudden increase in the flow rate through each nozzle during system startup, and this increase is constant for all five 210 mm diameter nozzles located at nodes 5, 15, 25, 35, and 45 on the flow rate graph. This is anticipated as the fluid accelerates through the nozzles when the system moves from a static state to a dynamic ones. Following the first surge, the flow rate through each nozzle stabilizes, signifying that the system has reached a quasi-steady state. This is characterized by balanced conditions at each nozzle position and uniform fluid flow across all restrictions. There is a noticeable decrease in the flow rate via each nozzle after about 2000 seconds. This means that the boundary conditions have changed, likely due to a drop in flow input, which has reduced the amount of fluid flowing through each nozzle. The flow rate through each nozzle seems to return quickly when the boundary condition changes, then settle at a new, lower plateau. This implies that the flow has attained a new steady state that is representative of the new boundary conditions and that the system has adjusted to them.

The uniform pattern observed in all five nozzles indicates that the nozzles are responding uniformly to changes in the system and that their flow characteristics are consistent. This is because the nozzles respond uniformly within the system since they have the same diameter and, most likely, the same flow characteristics.

- Case II: The nozzle's size is changed to $D_{nozzle} = 200\,\text{mm}$ to observe the change in flow rate and pressure

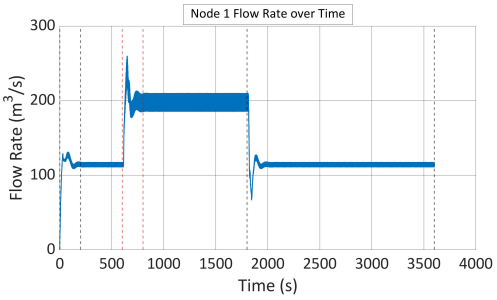

(a) Present study: Flow rate at Node 1 with $D_{nz} = 200\,\text{mm}$

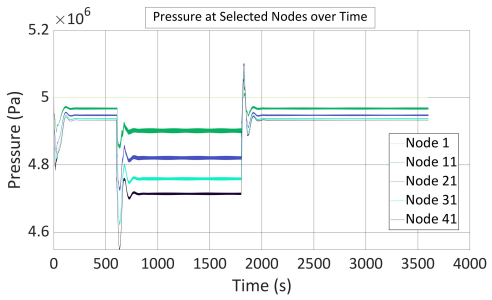

(b) Present study: Pressure at selected Nodes

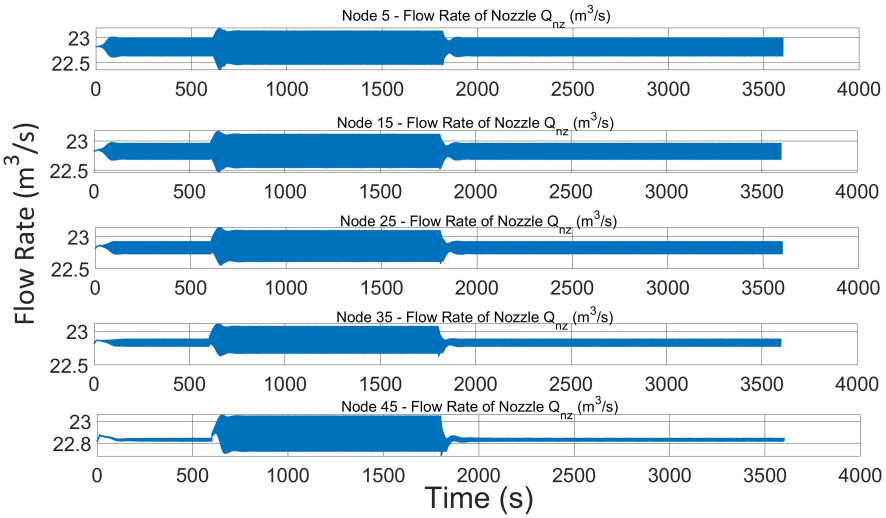

(c) Present study: Flow rate of nozzle at $D_{nz} = 200\,\text{mm}$

Figure 5.17: Node 1 flow rate, pressure, and Nozzle flow rate at $D_{nz} = 200\,\text{mm}$ for five nozzles

- Case III: The nozzle's size is changed to $D_{nozzle} = 150\,\text{mm}$ to observe the change in flow rate and pressure

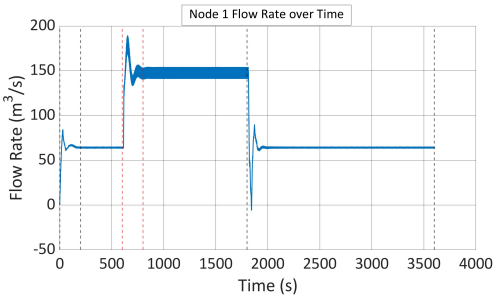

(a) Present study: Flow rate at Node 1 with $D_{nz} = 150\,\text{mm}$

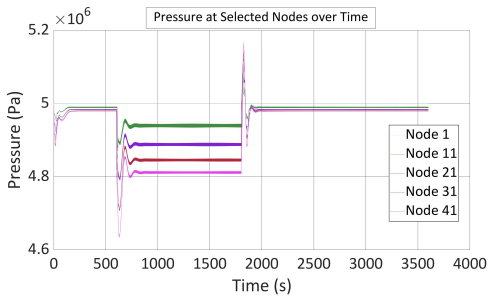

(b) Present study: Pressure at selected Nodes

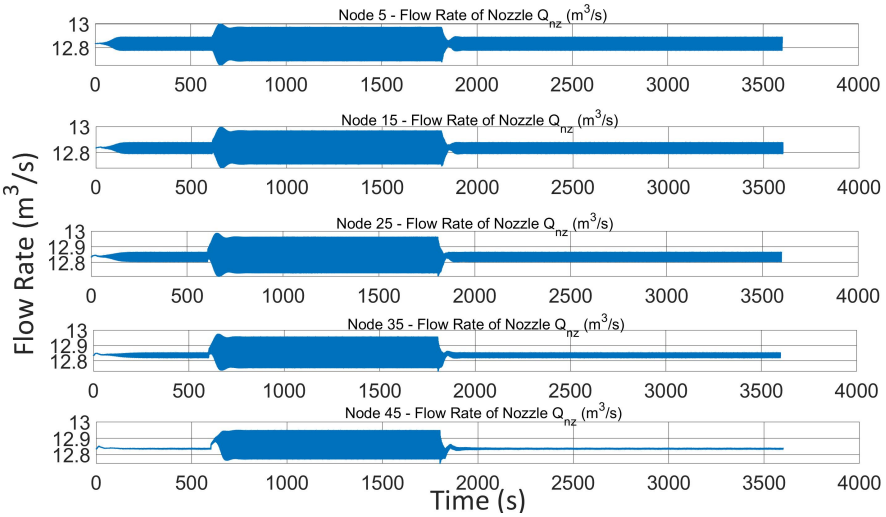

(c) Present study: Flow rate of nozzle at $D_{nz} = 150\,\text{mm}$

Figure 5.18: Node 1 flow rate, pressure, and Nozzle flow rate at $D_{nz} = 150\,\text{mm}$ for five nozzles

Overall Analysis

Each nozzle's flow rate and the system's total pressure dynamics are greatly affected by the presence of five nozzles of different diameters. Node 1 experiences a decrease in flow rate when the nozzle diameter is lowered because of increased flow resistance. The maximum peak flow rate was observed at 290 m^3/s for a diameter of 210 mm and 260 m^3/s for a 200 mm diameter. A further increase in flow rate to 190 m^3/s was observed for 150 mm diameter, reflecting the phenomenon of excess flow entering due to the presence of nozzles with varying sizes, which causes the flow rate at Node 1 to increase. This occurs approximately 600 seconds after the boundary condition changes. The quick stabilization of pressure and flow rates after early transients and boundary condition adjustments suggests that whereas nozzles increase complexity and create the potential for oscillations, they also have damping effects that support the equilibrium of the system. In addition to making the system more dynamically complicated, having more nozzles adds additional damping sites, which can aid in restoring flow stability following disruptions. The instability at increasing nozzle diameters is probably due to the greater difficulty in quantitatively capturing intricate wave dynamics. The combined damping effect of the five nozzles results in a rapid reduction of oscillations in both flow rate and pressure after 1800 seconds. Furthermore, an increase in diameter corresponds to a higher flow rate through the nozzle.

5.0.4. Comparative Analysis of Different Nozzle Configurations

Upon system startup, the single-nozzle model had an early spike, but it later settled to a high constant value, indicating steady-state flow. Around 1800 seconds, a boundary condition change resulted in a notable drop in flow rate. The second model with three nozzles had a greater stabilization flow rate after a similar initial surge as the single-nozzle variant. The model with three nozzles showed a less dramatic recovery after the boundary shift, which caused a steeper fall in the flow rate. Similarly, an initial rise in flow rate was seen upon the subsequent implementation of five nozzles. But before the boundary condition changed, it appeared that having more nozzles increased the maximum steady-state flow rate. Additionally, the system showed faster post-disturbance stability. Different nozzle sizes have an impact on all models, ranging from single-nozzle to five-nozzle models. As the nozzle diameter decreased, the flow rate at Node 1 for the steady-state condition decreased due to increased flow resistance. However, the peak flow rate was higher at 600 seconds, where the mass flow rate increased owing to a changed boundary condition since there was less resistance at larger diameters. Larger nozzle diameters produced higher pressures because there was less initial resistance. Smaller diameters increased resistance, which led to a bigger initial pressure drop. Larger diameter nozzles produced higher flow rates, whereas smaller diameter nozzles produced lower flow rates.

The updated model with a single nozzle demonstrated a comparable initial pressure drop, stability, and a significant decline at 1800 seconds, coinciding with the boundary condition shift. Furthermore, using three nozzles at nodes 15, 25, and 35 resulted in more noticeable pressure reductions at each nozzle, resulting in more complicated transient behaviors. Likewise, when the five nozzles were positioned at nodes 5, 15, 25, 35, and 45, more damping sites were generated, resulting in faster pressure stabilization following initial transients and disturbances. The behavior of the system as a whole was reflected in the flow rate through a single nozzle, initially rising before stabilizing. Each of the three nozzles demonstrated similar flow dynamics, with the system reaching a quasi-steady state following the first surge and exhibiting a discernible decline following the modification of the boundary condition. Additionally, the flow rates of the five-nozzle model showed fast stability following initial disruptions, demonstrating the cumulative damping effect of numerous nozzles.

The nozzle diameter had a significant impact on both the flow rate and pressure dynamics in all of the simulations. Because they could attenuate oscillations more effectively and had less resistance, larger diameters allowed for higher flow rates and pressures. Furthermore, when the number of nozzles increased, the system's complexity increased as well, which raised the numerical instability because of the more difficult wave dynamics and interactions. The overall behavior of the system indicates that although having many nozzles can complicate flow dynamics, they can also offer a variety of damping mechanisms to aid in the system's ability to recover to equilibrium following a disruption.

6
Analysis of Numerical Instability

6.0.1. Identification of Instability Issues

The instabilities observed in the previous chapter with the introduction of the first nozzle to the present pipeline system model are highlighted in subsection 5.0.1. In this research, the two primary causes of numerical instability were identified: the convective inertia components in the momentum equation and various discretization strategies. However, further verification is needed to confirm these findings.

- Discretization schemes
- Convective inertia

In particular, at Node 25, where a nozzle has been established, the model addresses the flow dynamics across the nodes by utilizing different discretization techniques. At this node, the intermediate calculations are performed to implement the nozzle in the pneumatic model by using both forward and backward discretization strategies as discussed in Chapter 5. However, numerical difficulties arise with such a method due to the abrupt transition between discretization approaches, which the numerical solver is unable to handle. These instabilities show up as irregularities or fluctuations in the solution; the pressure and flow rate graphs show this very well in figure 5.6. Additionally, when more nozzles are added, the instability increases, as shown in these two figures straight away: 5.11 and 5.16.

The momentum equation convective inertia term adds another level of complexity on top of the discretization approach. This intrinsically nonlinear term expresses how fluctuations in flow conditions and velocity affect the fluid's momentum. Steep gradients in the solution may result from convective inertia in areas of the pipeline where the flow is changed, such as at nozzles. The stability of the simulation can be negatively impacted by numerical fluctuations, which can be caused by the solver's inability to appropriately capture these gradients. As seen by the situations with three and five nozzles, the difficulties get even more challenging as more nozzles are added. The model's nonlinearity and potential for steep gradients are increased by the inclusion of each nozzle, which acts as a new point of flow change. With each additional nozzle, the ODE15s solver used in this research was unable to generate a stable solution due to the more complex interplay between flow dynamics and abrupt changes in boundary conditions.

Additionally, a more thorough discussion of these two numerical instabilities is provided in the next section. Furthermore, a deeper comprehension of these instability problems is essential to the creation of computational models that are more durable and trustworthy. It requires a close inspection of the discretization techniques used and the way nonlinear variables are handled in the fluid flow equations. The model may be improved to guarantee that it not only accurately represents the fundamental physics of the system but also yields reliable, convergent solutions for engineering analysis and design. This can be done by locating and resolving the causes of instability.

6.0.2. Impact of Convective Inertia Term

The significance of the convective inertia tern in the existing research Kiuchi model, which was used to verify the current model, has previously been discussed in Section 3.0.4. This section goes deeper into the ramifications of the convective inertia factor, which has resulted in numerical instability in the form of bulge graphs in the modified model with nozzles for this research. A crucial part of the momentum equation is the convective inertia term, which represents the change in momentum caused by the fluid velocity, which is represented by the mass flow rate m, as well as any modifications to the cross-sectional area or flow conditions. The convective-inertia term is the second term in the momentum equation 2.

The second term in the momentum equation, representing convective inertia, is particularly important in the context of the modified numerical model with nozzles implemented at different nodes. Because it relies on the square of the mass flow rate, this term is nonlinear and sensitive to variations in velocity across the nozzle, which causes sudden changes in area. These sudden shifts can result in steep or high gradients in the flow variables, which are difficult for numerical solvers to precisely control. Numerical stability was shown to be significantly affected by the convective inertia term in studies that evaluated models with one, three, and five nozzles. When discretization strategies are used at the nodes with nozzles, the complexity added by this term is further increased. Because each approach calculates derivatives differently, switching between forward, backward, and center discretization provided additional numerical problems.

The flow rate graphs in figures 5.11 and 5.16 show a notable bulge, which is a representation of the effects of inertia. The inertia term can result in transient surpasses or drops in the solution when the fluid suddenly accelerates or decelerates, especially after going through a nozzle. This is because the term describes the fluid's resistance to motion changes, which can result in fluctuations or spikes in a discretized numerical model. The existence of several nozzles contributes to these difficulties because flow disturbances induced by one nozzle can interact with disturbances caused by other nozzles, resulting in a compounding influence on overall system dynamics. When studying and enhancing the stability of numerical models with complicated geometries and boundary conditions, such as those with many nozzles, the interplay between convective inertia and the discretization scheme proves especially important.

6.0.3. Discretization Method Analysis

This section discusses the intricate effects related to using various discretization methods in numerical models, particularly ones with features such as nozzles. The process of converting differential equations into discrete ODEs that may be solved numerically in MATLAB is known as discretization. Furthermore, a full description of discretization is discussed in the section 3.0.3. At the nodes where nozzles are present in the current context, forward and backward discretization techniques are used. Usually, these approaches are used for directional flow characteristics, such as flow via a nozzle or boundary conditions. While backward discretization makes use of the data from the current and previous nodes, forward discretization employs information from the present and following nodes to estimate derivatives at a location. Moreover, center discretization provides a more balanced approach by taking into account the effect of nearby points on all sides of the node, whereas forward and backward discretization is inherently one sided.

The complexity of the flow dynamics grows with each new nozzle added to the system. The model exhibits fluctuations or instabilities due to discontinuities in the numerical solution caused by the localized application of forward and backward discretization at these nozzle nodes. This is so because, in contrast to central discretization, these schemes do not use a balanced pattern. Additionally, while central discretization, which is employed at nodes without nozzles, is often more accurate and stable for smooth solutions, it loses dependability in the context of abrupt changes in gradient or discontinuity, like those brought about by nozzle presence.The research reveals that the convective inertia term in the momentum equation makes a substantial contribution to numerical instability. The non-linear character of this component, particularly near nozzles, along with the use of multiple discretization methods, might worsen the instability of this research. The solution to the instability caused by convective inertia is explained in the next section of this research.

6.0.4. Simulation Adjustments and Rationale

This section discusses the methods used to deal with the numerical instability issues that occur, especially those related to the convective inertia term present in the momentum equation. To create a more stable and reliable simulation, the part outlines a methodical strategy for addressing the numerical issues that have been found.

The main modification entails a close examination of the convective inertia term. The model facilitates an understanding of the behavior and impact of this term on the momentum balance by isolating it. As previously mentioned, the convective inertia term, which is linked to changes in momentum as a result of fluctuations in area and velocity, can be extremely nonlinear and cause steep gradients that result in numerical instability. A detailed analysis is conducted of the convective inertia term's magnitude with the pressure gradient component. Both terms share units of ($kg/s \cdot m^2$) which offers a similar base for direct comparison in this research. Numerical attention is focused on determining whether or not the convective inertia term significantly affects the total momentum change. If the amplitude of the convective inertia component is found to be significantly lower than that of the pressure gradient term, the model can be adjusted to diminish the impact of the convective term. In cases where the contribution of convective inertia is negligible, the momentum equation may be simplified by excluding it. This might remove the nonlinearity and steep gradients generated by this component, potentially reducing the instability.

Results

Convective inertia Vs Pressure

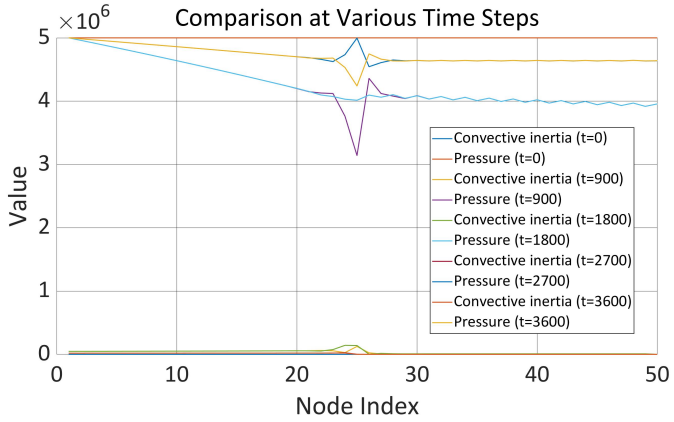

(a) Convective inertia Vs Pressure with a single nozzle model

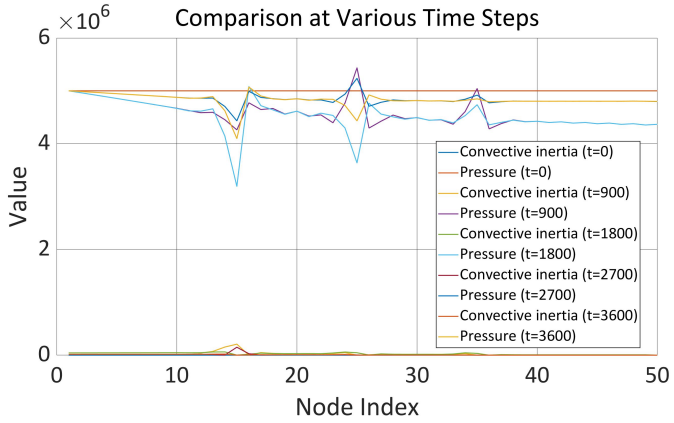

(b) Convective inertia Vs Pressure with a three nozzle model

Figure 6.1: Convective inertia Vs Pressure with a single and three nozzle model

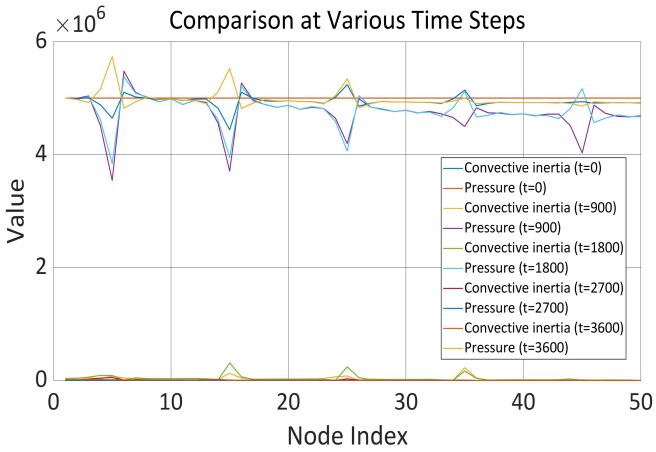

Figure 6.2: Convective inertia Vs Pressure with five nozzle model

The findings, as seen in the supplementary graph figures 6.1 and 6.2, demonstrate that the convective inertia term remains almost constant over the range of nodes and time intervals examined. This is a constant finding, independent of the amount of simulation time that has passed; the inertia term was found to be significantly smaller than the pressure at every node. Thus, it can be deduced from such a big difference that the convective inertia term plays a minor role in the system's momentum shifts in this research. Further, it may be deduced that such a big difference in inertia and pressure suggests that the inertia term can be safely ignored in the momentum equation, given its low value. When the convective inertia factor is removed from the calculations, the pressure profile no longer exhibits any abnormalities, indicating that this simplification significantly increases numerical stability for this research. Its elimination is further supported by the consistency of the results with and without the convective acceleration term. This suggests that in the dynamics of the specific system, the term is not highly significant. By removing this element, the numerical distortions, such as bulges in the graphs, introduced by the convective term causing nonlinearity and stiffness are also eliminated.

7 Comparative Analysis and Stability Improvement

7.0.1. Simulation without Convective Inertia Term

To increase the numerical stability, as covered in Section 6.0.4, the simulation are performed in this part by eliminating the convective inertia term. The current model's first simulation is conducted without a nozzle to see how the pressure and flow rate differ.

Flowrate at Node 1

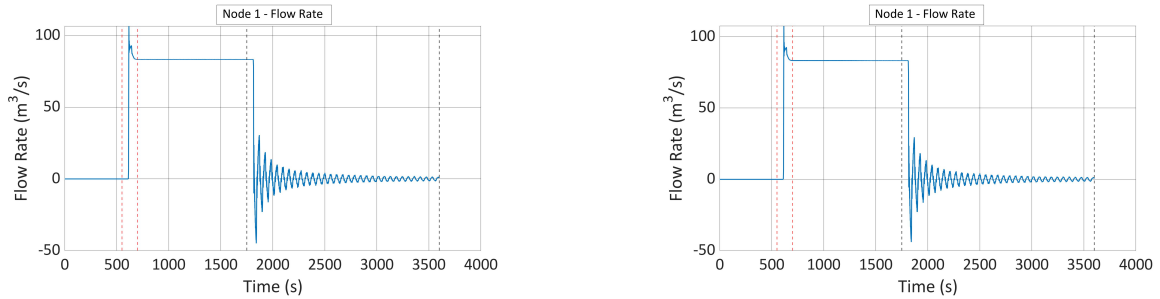

(a) Present study: Flow rate at node 1 with convective inertia

(b) Present study: Flow rate at node 1 without convective inertia

Figure 7.1: The flow rate at node 1 with and without convective inertia

Pressure at selected Nodes

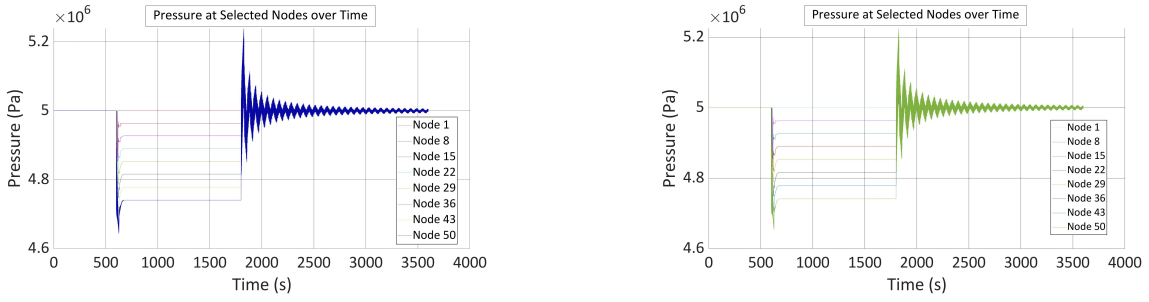

(a) Present study: Pressure with convective inertia

(b) Present study: Pressure without convective inertia

Figure 7.2: Pressure at selected nodes with and without convective inertia

The model's comparison of the flow rates at Node 1 and pressure with and without the convective inertia term points to an important finding. Results suggest that the flow rate results at Node 1 and pressure for the original model without any nozzles are not considerably affected by the removal of the convective inertia component. In the context of a particular model configuration, this suggests that the convective inertia factor might not have a major effect on the flow dynamics.

7.0.2. Stability Assessment for 1, 3, and 5 Nozzle Models

Single Nozzle

- The size of the nozzle is equivalent to the size of the pipe, which is considered to be an extreme condition. [$D_{pipe} = D_{nozzle} = 500\,\text{mm}$]

Flowrate at Node 1

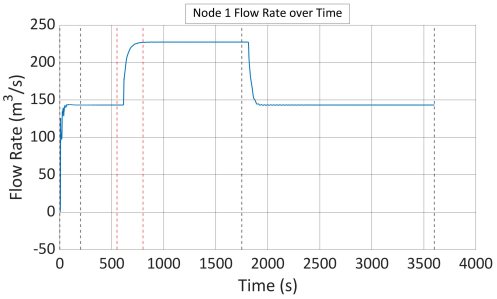

(a) Present study: Flow rate at node 1 with convective inertia

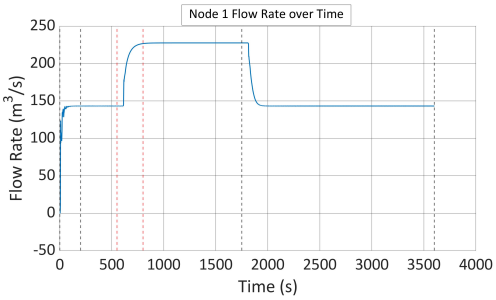

(b) Present study: Flow rate at node 1 without convective inertia

Figure 7.3: The flow rate at node 1 with and without convective inertia at $D_{nz} = 500\,\text{mm}$ for single nozzle

Pressure at selected Nodes

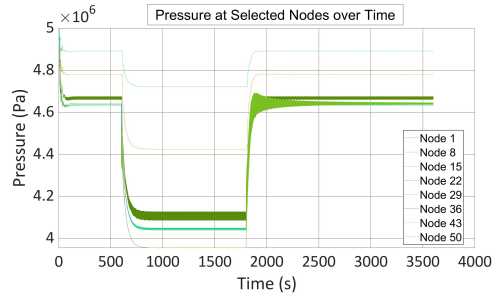

(a) Present study: Pressure with convective inertia

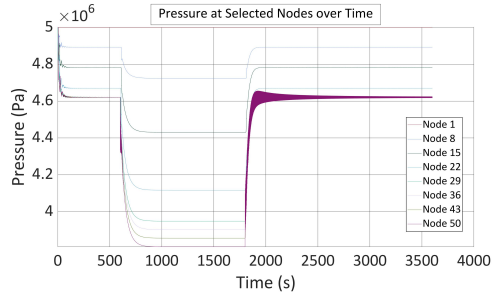

(b) Present study: Pressure without convective inertia

Figure 7.4: Pressure at selected nodes with and without convective inertia for single nozzle

Flow rate through nozzle

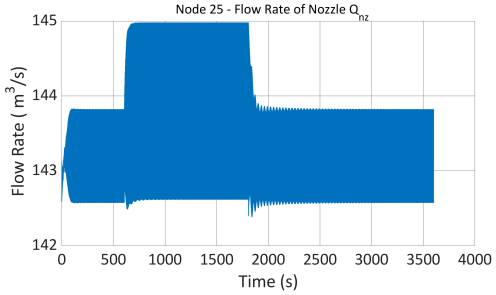

(a) Present study: Flow rate through nozzle with convective inertia

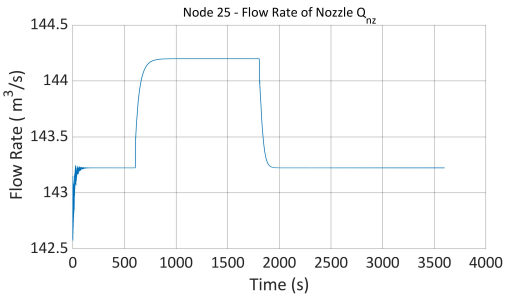

(b) Present study: Flow rate through nozzle without convective inertia

Figure 7.5: Flow rate through nozzle with and without convective inertia for single nozzle

The simulation results for the basic model with one nozzle, both with and without the convective inertia term, are displayed in the above graphs. Extreme circumstances were used for this simulation, with the pipe and nozzle diameters the same. The main findings from the graph show that, at around 600 seconds, the flow rate at Node 1 peaks at 230 m^3/s, which is consistent with a modification in the

boundary conditions that raises the mass flow rate. This peak flow rate suggests that the removal of the convective inertia element does not affect the model's output in terms of peak flow rates, since it is consistent with the results from the model that includes this term. Additionally, the model achieves a steady state flow rate of around 230 m^3/s in the 600–1800 second range, which is consistent with the outcomes that are attained when the convective inertia factor is taken into account. This provides additional support for the suggestion that, under these particular simulation settings, the convective inertia component might not play a major role in the system's flow dynamics. Furthermore, it seems that the graph is smoother when the convective inertia element is absent, especially after 1800 seconds when the transient brought on by an abrupt shift in boundary conditions is reduced. The pressure result is almost the same for both models with and without the convective inertia term. After 1800 seconds, the model without the inertia term exhibits a smoother transition compared to the model with the inertia term.

The flow rate graph for the nozzle at Node 25 exhibits consistent behavior with no bulges, indicating improved stability in the fluctuations. Previous models that incorporated the convective inertia term showed bulges, a sign of numerical instability. The momentum equation's convective inertia term, which can be sensitive to the spatial discretization and the solver's capacity to record steep gradients in the flow variables, is most likely what caused these instabilities. The results with and without the convective inertia factor show a slight variation of around 0.7%, which falls within allowable tolerance bounds and suggests that the simulations are not greatly affected by the absence of these components. This suggests that eliminating the convective inertia term can indeed enhance numerical stability by reducing fluctuations in the graphs for this research.

- Case II: The nozzle's size is changed to $D_{nozzle} = 200\,\text{mm}$ to observe the change in flow rate and pressure

The findings of a second simulation that was run with the nozzle diameter set to 200 mm and without the convective inertia term indicate that the flow dynamics for this specific system configuration are not significantly affected by the convective inertia. "Additionally, an appendix B including additional diameter changes and corresponding simulation results is included to offer complete information for reference".

Flowrate at Node 1

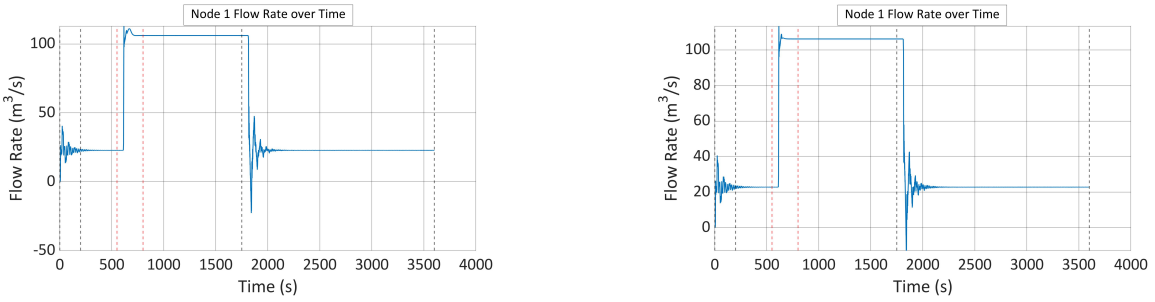

(a) Present study: Flow rate at node 1 with convective inertia

(b) Present study: Flow rate at node 1 without convective inertia

Figure 7.6: The flow rate at node 1 with and without convective inertia at $D_{nz} = 200\,\text{mm}$ for single nozzle

Pressure at selected Nodes

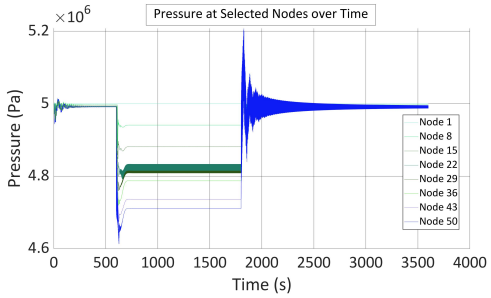

(a) Present study: Pressure with convective inertia

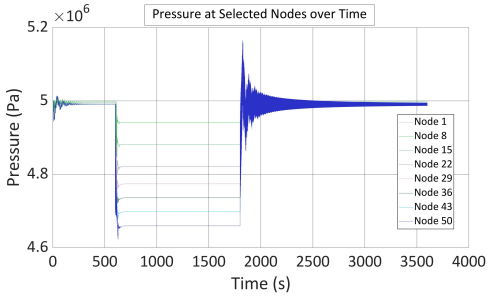

(b) Present study: Pressure without convective inertia

Figure 7.7: Pressure at selected nodes with and without convective inertia for single nozzle at $D_{nz} = 200\,\text{mm}$

Flow rate through nozzle

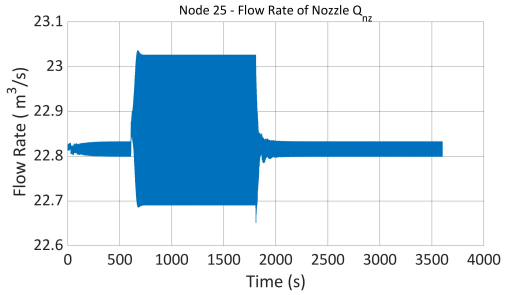

(a) Present study: Flow rate through nozzle with convective inertia

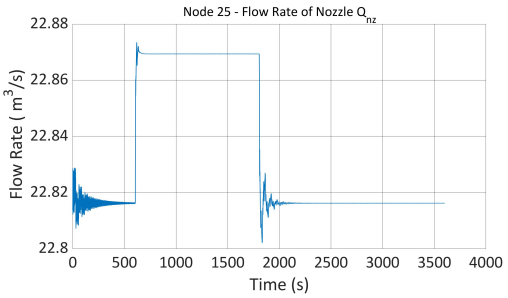

(b) Present study: Flow rate through nozzle without convective inertia

Figure 7.8: Flow rate through nozzle with and without convective inertia for single nozzle at $D_{nz} = 200\,\text{mm}$

Three nozzles

- Case I: The size of the nozzle is equivalent to $D_{nozzle} = 280\,\text{mm}$ which is considered to be an extreme condition.

Flowrate at Node 1

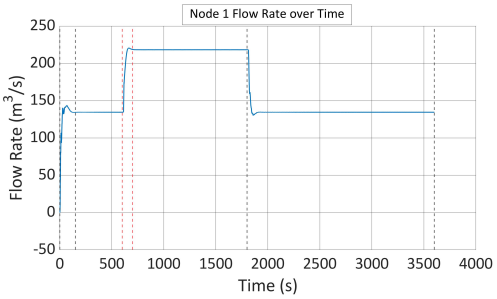

(a) Present study: Flow rate at node 1 with convective inertia

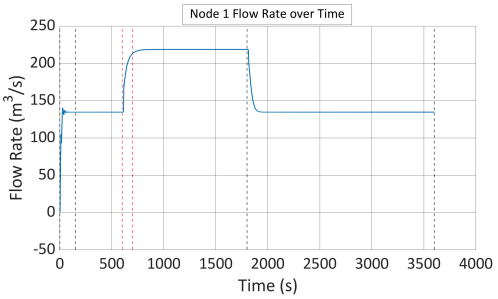

(b) Present study: Flow rate at node 1 without convective inertia

Figure 7.9: The flow rate at node 1 with and without convective inertia for three nozzles

Pressure at selected Nodes

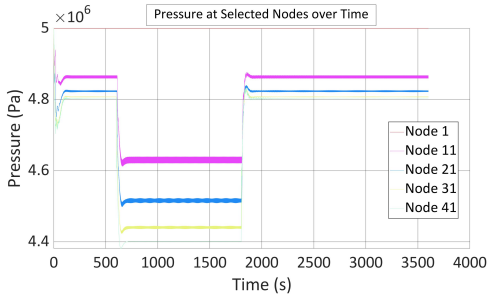

(a) Present study: Pressure with convective inertia

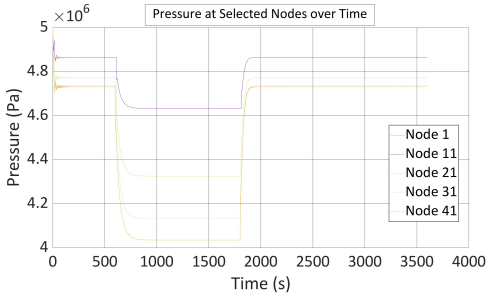

(b) Present study: Pressure without convective inertia

Figure 7.10: Pressure at selected nodes with and without convective inertia for three nozzles

Flow rate through nozzle

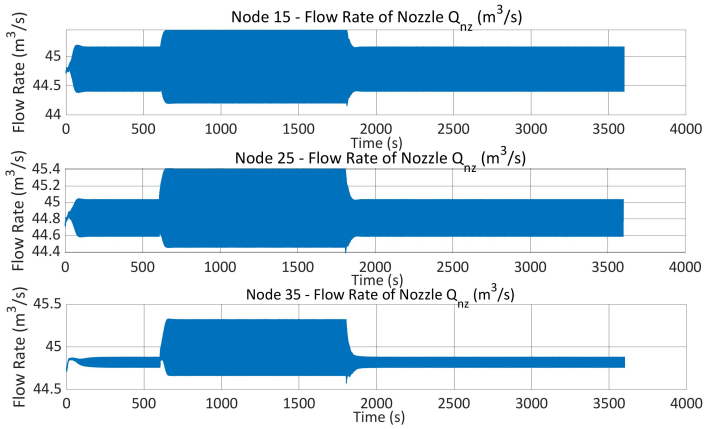

(a) Present study: Flow rate through nozzle with convective inertia

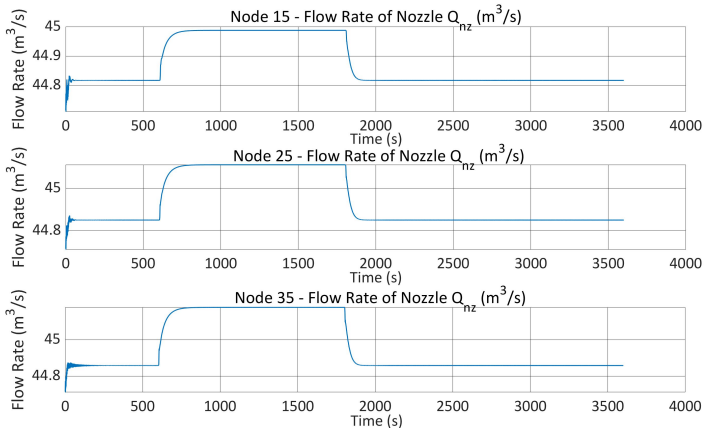

(b) Present study: Flow rate through nozzle without convective inertia

Figure 7.11: Flow rate through a nozzle with and without convective inertia for three nozzles

According to the graph, the flow rate at Node 1 stabilizes at around 230 m^3/s between 600 and 1800 seconds. These results are consistent with the estimates made by the model that incorporated the convective inertia component. The important finding here is that the model without the convective inertia factor exhibits a smoother transition to the new steady state with no noticeable oscillations at 1800 seconds when the boundary condition is changed to cease the mass flow. In comparison, there are minor variations during this transition in the model with the inertia term. Additionally, the model with the convective inertia part exhibits variation around 600 seconds when there is a pressure drop caused by an abrupt rise in the mass flow rate of the system owing to a change in the boundary condition, whereas the transition is smooth in the model without the convective inertia element. Furthermore, the pressure graph bulge found with the convective inertia factor has been eliminated in the model without the convective inertia term. Moreover, the model with convective inertia exhibits fluctuation at the point where the flow rate stops owing to a change in the boundary condition, but the graphs without the inertia term do not exhibit any fluctuation at 1800 seconds.

The flow rate through the three nozzles shows steady behavior without bulges, indicating that the problems with numerical instability caused by the inertia term have been eliminated. The results with and without the convective inertia factor show a variation of about 0.5%, which is within allowable tolerance ranges and suggests that the simulations are not greatly affected by the absence of this term. Without the convective inertia part, the model does not fluctuate, suggesting that this reduction results in a simulation that is more stable and numerically robust.

- Case II: The nozzle's size is changed to $D_{nozzle} = 200\,\text{mm}$ to observe the change in flow rate and pressure

The results of a second simulation, which was conducted with the nozzle diameter set to 200 mm and without the inertia, show that the convective inertia has no effect on the flow dynamics for this particular system configuration, as seen by the graphs below. To provide comprehensive information for reference, an appendix B with more diameter adjustments and matching simulation results is also provided.

Flowrate at Node 1

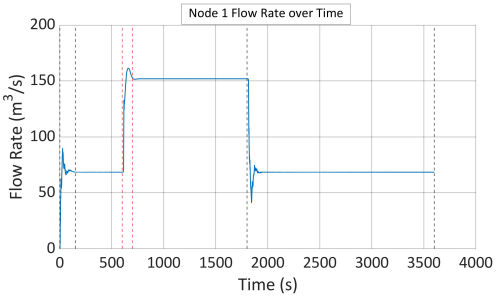

(a) Present study: Flow rate at node 1 with convective inertia

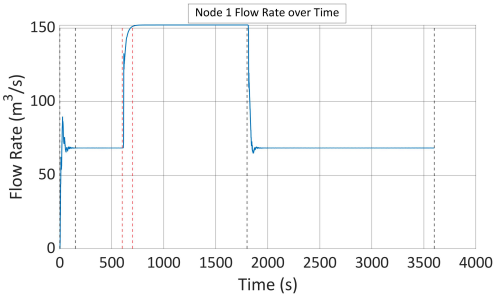

(b) Present study: Flow rate at node 1 without convective inertia

Figure 7.12: The flow rate at node 1 with and without convective inertia at $D_{nz} = 200\,\text{mm}$ for three nozzles

Pressure at selected Nodes

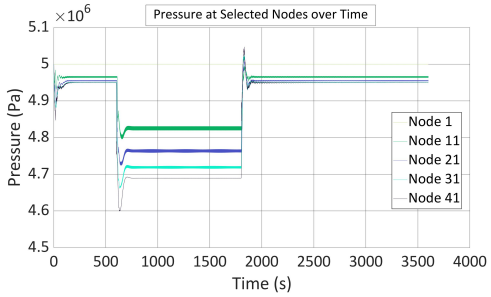

(a) Present study: Pressure with convective inertia

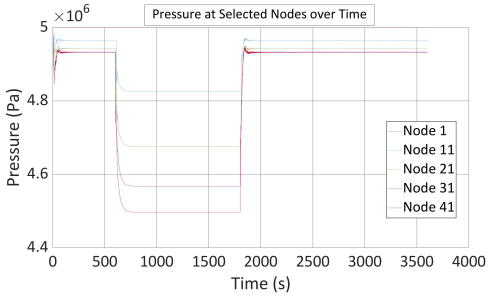

(b) Present study: Pressure without convective inertia

Figure 7.13: Pressure at selected nodes with and without convective inertia for three nozzles at $D_{nz} = 200\,\text{mm}$

Flow rate through nozzle

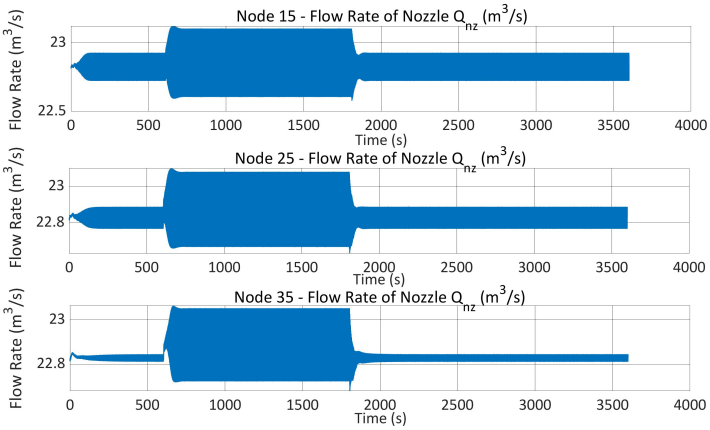

(a) Present study: Flow rate through nozzle with convective inertia

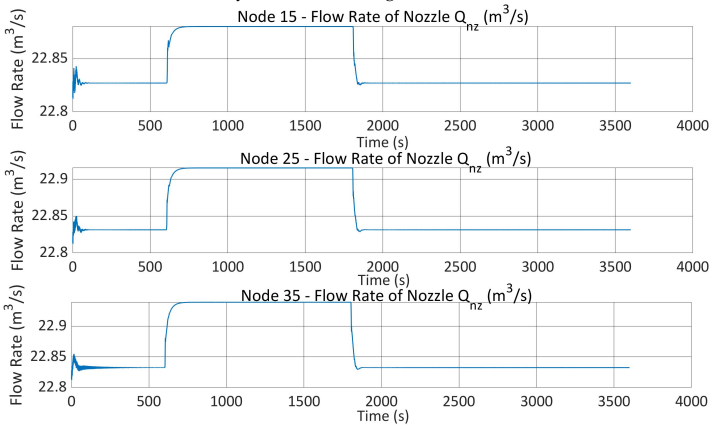

(b) Present study: Flow rate through nozzle without convective inertia

Figure 7.14: Flow rate through a nozzle with and without convective inertia for three nozzles at $D_{nz} = 200\,\text{mm}$

Five nozzles

- Case I: The size of the nozzle is equivalent to D_{nozzle} = 210 mm which is considered to be an extreme condition.

Flowrate at Node 1

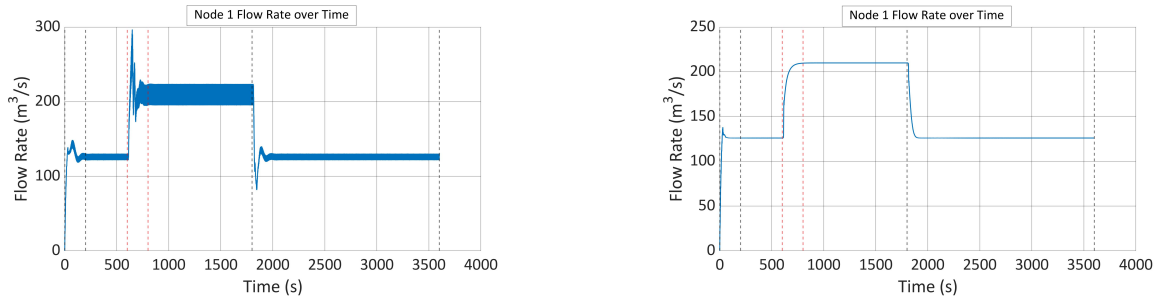

(a) Present study: Flow rate at node 1 with convective inertia

(b) Present study: Flow rate at node 1 without convective inertia

Figure 7.15: The flow rate at node 1 with and without convective inertia for five nozzles

Pressure at selected Nodes

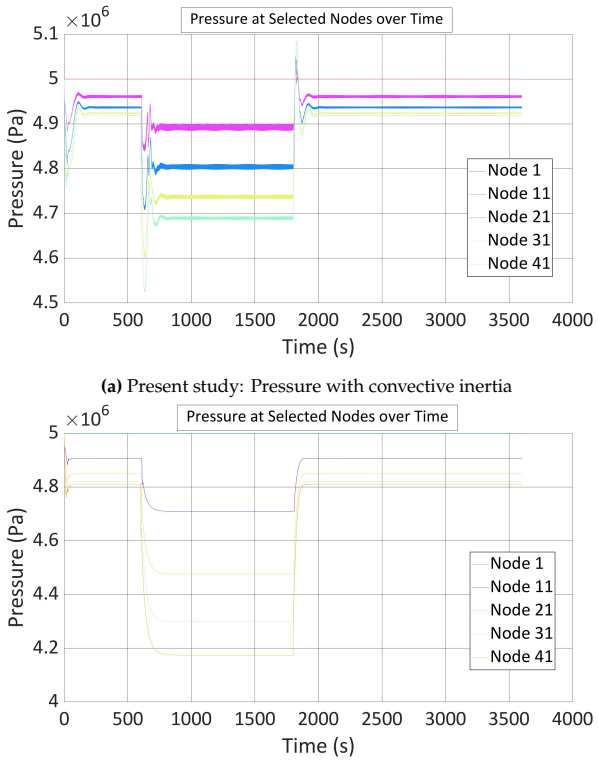

(a) Present study: Pressure with convective inertia

(b) Present study: Pressure without convective inertia

Figure 7.16: Pressure at selected nodes with and without convective inertia for five nozzles

Flow rate through nozzle

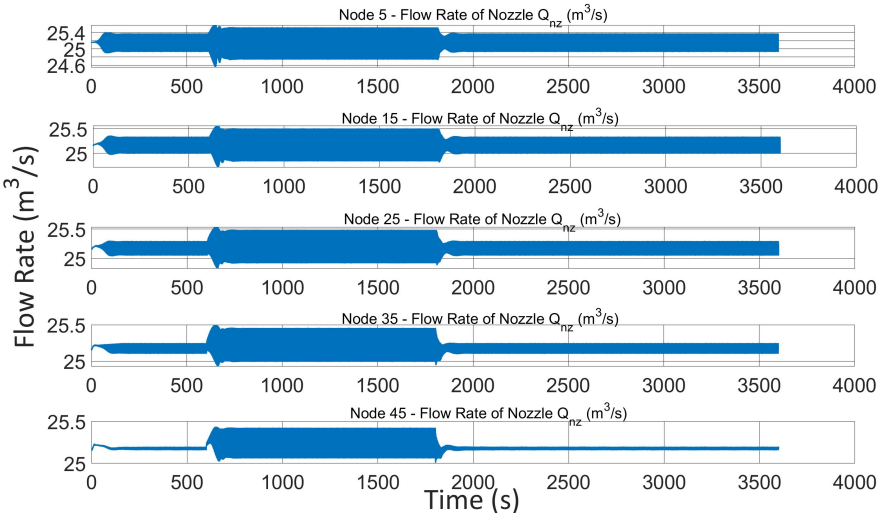

(a) Present study: Flow rate through nozzles with convective inertia

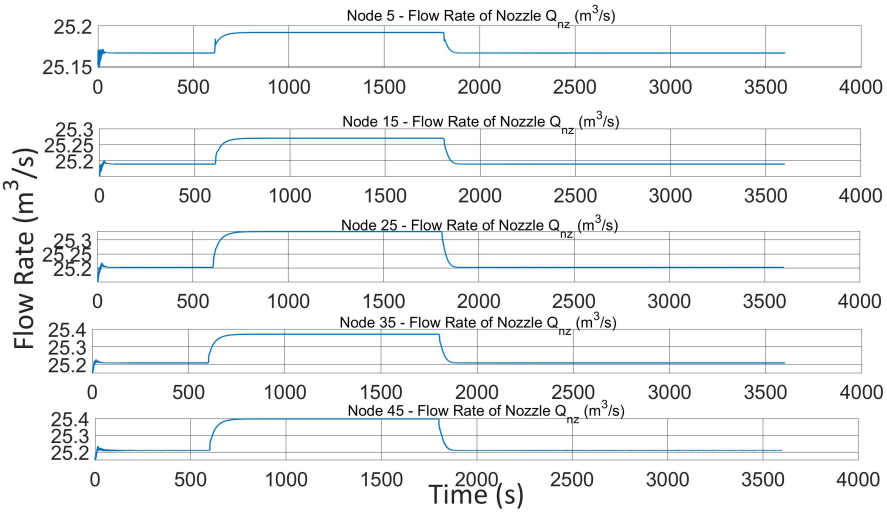

(b) Present study: Flow rate through nozzle without convective inertia

Figure 7.17: Flow rate through a nozzle with and without convective inertia for five nozzles at $D_{nz} = 210\,\text{mm}$

The graphs above show the simulation results for the current model with five nozzles, both with and without the convective inertia term. In the model without an inertia term, the numerical instability of bulge graphs shown in the model with convective inertia is fully eliminated. A change in the boundary condition causes the mass flow rate to abruptly increase at 600 seconds, causing the inertia term in the model to fluctuate, whereas the model without the convective inertia component exhibits continuous flow rate transactions. The maximum steady state condition, which spans 600–1800 seconds, is consistent both with and without the inertia term mode, indicating that the simulations remain unchanged. Furthermore, the system's mass flow rate drops to zero at 1800 seconds as a result of a change in the boundary condition, which causes the model containing the inertia term to fluctuate and produce bulges in the results. In contrast, the model eliminating the inertia term exhibits a smooth transition without any fluctuation.

The overall pressure drops at all nodes at 600 seconds when the system mass flow rate increases due to a change in the boundary condition. The model with the convective inertia term exhibits spikes in the drops, while the model without the inertia term exhibits a smooth transition without any fluctuations. Both the model with and without the inertia component maintain a steady state condition of pressure between 600 and 1800 seconds; however, the model with the inertia term exhibits bulge lines, whereas

the model without the inertia term displays smooth, straight lines without any numerical instability. The five nozzle's flow rates exhibit continuous, bulge-free behavior, proving that the inertia term's numerical instability issues have been solved. The findings, both with and without the convective inertia factor, exhibit a marginal variation of approximately 0.3%. This falls within the tolerance margins established for this research, implying that the absence of this component improves numerical stability by reducing fluctuations in the graphs.

- Case II: The nozzle's size is changed to $D_{nozzle} = 200\,\text{mm}$ to observe the change in flow rate and pressure

The graphs below demonstrate that convective inertia has no influence on the flow dynamics for this specific system configuration. A second simulation was run with the nozzle diameter set to 200 mm and without the inertia. A thorough appendix B with additional diameter modifications and corresponding simulation results is also included for reference.

Flowrate at Node 1

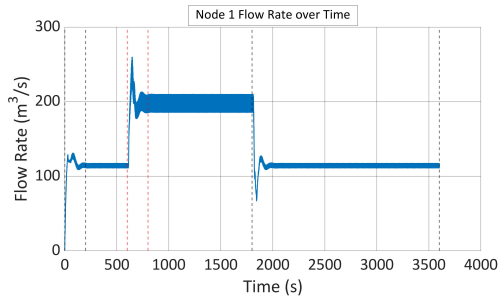

(a) Present study: Flow rate at node 1 with convective inertia

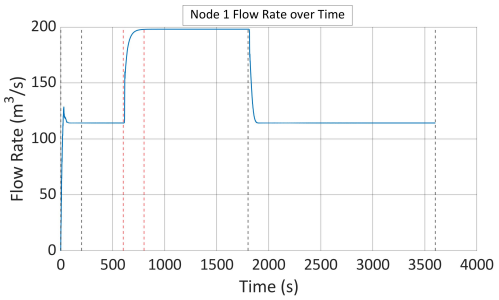

(b) Present study: Flow rate at node 1 without convective inertia

Figure 7.18: The flow rate at node 1 with and without convective inertia at $D_{nz} = 200\,\text{mm}$ for five nozzles

Pressure at selected Nodes

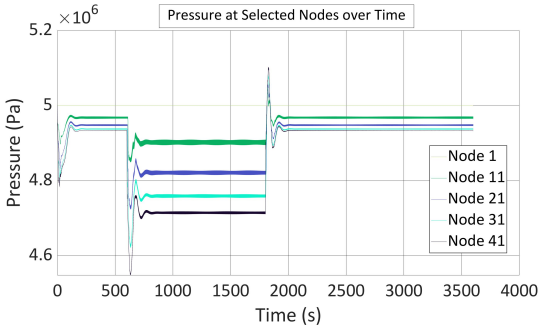

(a) Present study: Pressure with convective inertia

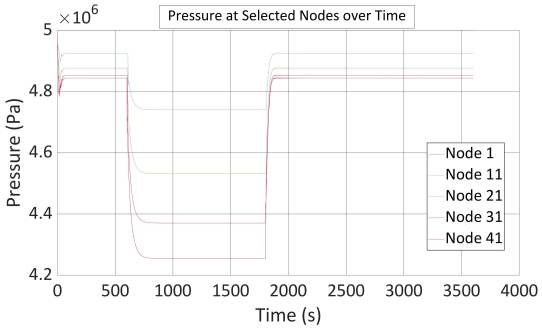

(b) Present study: Pressure without convective inertia

Figure 7.19: Pressure at selected nodes with and without convective inertia for five nozzles at $D_{nz} = 200\,\text{mm}$

Flow rate through nozzle

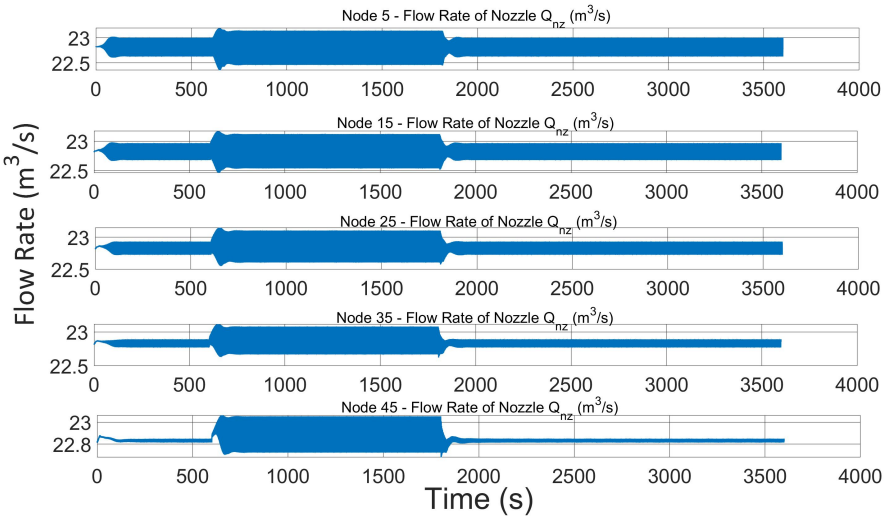

(a) Present study: Flow rate through nozzles with convective inertia

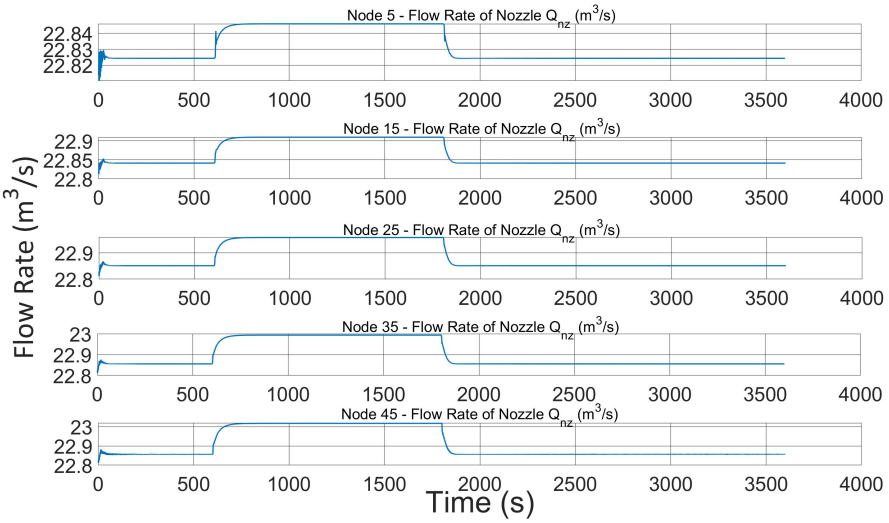

(b) Present study: Flow rate through nozzle without convective inertia

Figure 7.20: Flow rate through a nozzle with and without convective inertia for five nozzles at $D_{nz} = 200\,\text{mm}$

7.0.3. Comparative Analysis: With vs. Without Convective Inertia

Several important conclusions may be drawn from the comparison of fluid dynamics simulations among models with one, three, and five nozzles with and without the convective inertia term.

The addition of the convective inertia term to the single nozzle model causes variations in the flow rate at Node 1, which is a sign of the term's involvement in intricate transient behaviors at the boundary condition transition. Nevertheless, the model without the inertia term did not exhibit similar variations. For both the model with and without the inertia element, the magnitude of the steady state condition is 230 m^3/s between 600 and 1800 seconds, which is shown to be identical. Prominent spikes in pressure profiles with the inertia term are present during transitions, indicating the term's contribution to the system's non-linear response. When the inertia factor is included, there are oscillations in the flow rate through the nozzle, but these have a minor impact on the steady-state conditions.

With the three-nozzle configuration, the complexity rises as the inclusion of the inertia term exacerbates transient behaviors, making fluctuation at Node 1 more prominent. The system exhibits a smoother

response with suppressed transients when the inertia factor is absent, suggesting a more stable and consistent model. Including the inertia element causes the pressure across the system to respond to boundary changes more dramatically, with more sharp drops and spikes. The existence of an inertia factor causes the flow rate through the nozzle to bulge in the graphs; this is not the case in the model without an inertia term. However, there is a slight variation in the flow rate magnitude, 0.5%, which is considered to be negligible in terms of the fluctuations in the graphs for this research.

Transient complexity is further increased when two additional nozzles are added to the system, making it a five-nozzle setup. The inertia term in the flow rate at Node 1 exhibits a multiple peak response before stabilizing, but its absence causes a swift and smooth shift to a new equilibrium. With the inertia term during transients, the pressure responses are much more fluctuating, with notable differences during boundary condition changes. Without the term, the pressure at particular nodes gradually stabilizes following disturbances to the system more rapidly, and the flow rates through the nozzles more closely follow steady-state estimates without the fluctuation caused by the inertia component.

To summarize, the absence of the convective inertia term results in fewer fluctuations and a more stable numerical response for this research. The absence of the term in a model does not affect the flow rates or pressures; nonetheless, it makes the transient dynamics simpler, which can result in improved numerical stability by reducing fluctuations in the graphs.

8

Model Evolution from Pipeline to Scaled BCT Representation

General Description
Moving from a basic pipeline system to a scaled representation of Bubble Curtain Technology (BCT), this chapter represents a major transformation in the modeling methodology. The framework of the model's gradual development and the subtle complications of moving to a scaled BCT representation are explained in this chapter.

The first step of the research was to develop a basic model to represent compressible, unsteady flow in a pipeline system. This model functioned as a basic framework, providing a clear understanding of the fluid dynamics environment for the investigation. This fundamental model was verified by cross-referencing it with existing studies, which made sure it was accurate and dependable and provided a strong baseline for further modifications. After laying this foundation, the investigation progressed to include several nozzle arrangements inside the pipeline. The first indication of the changed flow dynamics that nozzles would bring about in the system arrived with the installation of a single nozzle in the center of the system. A further expansion of this incremental strategy to incorporate several nozzles at predefined intervals clarified the overall effect of nozzle quantity and location on the flow characteristics.

As these advancements took place, the establishment of numerical instability was a significant challenge for graphical representation. The convective inertia term, which caused these instabilities, was found and eliminated, which smoothed out the resulting graphs and improved numerical stability by reducing fluctuations in the graphs for this research. The final task was to develop a pneumatic model of the real BCT, which had a complicated configuration with a wide range of nozzles spread out across long distances. Assume, for instance, that the hose is 700 meters long and that the nozzles are spaced around 0.3 meters apart. Due to computational limitations, it is not possible to simulate the approximately 2500 nozzles that this real BCT system has. Therefore, the focus of this research will be on a scaled BCT model. Within a more computationally tractable framework, the model aimed to capture the essence of the Bubble Curtain Technology (BCT) by reducing the number of nozzles and the system's length. This approach seeks to replicate the proportions of a real BCT and serves as the foundation for developing a full-scale pneumatic model.

In this research, the number of nozzles in the model was selectively restricted to five due to increasing numerical artifacts associated with the transient flow dynamics as the number of nozzles expanded. These artifacts challenged our numerical solver's capabilities, and along with the project's time limits, we decided not to continue beyond this number. In the future, this model may be scaled up to a full-scale bubble curtain technology (BCT) system with more than a thousand nozzles by utilizing a methodology similar to this studies. This involves considering mass flow rates while adhering to mass conservation laws for integrating the hose-nozzle configuration. Furthermore, it may be helpful to investigate the usage of different numerical techniques better suited for dealing with the complexity of transient flow conditions.

8.0.1. Development of the 5-Nozzle Bubble Curtain Model

After incorporating five nozzles into the pipeline system's unsteady compressible flow, it is considered the final model that will be utilized to simulate the scaled BCT model. In this study, the actual Bubble Curtain Technology (BCT) parameters will be used in the scaled model. These parameters are derived from existing research with arbitrary changes, as per the pneumatic model, and are considered as a reference case. The reference case parameters are shown in the below tables as Environmental conditions and Variable and Operational and design properties of the BBC pneumatic system. However, the model also calls for new parameters, which have to be determined using model calculations. Other parameters, including the nozzle discharge coefficients, were calculated by using values that were either very similar to or identical to those found in the literature for the related parameters.

Inputs for the numerical model simulations

The numerical model's input parameters are separated into two categories: environment parameters and BBC pneumatic system parameters. Water depth is one of the environmental characteristics, as are the physical properties of both seawater and air, such as water density, air temperature, air dynamic viscosity, and air specific gas and adiabatic constant.

The pneumatic generating system's input parameters are further classified into geometrical and operational factors. The length, roughness, and diameter of the supply/riser lines and main hose, as well as the diameter and spacing of the nozzles, are all geometrical characteristics. The discharge coefficient of the nozzles is also incorporated within the geometrical attributes in this numerical model, although in reality it also relies on the operational air flow circumstances. The total volumetric flow rate provided by the sequence of compressors during free air delivery circumstances (FAD), expressed as the airflow rate in m^3/minutes/length of hose, is one of the operating parameters.

The first adjustment is conducted on the length of the hose in the actual BCT model; the complete length of the hose is around 700 m, but the length of the reference case is scaled down to 2.4 m with the total nozzle placed at a spacing of 0.3 m, as indicated in the general section that the scaled BCT model has been utilized. In addition, the length and spacing adjustments in the numerical model will be thoroughly detailed in the next section. The rest of the environmental and operational input parameters are displayed in the below tables. Additionally, in the final report of Nehls and M. Bellmann [39], the discharge coefficient for the typical drilled nozzle used for bubble curtain formation under pressures up to 3.6 bars was calculated, providing the empirical data required for the nozzle discharge coefficients. The coefficient's value was chosen such that the best possible match could be obtained when comparing the observed and computed mass flows. A discharge coefficient of $C\_d = 0.55$ was obtained by using a hose segment with a hole diameter of 2.0 mm, as per the existing literature.

Table 8.1: Input physical parameters for reference case of a bubble curtain application

Environmental conditions and Variable	Variable	Value	Unit
Water Depth	h	30 & 40	m
Density of water	ρ_w	1025	kg/m^3
Gravity acceleration	g	9.81	m/s^2
Atmospheric pressure	p_{atm}	1.013×10^5	Pa
Air Temperature	T	18	degC
Specific air gas constant	R	287	J/kg/K
Dynamic viscosity of air	μ	18×10^{-6}	Pa s
Air adiabatic constant	k	1.402	-
Ref temperature @ FAD conditions	T_{FAD}	20	degC
Ref pressure @ FAD conditions	p_{FAD}	1.013×10^5	Pa
Max Mach number	M_{max}	1.0	-

Boundary condition for reference scaled BCT numerical model

It was essential to include boundary conditions in the scaled Bubble Curtain Technology (BCT) model development process that closely resembled actual operating circumstances. A time-varying boundary

Table 8.2: Input parameters for reference case of the pneumatic hose-nozzle system for bubble curtain generation.

Operational and design properties of the BBC pneumatic system	**Variable**	**Value**	**Unit**
Air flow rate (per length)	Q_{FAD}	0.300 to 0.600	$m^3/min/m$
Nozzle size (diameter)	d	2	mm
Nozzle spacing	s	30	cm
Nozzle discharge coefficient	C_d	0.55	-
Internal nozzle hose diameter	D	104	mm
Total length of bubble curtain	L	2.4	m
Hose roughness	ε	1×10^{-3}	m
Diameter of supply hose & riser	D_{sup}	104	mm
Length of supply hose & riser	L_{sup}	40	mm
Supply hose roughness	ε_{sup}	$1e-3$	m

condition was used since it was acknowledged that a continuous supply of compressed air might not always required because of different operational and environmental circumstances. This time-varying boundary condition improves the realism of the model and makes it possible to forecast the behavior of the BCT more precisely under standard utilization scenarios.

Based on industry best practices as per existing research falling within the range of operating regulations, the airflow rate (Q_{FAD}) of $0.5\,m^3/min/m$ was selected for this research as reference case. This flow rate was adjusted to the scaled length of the hose to maintain proportionality in the scaled model; the result was a flow rate (Q) of $0.03\,m^3/sec$. The solution to the fluid dynamics governing equations inside the model required converting this volumetric flow rate to a mass flow rate. The mass flow rate (m) was found to be $2.94\,kg/s \cdot m^2$ after calculating the cross-sectional area of the hose (A_{hose}) and using an air density (ρ) of $1.2\,kg/m^3$, the mathematical expression of the conversion is explained further in this section. With an intake pressure (P) at the first node ($x = 1, t$) set to 8×10^5 Pa and a mass flow rate (m) at the final node ($x = L, t$)specified by the time-dependent function $f\_1(t)$, the boundary conditions were thus constructed to reflect these estimated values. This function exhibits the mass flow rate as a function of time, showing that there is no flow for the first 600 seconds, $2.94\,kg/s \cdot m^2$ of flow between 600 and 1800 seconds, and no flow between 1800 and 3600 seconds. By simulating possible disruptions in air supply and operational modifications, this type of temporal variation is intended to offer a thorough understanding of the system's responsiveness to dynamic boundary circumstances.

From table 8.2, the flow rate Q is obtained as $0.5 \times 10^5\,m^3/hr$. Further, it is converted to $0.02\,m^3/s$. Under FAD conditions, the density of air is given as,ρ_{air}=$1.2\,kg/m^3$, and the area of the hose is calculated using $A_{\text{hose}} = \frac{\pi}{4} \times Dia^2$, where the diameter of the hose is 2 mm.
The mass flow rate m can be calculated as $m = \frac{Q \times \rho_{\text{air}}}{A_{\text{hose}}}$, resulting in $m \approx 2.94\,kg/s \cdot m^2$.

Boundary conditions:

- $P(x = 1, t) = 8 \times 10^5$ Pa,
- $m(x = L, t) = f\_1(t)$.

$$f\_1(t) = \begin{cases} 0\,kg/s \cdot m^2 & \text{if } 0 \leq t < 600\,sec \\ 2.94\,kg/s \cdot m^2 & \text{if } 600 \leq t < 1800\,sec \\ 0\,kg/s \cdot m^2 & \text{if } 1800 \leq t < 3600\,sec \end{cases}$$

Matlab numerical model
The discretization scheme and methodological approach previously defined in Section 3 were used in the development of the numerical model for the scaled Bubble Curtain Technology (BCT) within MATLAB. This continuity ensures the consistency of the computational procedures used in previous sections to provide reliable results. To replicate the real BCT configuration, the hose length and nozzle spacing were modified for the scaled BCT model. Tables 8.1 and 8.2 provide certain parameters that are necessary to resolve the dynamics of the system; these tables can be referred to as more comprehensive

specifications. This scaled technique maintains an accurately scaled representation of the full-scale model by adjusting the hose length of the reference model to 2.4 meters, which corresponds to an inter-nozzle spacing of 0.3 meters.

The numerical domain is discretized into nine nodal points using the standard procedures for spatial division of the finite difference method. To calculate the spatial step dx, divide the hose's length by the total number of intervals ($Nx - 1$):

$$dx = \frac{\text{Length of hose}}{Nx - 1} = \frac{2.4}{9 - 1} = 0.3\,\text{m}$$

Following the scaled nozzle location, five nozzles are positioned at nodal points 3, 4, 5, 6, and 7. Using algebraic equations derived from the principles of fluid dynamics and the particular properties of the nozzles in use, the mass flow rate through each nozzle is calculated. Then, as part of the boundary conditions, this computed mass flow rate is added to the governing equations, which were covered in detail in Chapter 3. Both forward and backward discretization strategies are used to solve for the nodal points that have nozzles attached to them. Boundary conditions representing the system's physical limitations, such as intake pressure and exit mass flow rate, are assigned to the first and final nodal points. Central discretization is used for nodal locations that do not have nozzles. This technique is especially useful at internal domain points when there aren't any sudden changes in boundary circumstances since it balances the effect of neighboring nodes.

Convective inertia term

In fluid dynamics equations, the changes in cross-sectional area and momentum resulting from fluid flow are explained by the convective inertia term. This factor has the potential to generate nonlinear

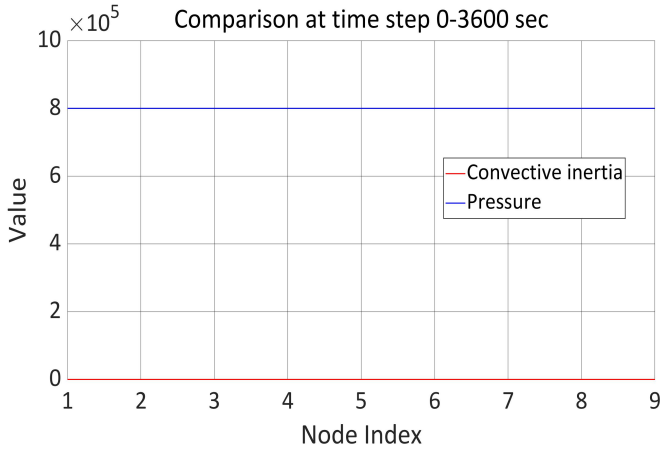

Figure 8.1: BCT scaled reference model convective inertia Vs Pressure with five nozzles

behavior in the equations, especially in systems that have changing cross-sections, such as nozzle systems. Steep solution gradients produced by nonlinear factors are frequently difficult for numerical solvers to manage and may result in numerical instability. These numerical instabilities were observed in section 6 of this work during simulations, including the convective inertia component. The convective inertia term's nonlinearity caused problems for MATLAB's ODE15s solver, which is meant to tackle stiff differential equations in this research. This implies that the numerical solution procedure is considerably more difficult when this factor is included.

The same method described in Section 6.0.4 has been applied to determine if the convective inertia term is crucial to the system's dynamics for this scaled BCT model in this research. This is because the two terms have the same units and can thus be directly compared in terms of magnitude. The convective inertia term's impact on the total momentum balance may be negligible if it is significantly lower than the pressure term. Therefore, it can be ignored to achieve stability by reducing fluctuations in the graphs for this research. Thus, the figures above illustrate that the convective inertia term for this particular case is significantly lower than pressure and can be ignored for this research.

8.0.2. Simulation with full scale BCT Parameters

Reference case results:
Flowrate at Node 1

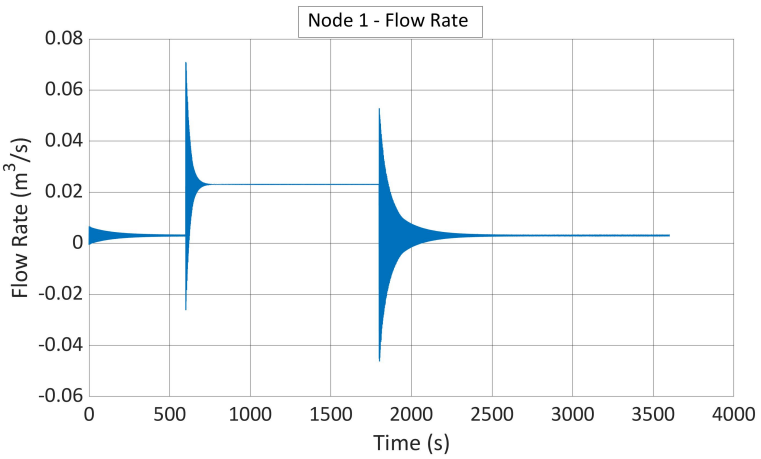

Figure 8.2: Reference Model: Flow rate at Node 1

The reference case's flow rate at Node 1 is depicted in the graph 8.2 above. With a flow rate that is zero, the system seems to be in a steady state before the initial spike. This implies that there isn't any flow at first, which the boundary condition accurately reflects. Furthermore, the flow rate increases sharply, reaching a peak at around 600 seconds slightly above 0.06 m^3/s, indicating that the mass flow rate has grown from zero to a value that satisfies the boundary condition. In addition, this surge may be an indication of an abrupt air injection into the system, perhaps as a result of the actual start of the bubble curtain.

The flow rate stabilizes for a short while, following the initial spike, before going through another abrupt reduction and increase. This time, at 1800 seconds, the flow rate becomes negative, indicating the possibility of a reversal or backflow situation, which is a reaction to a modification in the boundary conditions. After the second disruption, the flow rate stabilizes and stays that way for the rest of the time period that was observed. These spike's existence and the system's subsequent return to a steady state are signs of how the flow-controlling operating circumstances have changed inside the system. The graphs also have bulges, which are primarily caused by the different discretization schemes that were used in the calculation of this research. For instance, the forward and backward discretization method is used to incorporate nozzles at the location where they are placed, while the central discretization method is used at the location where they are not placed.

Pressure at selected Nodes

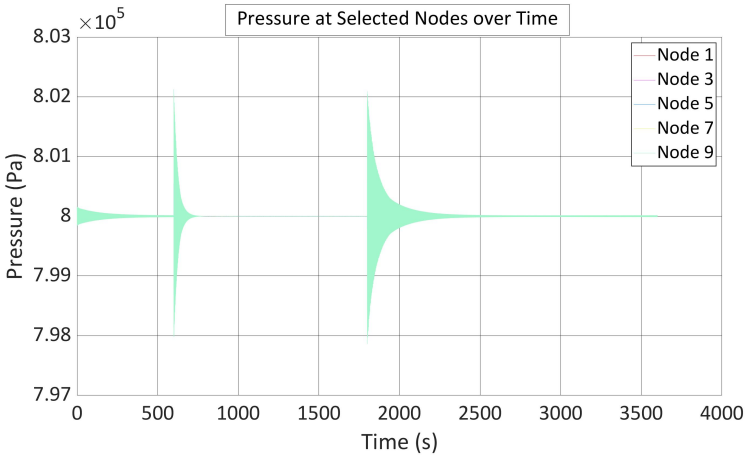

Figure 8.3: Reference Model: Pressure at all nodes

The fact that each node in the below figure 8.3 illustrates the behavior in the same way, which implies that there is a consistent distance between them. The consistent reaction to pressure fluctuations induced by the 0.3 m separation between each node would have an equal influence on the entire system. At first, every node has a constant pressure. This indicates that before any modifications or disruptions in functioning, the system is in a state of equilibrium. Two notable pressure increases occur at around 600 and 1800 seconds, respectively. This transition results from a change in boundary conditions. In terms of physical understanding, they might be the result of operational adjustments such as changes in air injection rates or other system manipulations. After each spike, the pressure returns to its former stable condition, suggesting that the system is well-regulated and capable of restoring equilibrium following disturbances. The magnitude of the spikes indicates that the changes are sudden rather than gradual. The rate of the pressure spikes looks uniform across nodes, suggesting that the change in operating conditions affects the whole system similarly.

Flow rate through nozzles

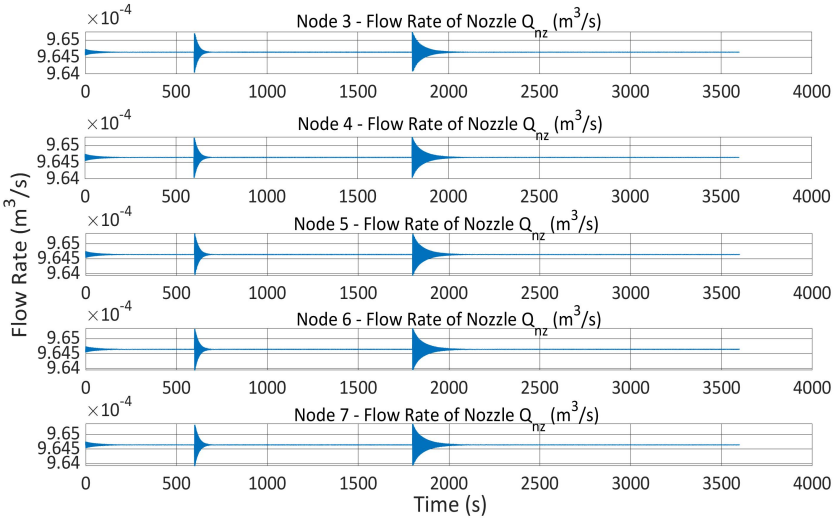

Figure 8.4: Reference Model: Flow rate through nozzles

The graph shows the flow rate at the nozzles in nodes 3, 4, 5, 6, and 7 of the simulated system. At certain times, noticeable spikes in flow occur. These probably correspond to the moments when the boundary conditions set at 600 and 1800 seconds change. Each nozzle appears to respond similarly to

these changes. This suggests that the effect of changing boundary conditions is system-wide and affects all nozzles in the same way. Between the peaks, the flow rate at each nozzle stabilizes at a constant value, suggesting that the system reaches a quasi-steady state during these periods. The uniformity of all nozzles suggests that the flow distribution system within the BCT is balanced. Additionally, when the boundary conditions change, the bulge of the plot is observed, which is mainly due to the instability caused by the different discretization schemes used to solve the numerical model.

8.0.3. Sensitivity analysis

A sensitivity analysis was conducted to identify the essential input parameters that have the greatest impact on the numerical model's output for the reference case of the pneumatic hose-nozzle arrangement. The sensitivity analysis was performed by varying each parameter between its maximum and minimum values while maintaining the other parameters constant. The analysis was conducted for operational parameters (discharge coefficient, flow rate of supplied air (*Q_FAD*), and water depth) in both maximum and minimum value ranges, as shown in table 8.3. Additionally, a sensitivity analysis was also conducted on the system's geometric characteristics (hose diameter, nozzle diameter, hose length, and nozzle spacing for both maximum and minimum value ranges, as shown in table 8.3). The existing research along with arbitrary changes, as per the pneumatic model provided acceptable maximum and minimum value ranges for the parameters, which included reasonable values from current practice. When simulating each parameter, the pneumatic model's boundary conditions were time-varying conditions that varied between 600 and 1800 seconds and remained constant for the remainder of the period, following the reference model. Since changing operational and environmental conditions don't always necessitate a constant supply of compressed air, this time-variable condition was thought to accurately reflect the real working conditions of BCT in this research.

The numerical model result showed the two significant effects of steady-state and transient effects because of time-varying boundary conditions. Sensitivity analysis helps to understand how a system will react to changes over time by looking at both steady-state and transient impacts. A comprehensive understanding of the system's long-term equilibrium under various situations is provided by the steady-state analysis, which is essential for evaluating Bubble Curtain Technology's (BCT) performance when operating continuously. However, transient impacts reflect an emphasis on the system's quick response to changes, which is crucial for assessing BCT's resilience and adaptation to unexpected operational or environmental changes.

Table 8.3: Range of input parameters of scaled BCT model

Variable	Reference value	Minimum value	Maximum value
Water depth [m]	40	30	50
Q FAD [$m^3/min/m$]	0.5	0.3	0.7
Hose length [m]	2.4	1.8	3
Discharge coefficient *C_d* [-]	0.55	0.3	0.7
Hose diameter D_{hose} [m]	0.102	0.076	0.127
Nozzle diameter d_{nz} [m]	0.002	0.001	0.003
Spacing [m]	0.30	0.20	0.40

Sensitivity analysis of operational parameters:
In a sensitivity analysis for a bubble curtain technology system, the flow rate of supplied air *Q_FAD* and the coefficient of discharge *C_d* are crucial because they have a direct impact on the flow dynamics of the system. Noise reduction and bubble dispersion underwater are impacted by *C_d*, which has an impact on how successfully the nozzles transform the supplied air into bubble curtains. The air supply capacity is determined by *Q_FAD*, which affects the bubble curtain's coverage and density. To understand the transient flow dynamics along the hose length under various circumstances and ensure optimum environmental protection, their magnitudes in the steady-state and transient states are compared with a reference model. The analysis results for both parameters are shown below. According to time-varying boundary conditions, the yellow color indicates the steady state's magnitude, the grey color shows the

first transient response, which was observed at 600 seconds, and the blue color highlights the second transient response, which was observed at 1800 seconds.

The graph 8.5 illustrates the vertical bars as positive and negative values that arise as a result of the transitory impact of time-varying boundary conditions. Additionally, a sudden increase in flow rate following the boundary condition is responsible for the positive flow rate obtained for the reference value, the maximum and minimum ranges, and the observed negative value, which occurred as the system adopted the change in condition, is due to reverse flow or backflow. By using the steady state as the baseline, the magnitude of both positive and negative flow rate values are measured. This method makes it possible to comprehend the dynamics in operation more concisely and aids in determining which factors most significantly affect how the system behaves under various circumstances. Finding these variations is essential to sensitivity analysis since it shows how sensitive the system is to variations in operating parameters.

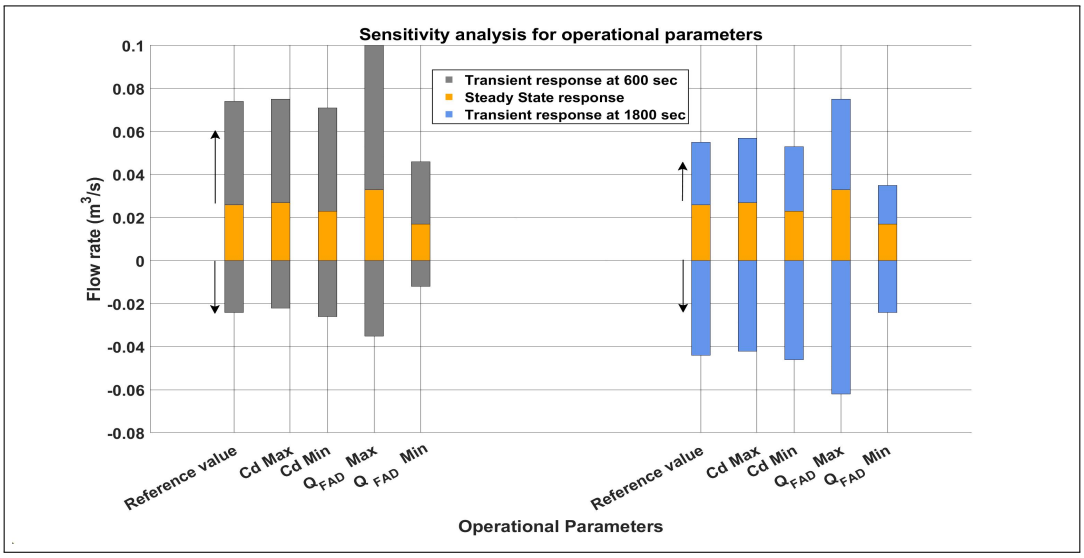

Figure 8.5: Sensitivity analysis: Operational parameters flow rate at Node 1

In the above graph, the reference case system's behavior during the first transient phase, which lasts for 600 seconds, shows a notable peak flow rate of 0.074 m^3/s, followed by a negative flow of -0.024 m^3/s, which indicates the reversal or backflow. This transient state establishes a baseline under standard circumstances and shows how the system adjusts to sudden changes in boundary conditions. When the maximum *C_d* value is introduced, required flow rates are marginally improved, as shown by a slightly higher peak flow rate of 0.075 m^3/s and a less severe negative flow of -0.022 m^3/s. On the other hand, the lower flow rate at the minimal *C_d* value is shown by a smaller peak of 0.071 m^3/s and a more prominent negative flow of -0.026 m^3/s, which indicates greater susceptibility to reverse flows during transients. The reference scenario shows a decline in flow rate to 0.055 m^3/s and a considerable reverse flow of -0.044 m^3/s when it shifts to transient 2 at 1800 seconds, where the flow rate drops to zero according to boundary conditions. The system shows higher resilience under maximum *C_d* circumstances, with values of 0.057 m^3/s and -0.042 m^3/s, indicating a more substantial recovery from the disruption. The minimal *C_d*, on the other hand, shows a more significant decline in flow and amplifies the impacts of the disturbance, as seen by values of 0.053 m^3/s and -0.046 m^3/s.

Under the reference scenario, the flow rate of supplied air, or *Q_FAD*, rises and falls at 0.074 m^3/s and -0.024 m^3/s, respectively. These patterns reveal the system's first reaction to a fluctuation that was caused by a sudden change in boundary conditions. Specifically, a higher peak of 0.1 m^3/s and a larger negative shift as -0.035 m^3/s at *Q_FAD* max show an enhanced dynamic response, implying that an increased air supply rate increases the system's reactivity. However, *Q_FAD* min shows a far greater negative variation as -0.062 m^3/s, even if its peak is just marginally above the reference at 0.075 m^3/s. This difference suggests that a reduced air supply rate causes a more noticeable flow reversal, which may indicate a less stable system response to disturbances. Moving on to the subsequent transient

state 2, the reference value shows a drop in flow rate to 0.055 m^3/s and a reversal at -0.044 m^3/s, which represents the system's attempt to stabilize after the disruption. A lower flow rate of 0.046 m^3/s and a smaller reversal at -0.012 m^3/s under *Q_FAD* max circumstances imply that a greater air supply rate would enable a quicker system stabilization. In contrast, *Q_FAD* min causes the flow rate to decrease to 0.035 m^3/s, with a reversal at -0.024 m^3/s. This suggests that the slow return to stability following a disturbance might be caused by a decreased air supply rate impeding the system's recovery.

When compared to the reference value, the sensitivity analysis for the operational parameter of water depth reveals relatively little variation in the flow rate at Node 1 for both the maximum and lowest water depth scenarios. Appendix D displays the graph from this sensitivity analysis. This stability across a variety of water depths indicates that, within the studied range, the flow rate at Node 1 is rather insensitive to variations in water depth. The nearly identical values indicate that other factors have a greater influence on the BCT system's flow dynamics, and the range of water depths studied has no substantial impact on the flow dynamics associated with the BCT's operating required flow rates in the aspect of the pneumatic model. In practical terms, this might imply that, within the tested range, the BCT system could be utilized reliably throughout a variety of water depths without requiring significant alterations to compensate for variations in depth. While this is a useful realization for the implementation of BCT systems in situations with variable water depth, further testing beyond this range may be required to completely comprehend the effects of water depth on system flow dynamics along the hose length.

A summary of the results for the sensitivity study of the operational parameters *Q_FAD* (flow rate of supplied air) and *C_d* (discharge coefficient) highlights their substantial effects on the flow dynamics in the BCT system's steady-state and transient states. Additionally, changes in *C_d* show a direct relationship with flow rates, meaning that both higher and lower values have a significant impact. Larger values of *C_d* are linked to more noticeable flow rates during transients, emphasizing their crucial function in influencing the behavior of the system. Regarding *Q_FAD*, the study reveals its significant impact on the BCT system's overall flow dynamics. Higher *Q_FAD* values are seen to increase the flow rate, suggesting better system response and required flow rates. On the other hand, larger negative flow rates are produced by lower *Q_FAD* values, which indicate possible operational difficulties and an extended return to steady-state conditions. Essentially, both parameters are crucial to a BCT system's operation, and figuring out their ideal values requires careful consideration of how to achieve a balance between maintaining system stability and responding rapidly to disturbances.

Sensitivity analysis of geometric parameters:
When evaluating a Bubble Curtain Technology (BCT) system, it is essential to perform a sensitivity analysis for geometric components including hose diameter, nozzle diameter, hose length, and nozzle spacing. This analytical method offers an invaluable understanding of how changes in physical dimensions may affect the overall functionality of the system. It is feasible to evaluate the durability of the system's design by meticulously analyzing the maximum and minimal ranges for these parameters. Thus, it enables to identification of crucial factors that have a big impact on both operational and achieving the desired outcomes.
From the above graph it can be observed that the hose diameter in the geometric parameter has a major impact on the flow dynamics, according to the results of sensitivity analysis. A maximum hose diameter of 0.12 m^3/s for the first transient response at 600 seconds shows a significant increase in flow rate over the reference value of 0.074 m^3/s, while a minimum diameter causes a lower magnitude of 0.066 m^3/s. This implies that the system's reaction is amplified by an increased hose diameter, producing a more noticeable transient effect. On the other hand, the minimal hose diameter results in a more intense negative reaction but a less intense positive transient response, suggesting higher susceptibility to flow reversals. Additionally, at 1800 seconds during the second transient response, the maximum diameter displays a lower negative flow rate drop to -0.011 m^3/s in comparison to the reference's -0.044 m^3/s. This suggests that hose diameters bigger than the reference can lessen the impact of abrupt flow rate declines. Its susceptibility to sudden fluctuations is highlighted by the minimal diameter's more significant negative flow of -0.022 m^3/s, indicating that smaller diameters could not be as successful at reducing the consequences of flow rate drops. These fluctuations demonstrate how crucial the hose diameter is to the transient behavior of the system, which in turn impacts the operating efficiency of the Bubble Curtain Technology (BCT).

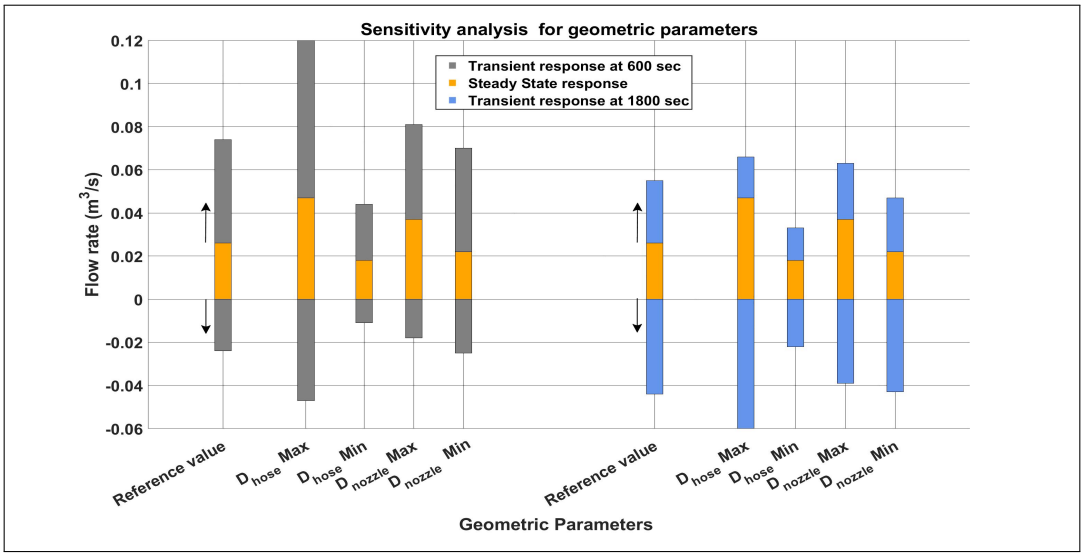

Figure 8.6: Sensitivity analysis: Geometric parameters flow rate at Node 1

When considering the sensitivity analysis for the nozzle diameter, significant trends appear across various scenarios. During the first transient response, the reference diameter produces a flow rate spike of 0.074 m^3/s, which is then followed by a drop to -0.024 m^3/s. On the other hand, the largest nozzle diameter causes a somewhat higher peak flow of 0.081 m^3/s along with a lesser impact of -0.018 m^3/s. This implies that a bigger nozzle diameter reduces the significant negative impacts seen in the reference situation while enabling a greater peak flow. However, the lowest nozzle diameter results in a somewhat more significant negative reaction at -0.025 m^3/s and a lower peak flow of 0.07 m^3/s, suggesting a possibly less stable system response to disturbances. Additionally, the flow rate falls to zero after a boundary condition at 1800 seconds, producing another transient effect. The reference diameter shows a peak flow rate of 0.055 m^3/s and a negative flow of -0.044 m^3/s in this secondary transient. A bigger nozzle diameter can minimize negative flow responses induced by reverse flow, as seen by the greater peak flow at 0.063 m^3/s and less evident negative flow at -0.039 m^3/s for the maximum diameter. On the other hand, the minimal diameter increases the negative flow, which is at -0.043 m^3/s, closer to the reference value and reduces the peak flow to 0.047 m^3/s. This extensive study highlights the complicated interaction between changes in nozzle diameter and how such changes affect system stability and flow dynamics.

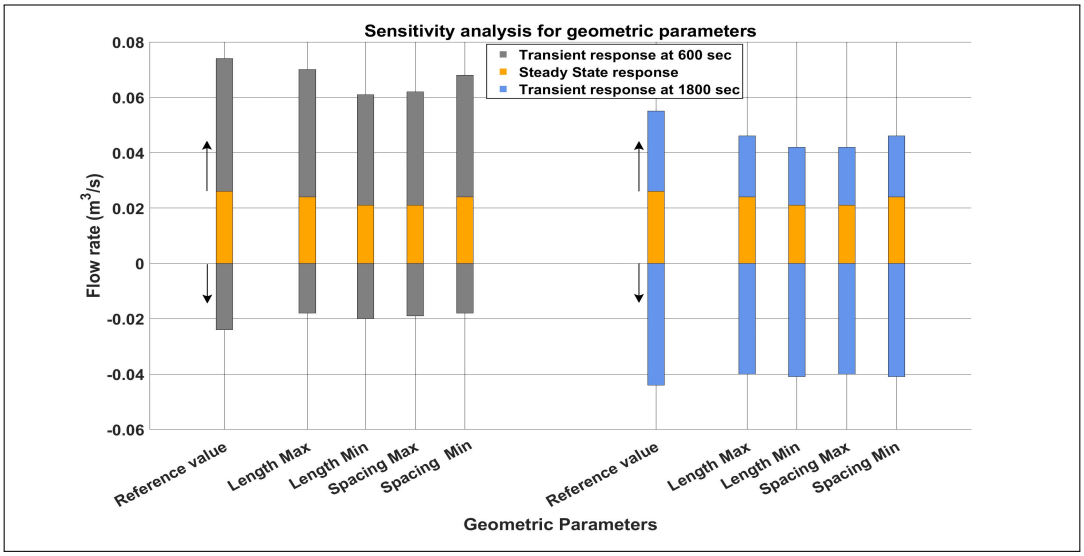

Figure 8.7: Sensitivity analysis: Length of hose and Spacing between nozzles

The sensitivity analysis of the nozzle spacing provides useful findings on how the system behaves in different configurations. A small decrease in peak flow rate to 0.062 m^3/s and a reduction in the severity of negative flow to -0.019 m^3/s are linked to increasing the space between nozzles. Conversely, a smaller nozzle spacing leads to a somewhat improved negative flow at -0.018 m^3/s and a slightly higher peak flow rate of 0.068 m^3/s. However, this decreased negative flow is especially noticeable in comparison to the maximum and reference values from the first transient reaction. In addition, the reference value shows a negative flow of -0.044 m^3/s and a peak flow rate of 0.055 m^3/s during the second transient reaction. When nozzle spacing is increased, the peak flow rate decreases to 0.042 m^3/s and the negative flow decreases a bit to -0.04 m^3/s. Reduced spacing, on the other hand, yields a peak flow rate of 0.046 m^3/s and a negative flow of -0.041 m^3/s, which are more in line with the reference numbers. When the boundary condition changes abruptly, the nozzle spacing with the smallest value is effective for adjusting the required flow rates in minimizing reverse flow. Furthermore, extending the hose length beyond the reference value causes the peak flow rate and the intensity of the negative flow to drop, suggesting that the system's reaction is becoming more stable. The peak flow is further decreased and the negative flow rate is slightly enhanced by reducing the length of the hose.

In summary, the geometric components of the Bubble Curtain Technology (BCT) system hose diameter, nozzle diameter, hose length, and nozzle spacing have a major influence on flow dynamics and system stability, as shown by the sensitivity analysis of these parameters. Larger hose and nozzle diameters increase the flow rate and lessen negative transient effects in response to disturbance. The system's responsiveness may also be affected by changing the hose length and nozzle spacing; longer hoses and smaller nozzle spacing are more successful in controlling flow rate peaks and reducing negative flow, respectively. These results highlight the requirement for accurate geometric designs for handling the transient flow dynamics along the length of the hose.

Sensitivity analysis of flow rate through nozzle :
Analyzing the flow through the nozzle's sensitivity was carried out using a similar technique to the one used to analyze the flow rate via node 1. At around 600 and 1800 seconds, respectively, there are two noticeable spikes in flow rate. Boundary conditions have changed, causing this transition. The observed two transitions had identical magnitudes. Because of the nozzle's uniform spacing inside the scaled BCT model, each nozzle's flow rate was constant. All five of the nozzles have a similar pattern that indicates they react to changes in the system in a uniform manner, exhibiting consistent flow characteristics. The reason for this consistent reaction is that the nozzles have the same sizes as well as similar flow characteristics. Except for the coefficients of discharge *C_d* and nozzle diameter, the sensitivity analysis of the geometric parameters (hose length, diameter, and spacing) and operational factors (*Q_FAD*, water depth) had a relatively lower influence on the nozzle flow rates. A higher flow rate magnitude was seen at the highest *C_d* value and maximum nozzle diameter, allowing for more flow through the nozzles. In specific, it was found that the increase in *C_d* max and maximum nozzle diameter was 2–3% more than the reference values.

Sensitivity analysis of Pressure:
The sensitivity analysis result indicates that there is no variation in pressure for either the geometric parameters (hose diameter, nozzle diameter, length of hose, and nozzle spacing) or the operational parameters (discharge coefficient, water depth, and flow rate of supplied air (*Q_FAD*) for both the maximum and minimum value range. Appendix D displays the graph from this sensitivity analysis. There are two significant spikes in flow rate, approximately around 600 and 1800 seconds, respectively. A modification in the boundary conditions causes this change to occur. The magnitudes of the two observed transitions were identical. This consistency demonstrates that, within their observed ranges, these parameters do not affect the pressure findings in this scaled model. Furthermore, it shows that the system attains a quasi-steady state rapidly generating no significant shift in pressure, an effect that might be due to the scaled model or the uniform spacing of the five nozzles for this research.

9 Discussion of Findings

9.0.1. Interpretation of Results

The focus of this thesis has been concurrent with the overall issue of "unsteady compressible flow along the hose of BCT." On the one hand, an investigation of the hydrodynamics of flow within the hose. On the other hand, the emphasis is on the influence of operational conditions on bubble curtain technology. This chapter discusses both topics, with the two sections below focusing on the scaled 1D model of unsteady compressible flow in the hose and the hose-nozzle system's influence on operating parameters.

Scaled 1D model of unsteady compressible flow in the hose

Establishing a foundation for a 1D unsteady state model of compressible flow inside a hose for application in bubble curtain technology was the main goal. This study was driven by one main research question and its supporting questions, as outlined in Section 1.0.2. The baseline simulation of unsteady compressible flow in a pipeline system served as the basis for the development of this one-dimensional model. The pipeline model served as the foundation for the later modeling of the scaled Bubble Curtain Technology (BCT) when it was verified against the existing researched model. With an emphasis on isothermal flow conditions, chapters 3 through 4 go into further detail on the approach, numerical modeling, and verification of this system. The model's creation was greatly aided by the conservation laws of mass and momentum, which are fundamental to the flow dynamics of pressured systems and are covered in detail in Section 3. The analysis of flow rates through the nozzles, pressures at various nodes, and flow rates at Node 1 were all essential to comprehending the dynamics of unsteady compressible flow along the length of the hose in the pneumatic aspects of the bubble curtain system. Figures 8.2, 8.4, and 8.3 show the results of using a reference example from the existing research to capture the scaled BCT model's unsteady behavior.

The dynamic response at Node 1, which reflects operational changes and suggests the intermittent nature of compressed air supply owing to operational and environmental variables, is captured by the flow rate graph 8.2. Time-varying boundary conditions were included in the model to resemble actual situations. The results showed that sudden variations in air injection might have a big effect on how well a system works. Notably, the system's responsiveness to operational changes is highlighted by spikes in the flow rate, which indicate the start and stop of air injection. The likelihood of a reversal or backflow scenario, which is a response to a change in the boundary conditions, is the primary cause of the negative spike shown in the graphs. The behavior of the flow rate was reflected in the pressure dynamics of a graph 8.3, reflecting a uniform systemic response to pressure variations at all nodes due to uniform nodal spacing. The uniformity of the pressure spike rate across nodes indicates that the system as a whole is affected comparably by changes in operating circumstances. The flow rate through the nozzle, which is evenly spaced at a distance of 0.3 meters, is displayed in the third graph. In a comparable way, a graph 8.4 flow rate across the nozzles showed a constant response from the nozzle to the nozzle, suggesting a balanced distribution system inside the BCT and a consistent result of modifications to operations. However, the observed numerical instabilities, as addressed in Chapter 6 "Analysis of Numerical Instability," were linked to the various discretization methods used in this research for pneumatic model.

In conclusion, the simulations of scaled BCT models show the ability to demonstrate the importance of nozzle design in affecting internal flow rates and pressures. The behavior of the system may thus be

controlled by modifying the operational parameters, which can be a crucial consideration during the operation of bubble curtains.

Hose-nozzle system's impact on operational parameters

The purpose of the study was to clarify how operational factors affect the Bubble Curtain Technology (BCT) system. This research was directed by two major topics, each with a set of particular sub-questions, as explained in Section 1.0.2. The results of the sensitivity analysis were used to address those research questions. The sensitivity analysis will look at the impacts of water depth, hose length, discharge coefficient (*C_d*), hose diameter, nozzle diameter, and spacing based on the table 8.3 that is given. A range of situations were simulated, with the parameters set to their lowest, maximum, and reference values. The bar graphs (8.5, 8.6, and 8.7) illustrate the results of measuring the system's reaction in terms of flow rate at node 1.

The flow dynamics in the BCT system during both transient states and steady-state circumstances are impacted by the sensitivity analysis performed on the operational parameters *C_d* (discharge coefficient) and *Q_FAD* (flow rate of supplied air). Importantly, changes in *C_d* show a clear relationship with flow rates, meaning that both higher and lower values have a significant impact. An important role that *C_d* values play in influencing system behavior is shown by the fact that they are linked to more prominent flow rates during transients resulting in modifications in boundary conditions. When comparing the maximum *C_d* value to the reference (-0.024 m^3/s) and the minimum range (-0.026 m^3/s), a noticeable drop in reverse flow -0.022 m^3/s was seen during the initial transient reaction. Similar to the first transient reaction, higher *C_d* showed a decrease in reverse flow -0.042 m^3/s relative to the reference -0.044 m^3/s and the minimal *C_d* values -0.046 m^3/s. Upon examining *Q_FAD*, the analysis highlights its significant impact along the length of the hose. An increased flow rate is observed to be associated with higher *Q_FAD* values, suggesting effective for adjusting the required flow rates and faster system response. On the other hand, smaller *Q_FAD* values indicate reverse flow due to abrupt boundary conditions will result in higher negative flow rates. Overall, both parameters are critical to a BCT system's functioning, and their ideal values must be carefully chosen to strike a balance between rapid response to disturbances and conserving system stability. Moreover, when compared to the reference value, the water depth exhibits minimal variation in the flow rate at Node 1 for both the maximum and minimum water depth scenarios; this consistency across a range of water depths indicates that in practical terms, the BCT system could be reliably used across various water depths without requiring major adjustments to accommodate changes in depth, within the range tested

It is evident from the findings of sensitivity analysis of the Bubble Curtain Technology (BCT) system's geometric parameters hose diameter, nozzle diameter, hose length, and nozzle spacing indicate their important influence on the dynamics of flow and stability of the system in this research. When compared to the reference value 0.074 m^3/s and lowest value 0.066 m^3/s, larger hose diameters increase the flow rate by up to 0.12 m^3/s. Furthermore, the larger hose diameter showed a decrease in the magnitude of the negative transitory effects carried on by reverse flow after a boundary condition modification. When compared to the reference value of -0.044 m^3/s and the minimum value of -0.022 m^3/s, the greater diameter shows a reduction of -0.011 m^3/s. Moreover, larger nozzle sizes provide greater peak flows and reduce negative responses to disturbances. Modifying the hose length and nozzle spacing also affects how the system responds; longer hose lengths and smaller nozzle spacing proved effective for adjusting the required flow rates and reducing negative flow, respectively. These results emphasize the necessity of modifications to improve required flow rates. and stability, underscoring the crucial relevance of precise geometric configurations to handle transient flow along the length of the BCT hose.

Along with the flow rate at Node 1, the sensitivity analysis of the pressure and flow rate through the nozzle was also performed for both the geometric and operational parameters within the lowest and maximum value ranges. The identical pattern observed in all five nozzles indicates that they exhibit consistent flow characteristics and respond evenly to variations in the system. The consistent reaction can be attributed to the nozzle's same sizes and likely similar flow characteristics. It's interesting to note that, except the coefficients of discharge *C_d* and nozzle diameter, the sensitivity analysis of both geometric (hose diameter, length, and spacing) and operational (*Q_FAD*, water depth) parameters did not show any notable variations in the flow rate. A higher flow rate magnitude was seen at the highest *C_d* value and maximum nozzle diameter, allowing for more flow through the nozzles. For the reference

values, it was observed that the increase in *C_d* max and maximum nozzle diameter was 2 to 3% greater. The sensitivity analysis result does not indicate any variation in pressure for either the geometric or operational variables. There are two significant spikes in pressure, approximately around 600 and 1800 seconds, respectively. A modification in the boundary conditions causes this transition. The magnitudes of the two observed transitions were similar. This consistency demonstrates that these parameters have minimal impact on the pressure values in this scaled model when they are within their observed limits. Furthermore, it shows that the system attains a quasi-steady state rapidly, generating no significant shift in pressure, an effect that might be due to the scaled model or the uniform spacing of the five nozzles.

The results of the study highlight how much operational factors affect the BCT system. The findings open the way for enhancing the understanding of unsteady compressible flow inside BCT hoses and examine the impact of operational parameters on the pneumatic aspects of the bubble curtain system along the hose length. Therefore, answering the whole sub-question, the sensitivity analysis carried out in Section 8.0.3 provides insight into how operational and geometric factors affect the bubble curtain's flow characteristics.

10 Conclusion

The offshore wind industry is rapidly advancing, expected to play a crucial role in renewable energy production, with a growing emphasis on addressing associated environmental concerns, particularly the impact of underwater noise generated during the installation of wind turbines. In response, bubble curtain technology (BCT) has emerged as a potential solution. The purpose of this study is to study the unsteady compressible flow dynamics within the hose and examine how the Bubble Curtain Technology (BCT) system is influenced by various operating parameters. A thorough examination of the intricacies of bubble curtain systems was guided by the research's well-defined objectives and meticulously organized research questions.

The study began with the development of a 1D unsteady state model for compressible flow in pipes. This foundational model was carefully evaluated against the existing research to ensure the dependability of subsequent studies and adjustments. The flow rates and pressure responses in the current research differed by 2%-4% from those observed in existing research. Differences in the magnitudes of flow rate changes as well as the frequency and amplitude of pressure oscillations after boundary condition changes were observed. These variations may be attributed to the different numerical methods applied to solve the governing equations in each research study, as per this study; however, further validation is required. The existing research, called the Kiuchi model, solved the system's (ODEs) using a completely implicit finite difference approach. On the other hand, in this research, MATLAB ode15s solver was used. Section 4.0.2 provides a general explanation of differences in verification. Going beyond verification, the study examined the addition of nozzles, looking at setups with one, three, and five nozzles, among other combinations. The results of this analysis demonstrated the complex relationship between flow dynamics and design parameters and offered an understanding of how nozzle size and spacing affect system flow dynamics. Furthermore, the characteristics such as flow rate at Node 1, pressure, and flow rate via the nozzle of this modified model were simulated with the use of nozzles of different sizes. The results of this revised model show that in every simulation, the nozzle diameter significantly affected the dynamics of pressure and flow rate. Larger diameters allow for higher flow rates and pressure since they damp out oscillations more efficiently and have less resistance. The system's overall behavior suggests that while having a large number of nozzles might complicate flow dynamics, they can also provide a range of damping mechanisms to help the system recover from disruptions and return to equilibrium.

Furthermore, the complexity of the system increased with the number of nozzles, increasing the numerical instability due to the more complicated wave dynamics and interactions. In this research, the two primary causes of numerical instability were identified: the convective inertia term in the momentum equation and various discretization strategies. However, further verification is needed to confirm these findings. A thorough examination of the magnitude of the convective inertia term with the pressure gradient component of the momentum equation is done to improve this instability in the research. Over the range of nodes and time periods investigated, the results demonstrated that the convective inertia term is nearly equal to zero for this research. It appears from this that the term has a minimal impact on the dynamics of our particular system. In addition, the convective inertia term is eliminated from the updated model using nozzles for this research, and the models with and without convective inertia are compared in Section 6.0.4. Following a comparative examination, it was shown that in all configurations, the lack of the convective inertia factor leads to fewer transient fluctuations and a more stable numerical response. Removing the term from the model had a relatively lower influence

on pressures and flow rates. However, it simplifies transient dynamics, leading to smoother transitions and contributing to stability by reducing fluctuations in the graphs for this research.

As these developments progressed, the final model with five nozzles was chosen as the foundation for the BCT model. Scaled BCT model: Developed to replicate the real BCT and fulfill the computing requirements of simulating a full-scale BCT system in MATLAB. This scaled model utilized actual Bubble Curtain Technology (BCT) values based on the existing literature. Parameters related to the environment and the BBC pneumatic system are the two groups of input parameters for the numerical model. A constant supply of compressed air is not always necessary due to various operational and environmental situations, which is the reason for time-varying boundary conditions were chosen. The steady state and transient effects are two significant effects that are observed in the numerical model's output because of time-varying boundary conditions. Sensitivity analysis uses both steady-state and transient impacts to help comprehend how the system responds to changes in operational and geometric parameters over time.

Due to a change in the flow condition, the highest *C_d* value indicated a reduction in the magnitude of the reverse flow, and the minimum value of *C_d* indicated an increase in the magnitude of backflow in both transient stages. Higher *Q_FAD* values correlate with increased flow rates, suggesting reduced transient flow dynamics along the length of the hose. Conversely, lower *Q_FAD* values reflect reverse flow, which is caused by abrupt boundary conditions and will lead to larger negative flow rates. Additionally, throughout the measured range, the water depth revealed the same variation in flow rate. When considering the practical aspects, this uniformity in flow rate suggests that the BCT system may be utilized over a range of water depths without requiring significant modifications to account for variations in depth. In comparison to the reference value, the larger hose and nozzle diameters showed an increase in flow rate in both transient phases and a further drop in the magnitude of reverse flow, whereas the minimum hose and nozzle diameters demonstrated a rise in the magnitude of backflow. In addition, adjusting the hose length and nozzle spacing has an impact on the system's response; longer hose lengths and smaller nozzle spacing are prominent in minimizing negative flow and proved effective for adjusting the required flow rates. Except for the nozzle diameter and coefficients of discharge *C_d*, the sensitivity analysis of the flow rate via the nozzle reveals no difference in flow rate at any other parameters. It was found that the increase in *C_d* max and maximum nozzle diameter was 2-3% higher when compared to reference values. The sensitivity analysis results show no fluctuation in pressure for either the geometric or operational factors within the observed ranges. Furthermore, it demonstrates that the system quickly achieves a quasi-steady state, generating no significant shift in pressure, an effect that might be due to the scaled model or the uniform spacing of the five nozzles.

Finally, this thesis contributes to the pneumatic knowledge of BCT systems while also providing an understanding of transient flow in the hose that might not be homogeneous for the full-scale BCT. The progression from a simple pipeline model to a comprehensive concept of scaled BCT systems illustrates rigorous and systematic academic study.

Recommendation

- The outcomes of this study provide a foundation for future research in this field. For a more comprehensive study, future studies should simulate a full-scale BCT model. This would most likely need enhanced computational resources or the application of more efficient algorithms capable of handling the complexity of a larger system.

- Future models also take into account non-isothermal conditions. Such settings are more realistic than real underwater environments and may have a significant impact on the behavior of bubble curtains, particularly during longer periods of operation. Furthermore, while the proposed model is limited to isothermal flow conditions, investigating the impact of temperature gradients on flow dynamics may give new insights into the dynamics of BCT systems. This might entail studying heat transmission between the air in the bubbles and the surrounding water, as well as the effects of various water temperatures at different depths.

- Finally, alternate discretization techniques other than the center, backward, and forward procedures implemented in this work should be investigated. These may include more advanced numerical algorithms capable of providing higher stability and precision in the solutions to the governing equations. Future models that investigate these discretization approaches may be able to overcome some of the numerical instabilities identified in this study.

References

1. Rumes, B. *et al.* Environmental Impacts of Offshore Wind Farms in the Belgian Part of the North Sea: Assessing and Managing Effect Spheres of Influence (2018).
2. Bulson, P. in *Coastal Engineering 1968* 995–1015 (1968).
3. ThayerMahan. https://www.thayermahan.com/systems/big-bubble-curtain.
4. Rodrigues, S., Restrepo, C., Kontos, E., Teixeira Pinto, R. & Bauer, P. Trends of offshore wind projects. *Renewable and Sustainable Energy Reviews* **49,** 1114–1135. ISSN: 1364-0321. https://www.sciencedirect.com/science/article/pii/S1364032115003627 (2015).
5. Kallehave, D., Byrne, B. W., LeBlanc Thilsted, C. & Mikkelsen, K. K. Optimization of monopiles for offshore wind turbines. *Philosophical Transactions of the Royal Society A: Mathematical, Physical and Engineering Sciences* **373,** 20140100 (2015).
6. Koschinski, S. & Lüdemann, K. Noise mitigation for the construction of increasingly large offshore wind turbines. *Technical Options for Complying with Noise Limits; The Federal Agency for Nature Conservation: Isle of Vilm, Germany* (2020).
7. Mooney, T. A., Andersson, M. H. & Stanley, J. ACOUSTIC IMPACTS OF OFFSHORE WIND ENERGY ON FISHERY RESOURCES: An Evolving Source and Varied Effects Across a Wind Farm's Lifetime. *Oceanography* **33,** 82–95. ISSN: 10428275, 2377617X. https://www.jstor.org/stable/26965752 (2023) (2020).
8. Würsig, B., Greene Jr, C. & Jefferson, T. Development of an air bubble curtain to reduce underwater noise of percussive piling. *Marine environmental research* **49,** 79–93 (2000).
9. Tsouvalas, A. & Metrikine, A. Noise reduction by the application of an air-bubble curtain in offshore pile driving. *Journal of Sound and Vibration* **371,** 150–170 (2016).
10. Fulton, N. & Kuo, C. *Minimising Underwater Noise Impact from Offshore Activities* in *SPE Offshore Europe Conference and Exhibition* (2013), SPE–166552.
11. Thomsen, F., Verfuss, T. & Perrow, M. Mitigating the effects of noise. *Wildlife and Wind Farms-Conflicts and Solutions: Offshore: Monitoring and Mitigation,* 207–241 (2019).
12. Song, Z. *et al. Investigation on Pile Driving Noise Production and Mitigation Through Bubble Curtain* in *International Conference on Marine Equipment & Technology and Sustainable Development* (2023), 1–9.
13. Vagle, S. On the impact of underwater pile-driving noise on marine life. *Ocean Science Productivity Division, Institute of Ocean Sciences, DFO/Pacific* (2003).
14. *Noordzeeloket* https://www.noordzeeloket.nl/en/policy/europese/background-documents/background-documents-0/. Accessed May 18, 2023.
15. Petrie, F. *Washington State Ferries' Experience with Bubble Curtains: Purpose, Hardware, and Use* in *2005 Summer Meeting/Conference of the Transportation Research Board ADC40 (A1F04) Noise & Vibration Committee* (2005).
16. Koschinski, S. Underwater Unexploded Ordnance - Methods for a Cetacean-friendly Removal of Explosives as Alternatives to Blasting.
17. Effects of Pile Driving on Marine Animals. https://dosits.org/animals/effects-of-sound/anthropogenic-sources/pile-driving/.
18. Thorley, A. & Tiley, C. Unsteady and transient flow of compressible fluids in pipelines—A review of theoretical and some experimental studies. *International journal of heat and fluid flow* **8,** 3–15 (1987).
19. Hai, W., Xiaojing, L. & Weiguo, Z. Transient flow simulation of municipal gas pipelines and networks using semi implicit finite volume method. *Procedia Engineering* **12,** 217–223 (2011).
20. Quintela, P., Pérez Parra, J. C., Useche Castro, L. & Lapo Palacios, M. Simulation of transient flow in gas pipelines using the finite volume method (2021).

21. Ouchiha, Z. *et al.* An investigation of highly pressurized transient fluid flow in pipelines. *International journal of pressure vessels and piping* **92,** 106–114 (2012).
22. Colebrook, C. F. *et al.* Correspondence. turbulent flow in pipes, with particular reference to the transition region between the smooth and rough pipe laws.(includes plates). *Journal of the Institution of Civil engineers* **12,** 393–422 (1939).
23. Panton, R. L. *Incompressible flow* (John Wiley & Sons, 2024).
24. Novotny, A. & Straskraba, I. *Introduction to the mathematical theory of compressible flow* (OUP Oxford, 2004).
25. Terenzi, A. *Flow Analysis for Hydrocarbon Pipeline Engineering* (Gulf Professional Publishing, 2022).
26. Kiuchi, T. An implicit method for transient gas flows in pipe networks. *International Journal of Heat and Fluid Flow* **15,** 378–383 (1994).
27. Chua, T.-S. *Mathematical software for gas transmission networks* PhD thesis (University of Leeds, 1982).
28. Van Reet, J. & Skogman, K. *The Effect of Measurement Uncertainly on Real Time Pipeline Modeling Applications* in *ASME Pipeline Engineering Symposium* (1987), 29–33.
29. Ke, S. & Ti, H. Transient analysis of isothermal gas flow in pipeline network. *Chemical Engineering Journal* **76,** 169–177 (2000).
30. Schiesser, W. E. & Griffiths, G. W. *A compendium of partial differential equation models: method of lines analysis with Matlab* (Cambridge University Press, 2009).
31. Lecheler, S. *Computational Fluid Dynamics: Getting Started Quickly with ANSYS CFX 18 Through Simple Examples* (Springer Nature, 2022).
32. Inc., T. M. *MATLAB version: 9.13.0 (R2022b)* Natick, Massachusetts, United States, 2022. `https://www.mathworks.com`.
33. Chaczykowski, M. Transient flow in natural gas pipeline–The effect of pipeline thermal model. *Applied Mathematical Modelling* **34,** 1051–1067 (2010).
34. Abbaspour, M., Chapman, K. S. & Keshavarz, A. *Dynamic modeling of non-isothermal gas pipeline systems* in *International Pipeline Conference* **41766** (2004), 2155–2163.
35. Abbaspour, M. & Chapman, K. Nonisothermal transient flow in natural gas pipeline (2008).
36. Shapiro, A. H. The dynamics and thermodynamics of compressible fluid flow. *New York: Ronald Press* (1953).
37. Kayser, J. C. & Shambaugh, R. L. Discharge coefficients for compressible flow through small-diameter orifices and convergent nozzles. *Chemical engineering science* **46,** 1697–1711 (1991).
38. Mazzei, L., Winchler, L. & Andreini, A. Development of a numerical correlation for the discharge coefficient of round inclined holes with low crossflow. *Computers & Fluids* **152,** 182–192 (2017).
39. Nehls, G. & Bellmann, M. *Weiterentwicklung und Erprobung des" Großen Blasenschleiers" zur Minderung der Hydroschallemissionen bei Offshore-Rammarbeiten: Schlussbericht* (BioConsult SH GmbH & Company KG; itap GmbH Oldenburg; Hydrotechnik Lübeck . . ., 2016).

A

Modification of the current research model with minimum nozzle diameter

The appendix examines the changes in flow rate and pressure impact while using a minimal nozzle model. There won't be any significant difference in the outcomes between the 1 mm diameter and the Kuchi mode.

Single Nozzle

- Case I: The nozzle's size is changed to $D_{nozzle} = 1\,\text{mm}$ to observe the change in flow rate and pressure

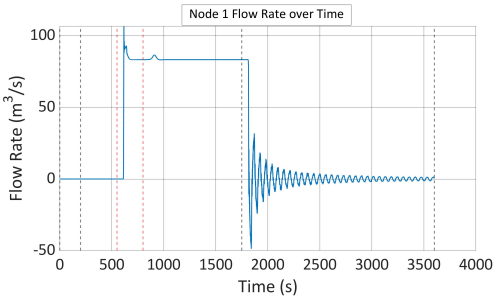

(a) Present study: Flow rate at Node 1 with $D_{nz} = 1\,\text{mm}$

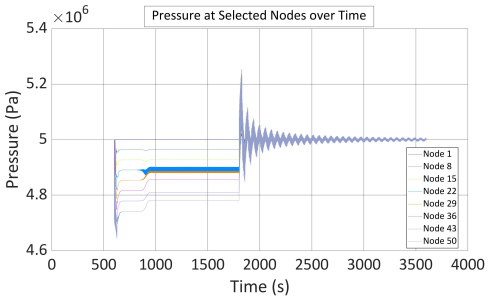

(b) Present study: Pressure at selected Nodes

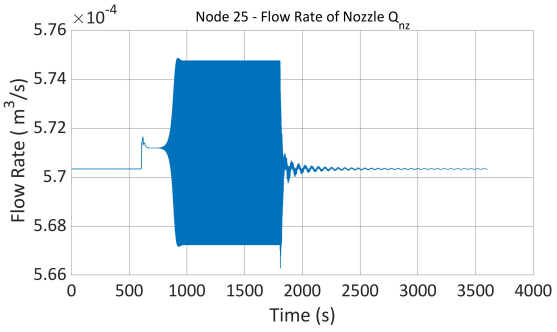

(c) Present study: Flow rate of nozzle at $D_{nz} = 1\,\text{mm}$

Figure A.1: Node 1 flow rate, pressure, and Nozzle flow rate at $D_{nz} = 1\,\text{mm}$ for single nozzles

The nozzle diameter being lowered to 1 mm results in a reduced capacity to dampen oscillations when evaluating the flow rate at Node 1. This is because less fluid can travel per unit of time, as can be seen after 1800 seconds. Furthermore, the flow at the node at 600 and 1800 seconds exhibits two transient effects that are nearly identical to the model without nozzles. This demonstrates very clearly the importance of nozzle sizes. A reduced damping mechanism is discovered to be the cause of the large-scale pressure fluctuation at 1800 seconds. With a low magnitude of 5.75×10^{-4} m^3/sec, the flow

rate via nozzles shows that less extra flow rate is entering the pipe through nozzles. However, with such a small diameter, the graph exhibits instability due to the inertia term.

Three nozzles

- Case I: The nozzle's size is changed to $D_{nozzle} = 1\,\text{mm}$ to observe the change in flow rate and pressure

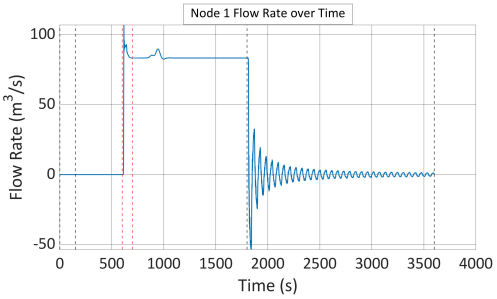

(a) Present study: Flow rate at Node 1 with $D_{nz} = 1\,\text{mm}$

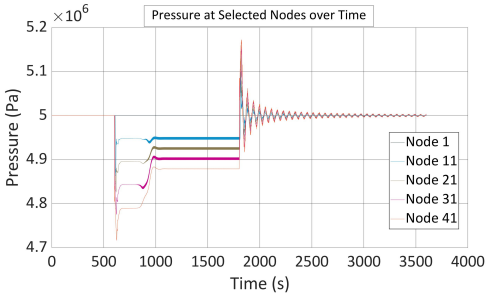

(b) Present study: Pressure at selected Nodes

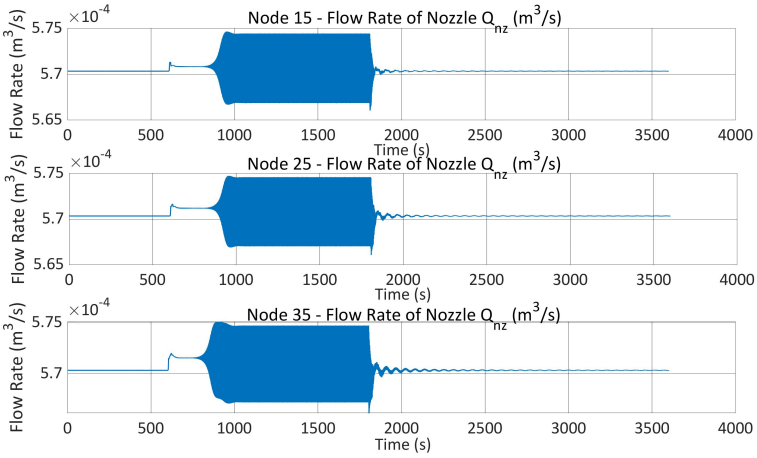

(c) Present study: Flow rate of nozzle at $D_{nz} = 1\,\text{mm}$

Figure A.2: Node 1 flow rate, pressure, and Nozzle flow rate at $D_{nz} = 1\,\text{mm}$ for three nozzles

The above figure A.2 shows that the model without a nozzle is not significantly affected by the implementation of three nozzles with a 1mm diameter nozzle at node locations 25, 25, and 35. Slight fluctuations are seen at 800 seconds; the peaks indicate extra flow that is passing through the nozzle and into the pipe. Given that the cumulative dampening of all three nozzles is modest and does not result in the removal of oscillation, the oscillation observed after 1800 seconds is caused by a sudden shift in boundary conditions. A change in the boundary condition caused an abrupt rise in flow rate, which is what caused the pressure decrease that was seen at 600 seconds. Furthermore, because of the lower nozzle size, the oscillation that was seen after 1800 seconds demonstrates the minimal damping mechanism. When other diameter variations of nozzles are compared, the flow rate via nozzles is the lowest flow rate that can be seen.

A.0.1. Five nozzles

- Case I: The nozzle's size is changed to $D_{nozzle} = 1\,\text{mm}$ to observe the change in flow rate and pressure

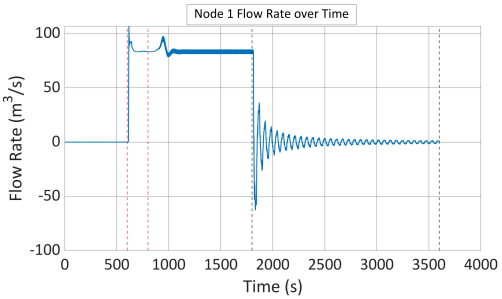

(a) Present study: Flow rate at Node 1 with $D_{nz} = 1\,\text{mm}$

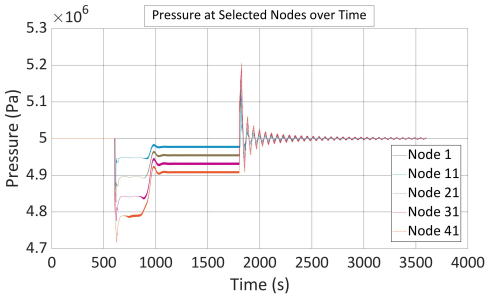

(b) Present study: Pressure at selected Nodes

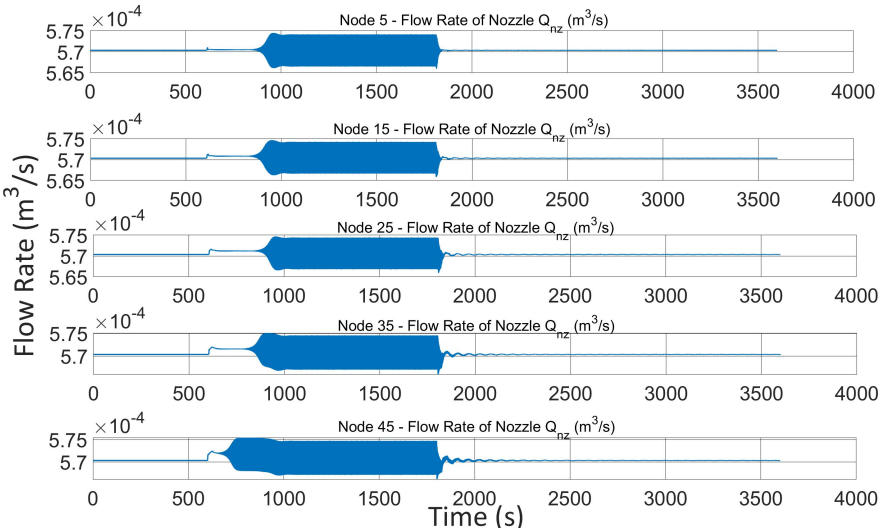

(c) Present study: Flow rate of nozzle at $D_{nz} = 1\,\text{mm}$

Figure A.3: Node 1 flow rate, pressure, and Nozzle flow rate at $D_{nz} = 1\,\text{mm}$ for five nozzles

The flow rate and pressure variations after the placement of nozzles at node positions 5, 15, 25, 25, and 45 are shown in the above figure. Similar to the situation of single and three nozzles, the influence of the small diameter of the nozzles has little impact on the pressure and flow rate. Because of the nozzles, more fluid can enter the pipe, which causes the flow rate at Node 1 to surge at 800 seconds. Even though the nozzle is tiny, there is still diversity observed. Since there is less cumulative damping than in other 210 mm and 150 mm diameters, the oscillation seen as a result of the rapid shift in the boundary condition at 1800 seconds does not result in elimination. For the model with five nozzles, the pressure and flow rate exhibit a similar pattern to those of the single and three nozzles model.

B

Nozzle diameter variation for models with and without the inertia term

The comparative study of the with and without convective inertia term is carried out for diameters of 500 mm and 200 mm for a single nozzle, 280 mm and 200 mm for three nozles, and 210 mm and 200 mm for five nozzles in Section 7 of this thesis. This appendix will address the 150mm and 1mm diameters.

Single Nozzle

- The size of the nozzle is equivalent $D_{nozzle} = 150\,\text{mm}$

Flowrate at Node 1

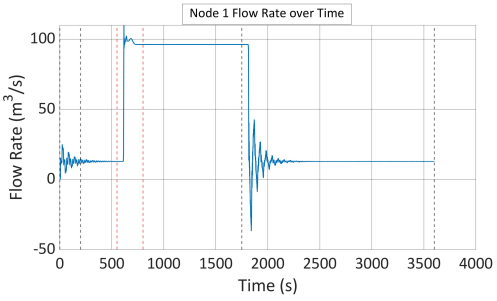

(a) Present study: Flow rate at node 1 with convective inertia

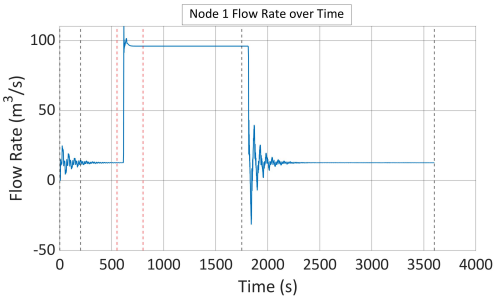

(b) Present study: Flow rate at node 1 without convective inertia

Figure B.1: The flow rate at node 1 with and without convective inertia at $D_{nz} = 150\,\text{mm}$ for single nozzle

Pressure at selected Nodes

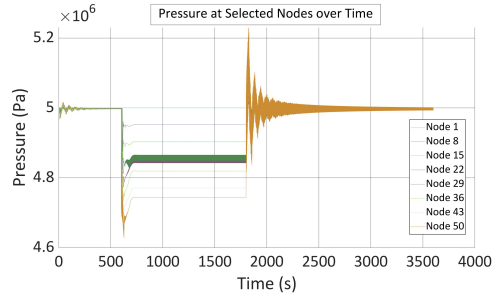

(a) Present study: Pressure with convective inertia

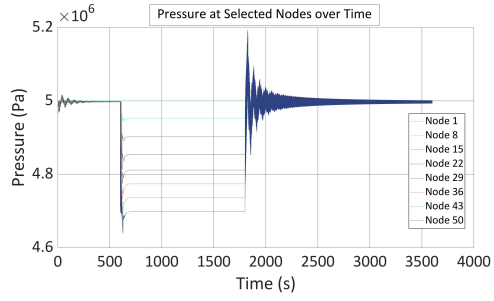

(b) Present study: Pressure without convective inertia

Figure B.2: Pressure at selected nodes with and without convective inertia for single nozzle with $D_{nz} = 150\,\text{mm}$

Flow rate through nozzle

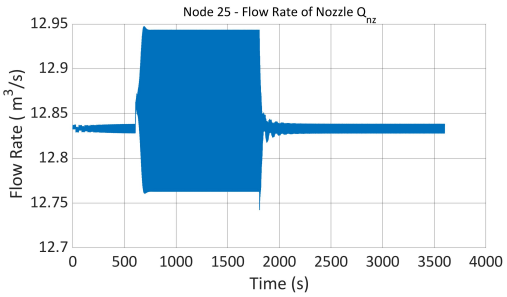

(a) Present study: Flow rate through nozzle with convective inertia

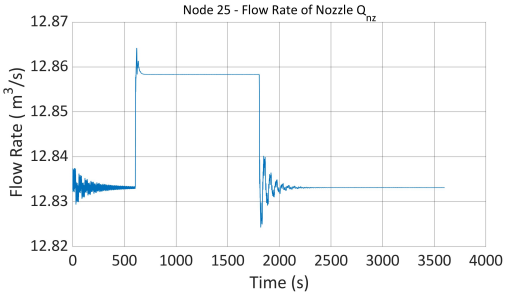

(b) Present study: Flow rate through nozzle without convective inertia

Figure B.3: Flow rate through a nozzle with and without convective inertia for the single nozzle with $D_{nz} = 150\,\text{mm}$

- The size of the nozzle of minimum $D_{nozzle} = 1\,\text{mm}$

Flowrate at Node 1

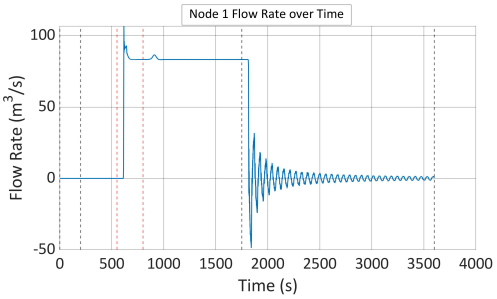

(a) Present study: Flow rate at node 1 with convective inertia

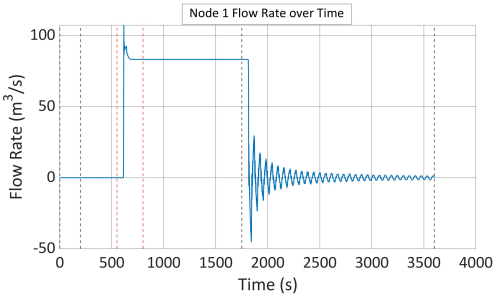

(b) Present study: Flow rate at node 1 without convective inertia

Figure B.4: The flow rate at node 1 with and without convective inertia at $D_{nz} = 1\,\text{mm}$ for single nozzle

Pressure at selected Nodes

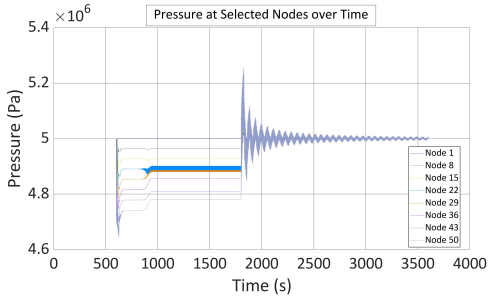

(a) Present study: Pressure with convective inertia

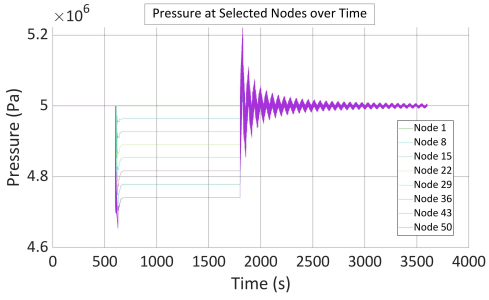

(b) Present study: Pressure without convective inertia

Figure B.5: Pressure at selected nodes with and without convective inertia for single nozzle with $D_{nz} = 1\,\text{mm}$

Flow rate through nozzle

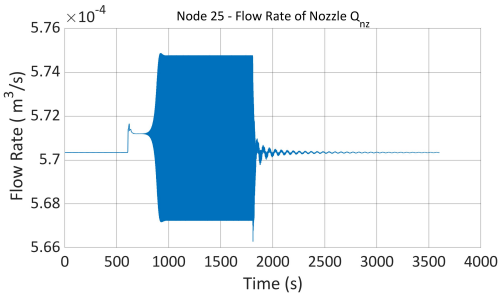

(a) Present study: Flow rate through nozzle with convective inertia

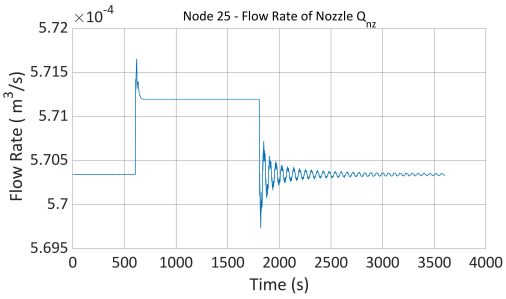

(b) Present study: Flow rate through nozzle without convective inertia

Figure B.6: Flow rate through a nozzle with and without convective inertia for the single nozzle with $D_{nz} = 1\,\text{mm}$

The flow rate graph for the nozzle at Node 25, which has a 150 mm and a 1 mm diameter, exhibits consistent behavior and no bulges, suggesting that the numerical instability issues that the model with the inertia term had have been reduced. These instabilities were probably induced by the convective inertia factor in the momentum equation, which can be sensitive to spatial discretization and the solver's ability to record steep gradients in the flow variables. The results, both with and without the convective inertia factor, indicate a small variation of about 0.07% in the model with a nozzle diameter of 1 mm and 0.03% with a nozzle diameter of 1 mm. This variation is within allowable tolerance bounds and indicates that the absence of these components does not significantly affect the simulation. This demonstrates how removing the convective inertia component may improve numerical stability by simplifying the behavior of the system with stable graphs and reducing fluctuations.

Three Nozzle

- The size of the nozzle is equivalent to $D_{nozzle} = 150\,\text{mm}$

Flowrate at Node 1

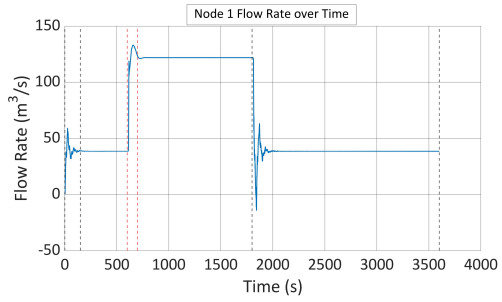

(a) Present study: Flow rate at node 1 with convective inertia

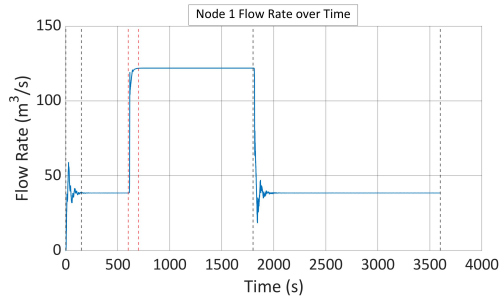

(b) Present study: Flow rate at node 1 without convective inertia

Figure B.7: The flow rate at node 1 with and without convective inertia at $D_{nz} = 150\,\text{mm}$ for three nozzles

Pressure at selected Nodes

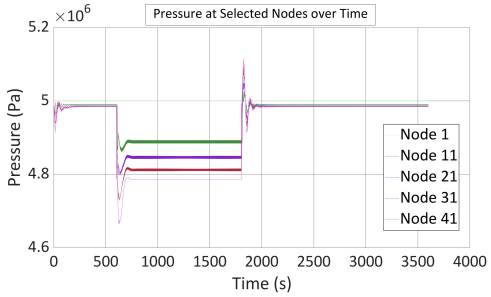

(a) Present study: Pressure with convective inertia

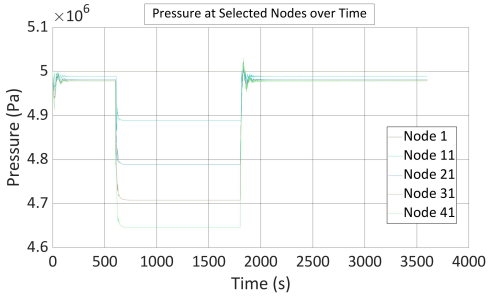

(b) Present study: Pressure without convective inertia

Figure B.8: Pressure at selected nodes with and without convective inertia for three nozzles with $D_{nz} = 150\,\text{mm}$

Flow rate through nozzle

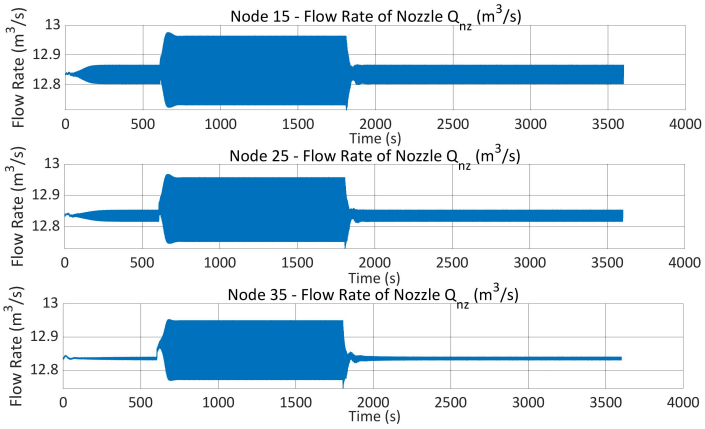

(a) Present study: Flow rate through nozzle with convective inertia

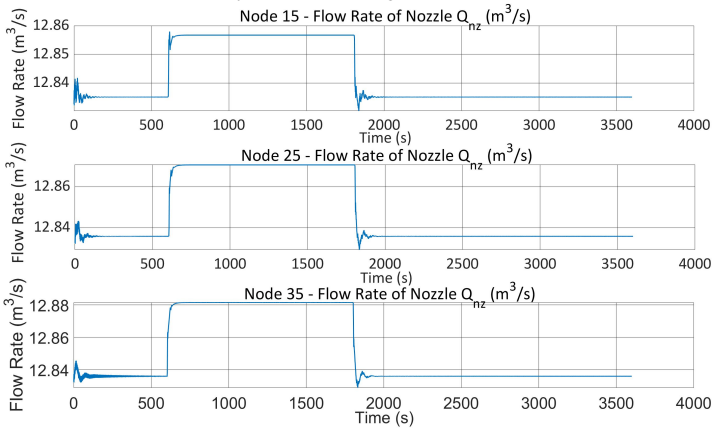

(b) Present study: Flow rate through nozzle without convective inertia

Figure B.9: Flow rate through a nozzle with and without convective inertia for the three nozzles with $D_{nz} = 150\,\text{mm}$

- The size of the nozzle of minimum $D_{nozzle} = 1\,\text{mm}$

Flowrate at Node 1

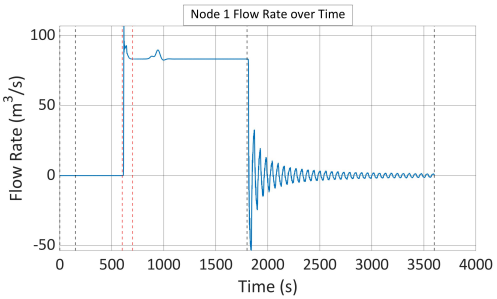

(a) Present study: Flow rate at node 1 with convective inertia

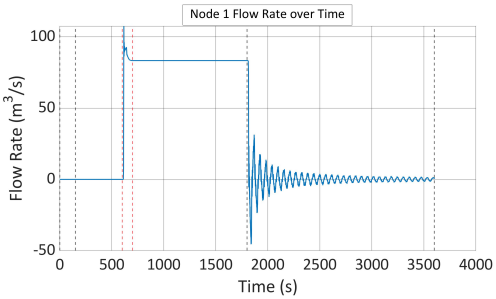

(b) Present study: Flow rate at node 1 without convective inertia

Figure B.10: The flow rate at node 1 with and without convective inertia at $D_{nz} = 1\,\text{mm}$ for three nozzles

Pressure at selected Nodes

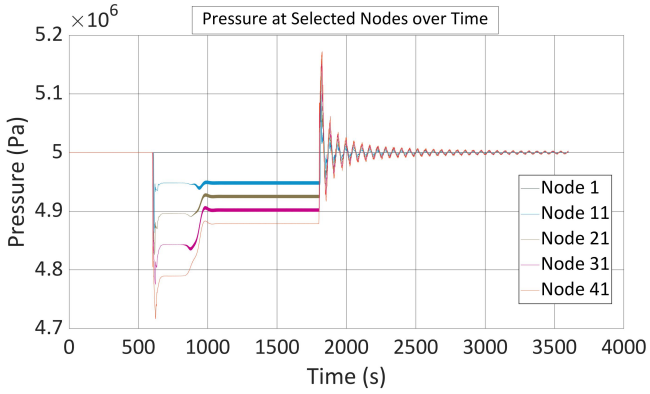

(a) Present study: Pressure with convective inertia

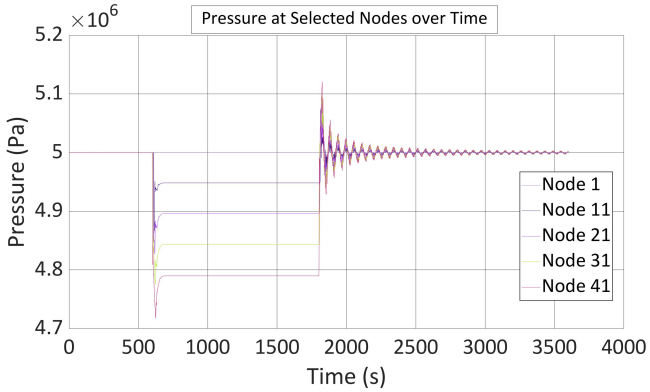

(b) Present study: Pressure without convective inertia

Figure B.11: Pressure at selected nodes with and without convective inertia for three nozzle with $D_{nz} = 1\,\text{mm}$

Flow rate through nozzle

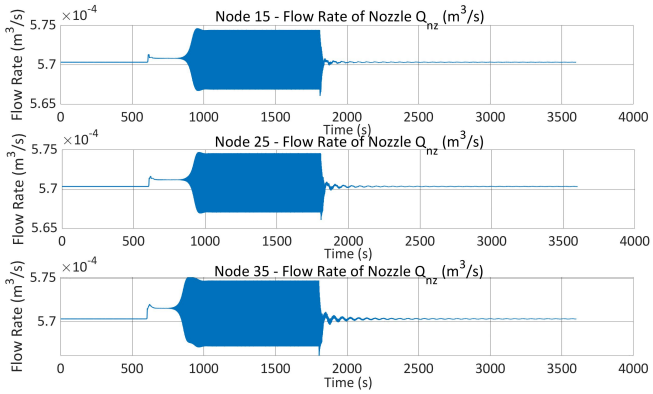

(a) Present study: Flow rate through nozzle with convective inertia

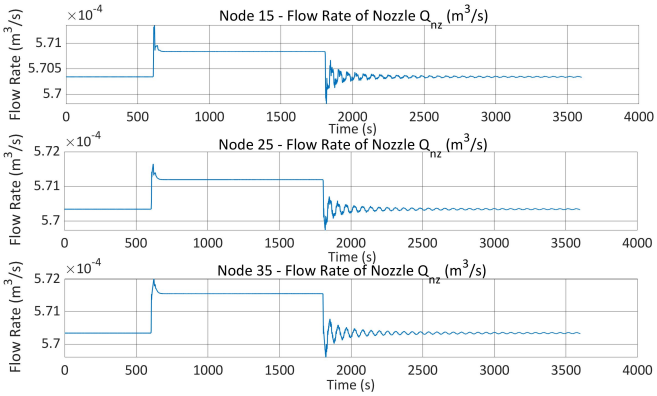

(b) Present study: Flow rate through nozzle without convective inertia

Figure B.12: Flow rate through a nozzle with and without convective inertia for the three nozzles with $D_{nz} = 1\,\text{mm}$

The flow rate through the three nozzles exhibits a bulge-free, stable behavior, proving that the inertia term's numerical instability issues have been resolved. The results indicate that the absence of the convective inertia factor does not significantly affect the simulation. It varies by approximately 0.14% for nozzle diameters of 150 mm and 0.03% for nozzle diameters of 1 mm, both of which are within permissible tolerance ranges. The model does not vary in the absence of the convective inertia component, indicating that this reduction produces a simulation that is more numerically robust and stable.

Five Nozzle

- The size of the nozzle is equivalent to $D_{nozzle} = 150\,\text{mm}$

Flowrate at Node 1

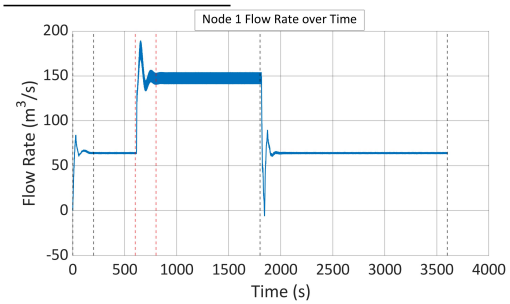

(a) Present study: Flow rate at node 1 with convective inertia

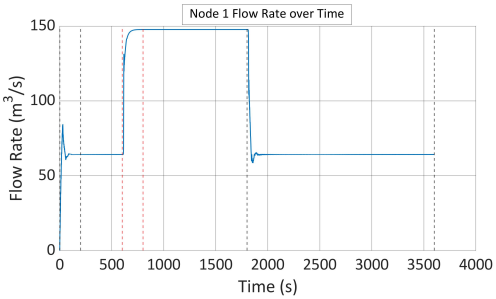

(b) Present study: Flow rate at node 1 without convective inertia

Figure B.13: The flow rate at node 1 with and without convective inertia at $D_{nz} = 150\,\text{mm}$ for five nozzles

Pressure at selected Nodes

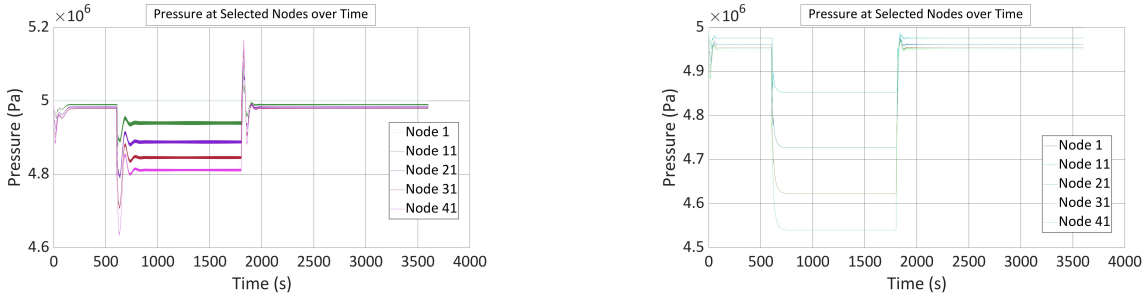

(a) Present study: Pressure with convective inertia

(b) Present study: Pressure without convective inertia

Figure B.14: Pressure at selected nodes with and without convective inertia for five nozzles with $D_{nz} = 150\,\text{mm}$

Flow rate through nozzle

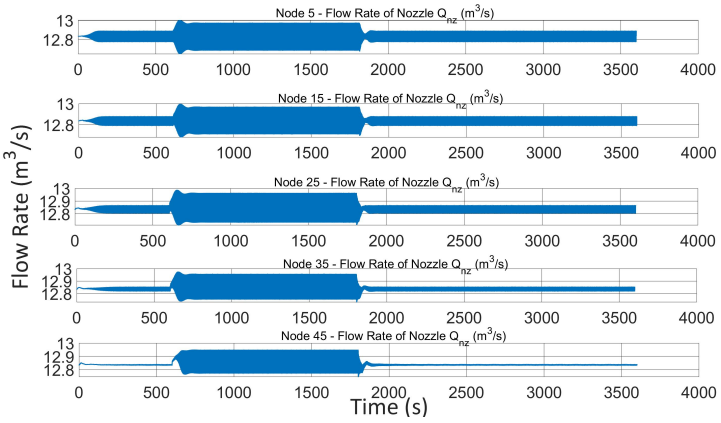

(a) Present study: Flow rate through nozzle with convective inertia

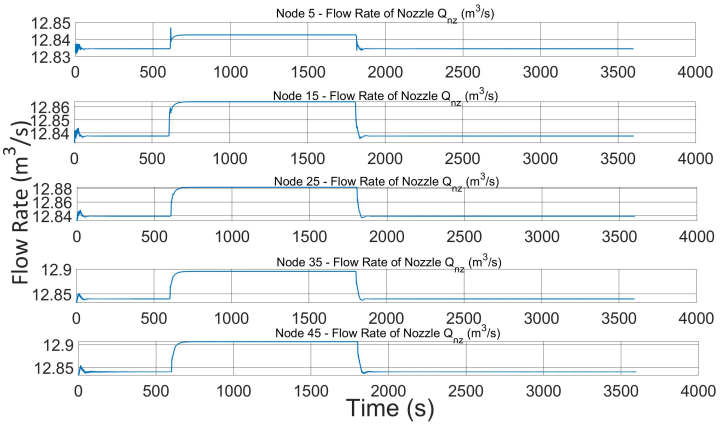

(b) Present study: Flow rate through nozzle without convective inertia

Figure B.15: Flow rate through a nozzle with and without convective inertia for the five nozzles with $D_{nz} = 150\,\text{mm}$

- The size of the nozzle of minimum $D_{nozzle} = 1\,\text{mm}$

Flowrate at Node 1

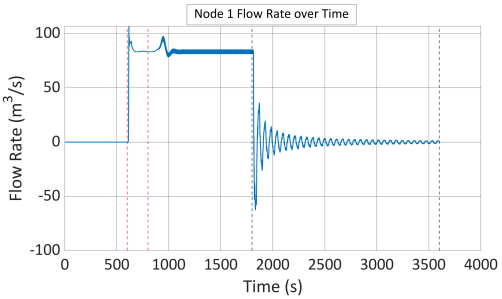

(a) Present study: Flow rate at node 1 with convective inertia

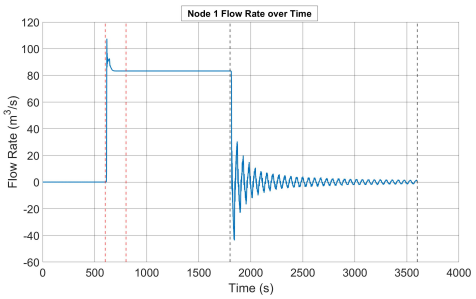

(b) Present study: Flow rate at node 1 without convective inertia

Figure B.16: The flow rate at node 1 with and without convective inertia at $D_{nz} = 1\,\text{mm}$ for five nozzles

Pressure at selected Nodes

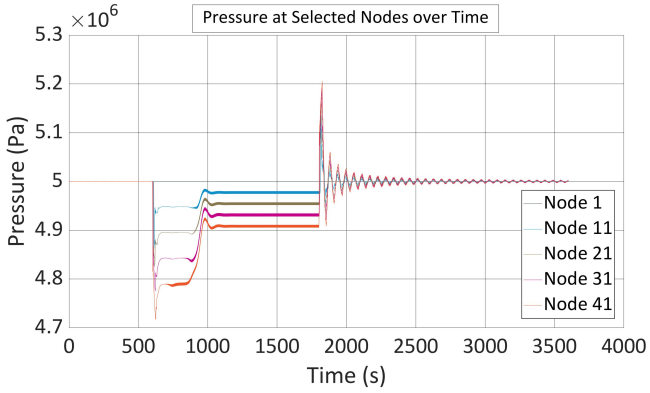

(a) Present study: Pressure with convective inertia

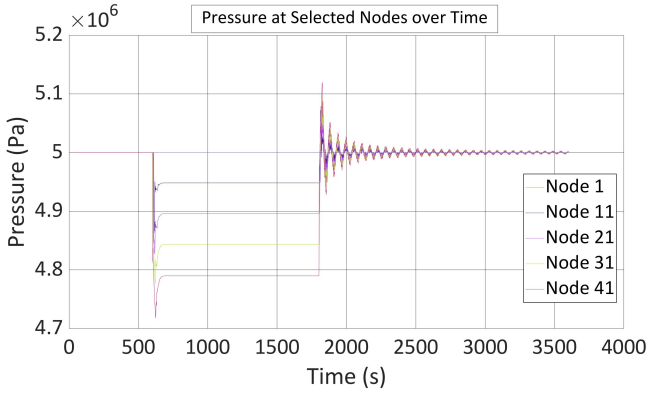

(b) Present study: Pressure without convective inertia

Figure B.17: Pressure at selected nodes with and without convective inertia for five nozzle with $D_{nz} = 1\,\text{mm}$

Flow rate through nozzle

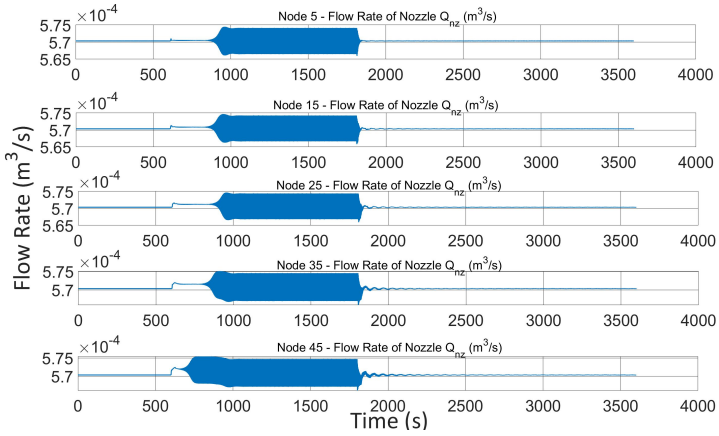

(a) Present study: Flow rate through nozzle with convective inertia

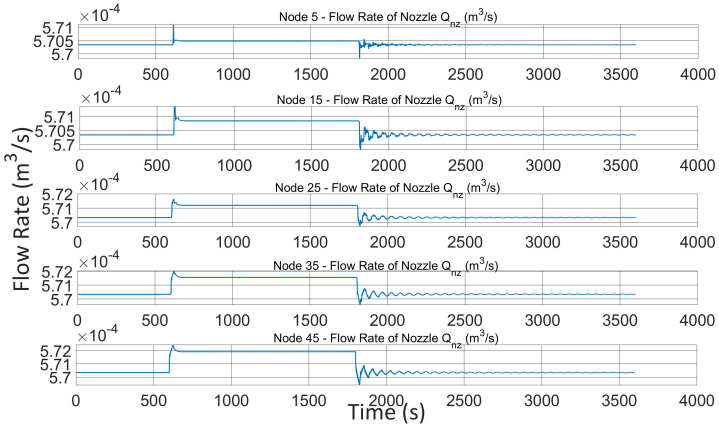

(b) Present study: Flow rate through nozzle without convective inertia

Figure B.18: Flow rate through a nozzle with and without convective inertia for the five nozzles with $D_{nz} = 1\,\text{mm}$

The flow rates of the five nozzles show a continuous, bulge-free behavior, indicating that the numerical instability problems with the inertia term have been resolved. The results show that the absence of the convective inertia factor has minimal impact on the simulation, with variations of about 0.15% and 0.03%, respectively, for nozzle diameters of 150 and 1 mm, respectively. These variations are within tolerance limits. When the convective inertia component is eliminated, the model maintains its stability, suggesting that this reduction leads to more stable graphs and reduced fluctuations.

C

Scaled BCT model with different cases

This type of boundary condition might be an operating profile or a controlled testing sequence where the BCT is turned on and off in two separate phases to meet various operational targets or adapt to shifting environmental circumstances. By giving a simplified representation of how the system could be operated in response to external needs or internal regulations, the two-step boundary condition in the script represents various operational possibilities.

Boundary conditions: Two step-wise

- $P(x = 1, t) = 8 \times 10^5\,\text{Pa}$,
- $m(x = L, t) = f\_1(t)$.

$$f\_1(t) = \begin{cases} 0\,\text{kg/s} \cdot \text{m}^2 & \text{if } 0 \leq t < 200\,\text{sec} \\ 2.1\,\text{kg/s} \cdot \text{m}^2 & \text{if } 200 \leq t < 800\,\text{sec} \\ 3.54\,\text{kg/s} \cdot \text{m}^2 & \text{if } 800 \leq t < 1800\,\text{sec} \\ 0\,\text{kg/s} \cdot \text{m}^2 & \text{if } 1800 \leq t < 3600\,\text{sec} \end{cases}$$

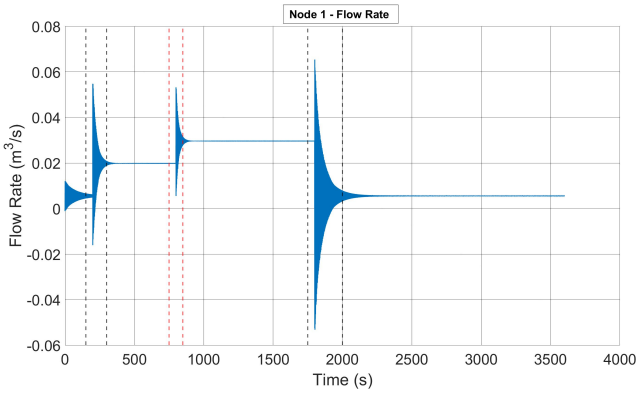

(a) Reference model: Flow rate at node 1

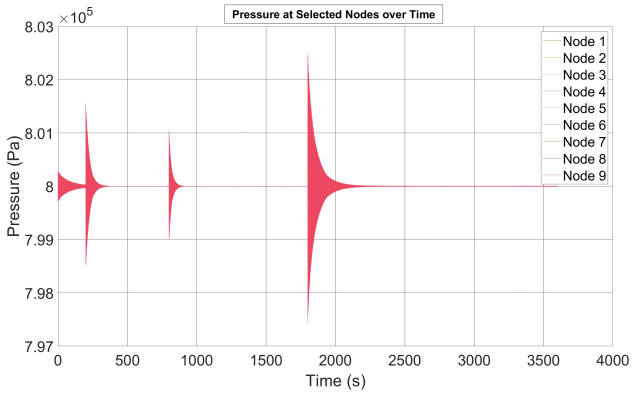

(b) Reference model: Pressure at selected nodes

Figure C.1: The flow rate at node 1 and pressure of BCT reference model with two-step boundary condition

The mass flow rate suddenly increases following the boundary condition, causing the flow rate to abruptly decline after an initial spike of around 200 seconds. Following the first surge, the flow rate levels drop to around 0.02 m^3/s, which is a steady state. A second, more noticeable spike occurs at 600 seconds, during which the flow rate increases as a result of a modification in the boundary condition. It then stabilizes between 800 and 1800 seconds. A shift in the system's circumstances, such as a two-step control action, is the reason for the behavior. When the flow rate ceases after 1800 seconds, it exhibits a sharp decline until it approaches the steady-state condition. There are distinct pressure spikes that occur at 200, 800, and 1800 seconds, among other intervals. These spikes occur in all nodes and are sharp, suggesting sudden and substantial occurrences in the system reflecting the two-step boundary condition. All nodes exhibit the same spike pattern, which suggests that the pressure disturbance spreads rapidly throughout the system.

Flowrate through nozzles

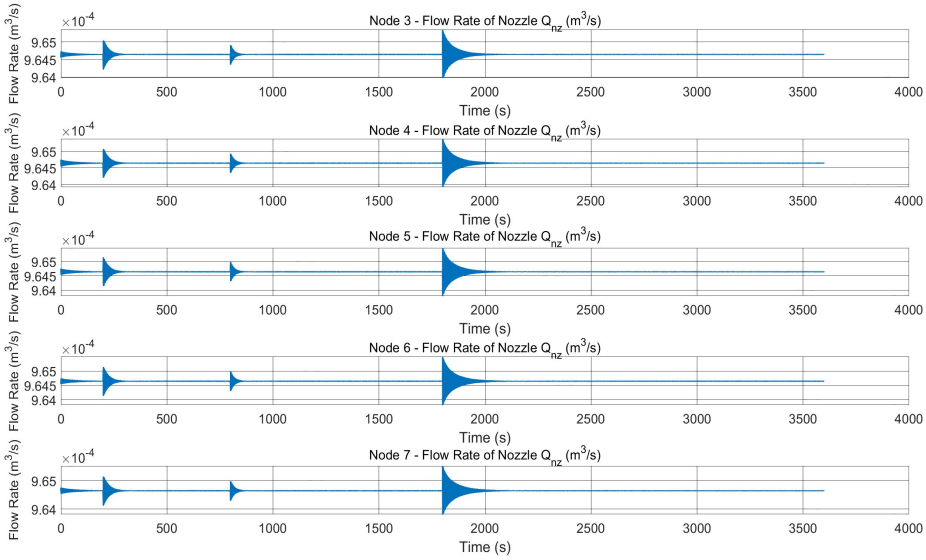

Figure C.2: The flow rate through nozzle of BCT reference model with two-step boundary condition

The flow rate via the nozzles at Nodes 3, 4, 5, 6, and 7 is shown against time in the graph. The flow rate of each node has a significant initial increase before swiftly falling back to its baseline level. Every node exhibits this behavior at roughly the same time, suggesting a coordinated event that affects every node at once due to equal spacing between the nozzles. The spikes exhibit asymmetry, exhibiting an abrupt rise followed by a more gradual decline. This implies a quick reaction to alterations in the two-step boundary conditions, followed by a gradual restoration of the standard operating circumstances. The strong spikes indicate a scenario in which a change in the boundary condition causes the flow rate to increase quickly.

Boundary conditions: Constant supply

- $P(x = 1, t) = 8 \times 10^5$ Pa,
- $m(x = L, t) = 2.94\text{kg/s} \cdot \text{m}^2$.

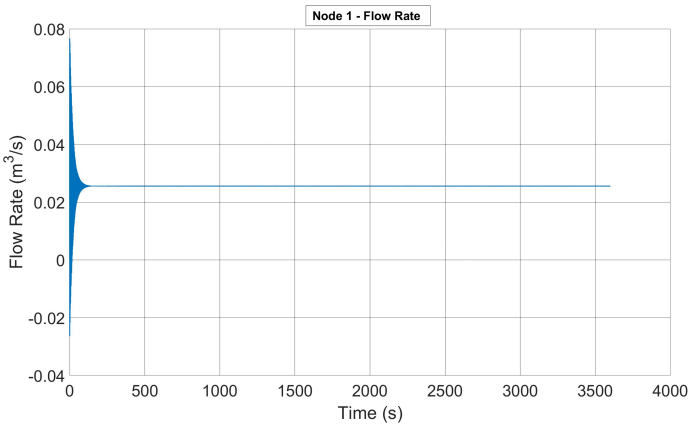

(a) Reference model: Flow rate at node 1

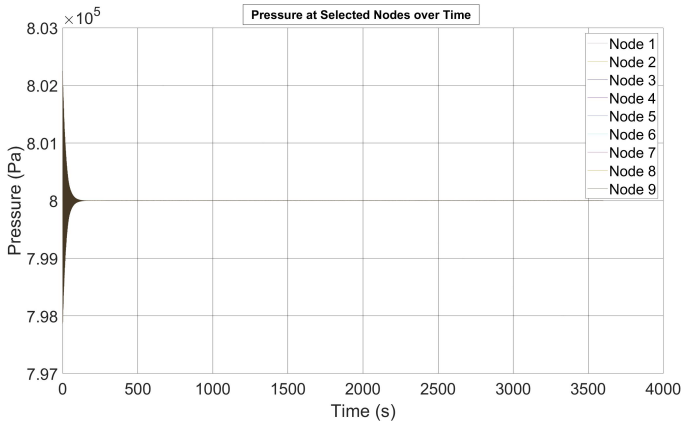

(b) Reference model: Pressure at selected nodes

Figure C.3: The flow rate at node 1 and pressure of BCT reference model with constant boundary condition

The flow rate suddenly spikes at first and then falls gradually. This is characteristic of systems in which initial circumstances are abruptly changed. Following the first transient, the flow rate returns to a steady state. This is the result of the final node's constant boundary condition being set. The system has attained equilibrium when the input and output are balanced, as shown by the constant flow rate. According to the graph, the BCT system maintains a steady operating condition after reacting swiftly to the initial change. At Node 1, the pressure and flow rate exhibit a similar pattern. After the first drop, all nodes see a stabilization of pressure. This suggests that the system has reached a stable state in which all of the pressures are equal. This stability is facilitated by the mass flow rate boundary condition being constant.

Flowrate through nozzles

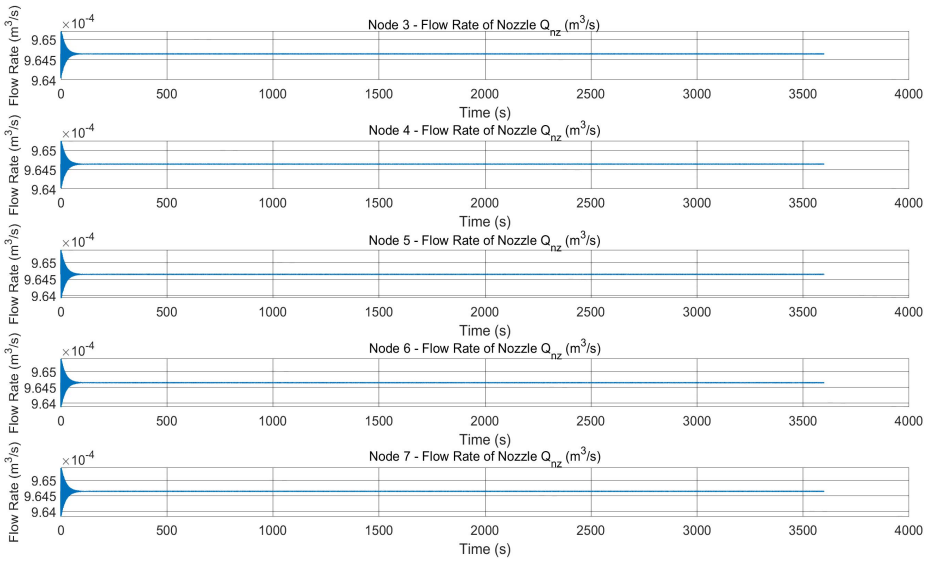

Figure C.4: The flow rate through nozzle of BCT reference model with constant boundary condition

Every node displays a quick initial flow rate surge before stabilizing. The system's reaction to the abrupt start of a consistent flow rate is probably what caused this first surge before it reached a steady state. The flow rate at each nozzle settles to a consistent value following the transient. This represents the new constant boundary condition and is consistent across all nodes. According to the steady-state condition, the pressure drop between the nozzles doesn't change over time. The similar responses seen in all nodes suggest that the nozzles are spaced equally apart.

D

Graphical representation of sensitivity analysis

Water depth

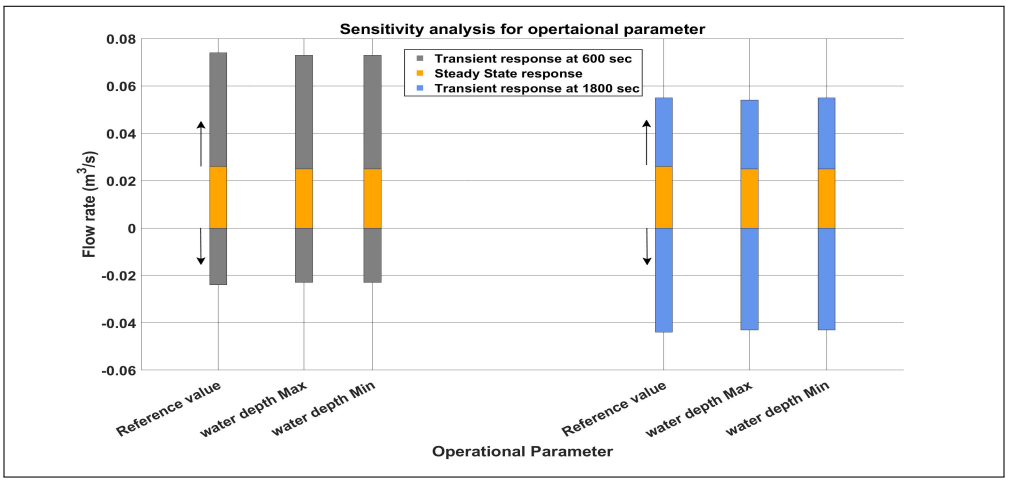

Figure D.1: Sensitivity analysis: Water depth flow rate at Node 1

Sensitivity analysis of pressure for operational parameters

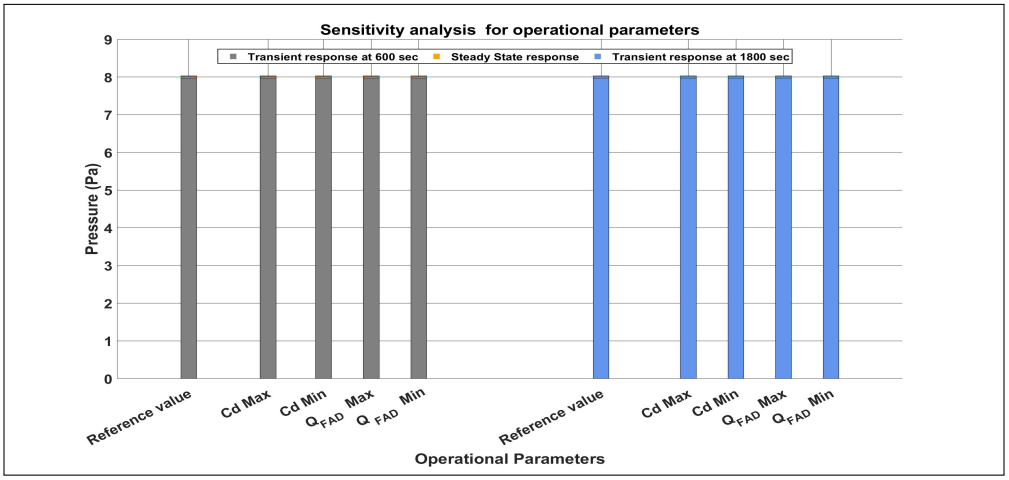

Figure D.2: Sensitivity analysis: Pressure for operational parameters

Sensitivity analysis of pressure for geometric parameters

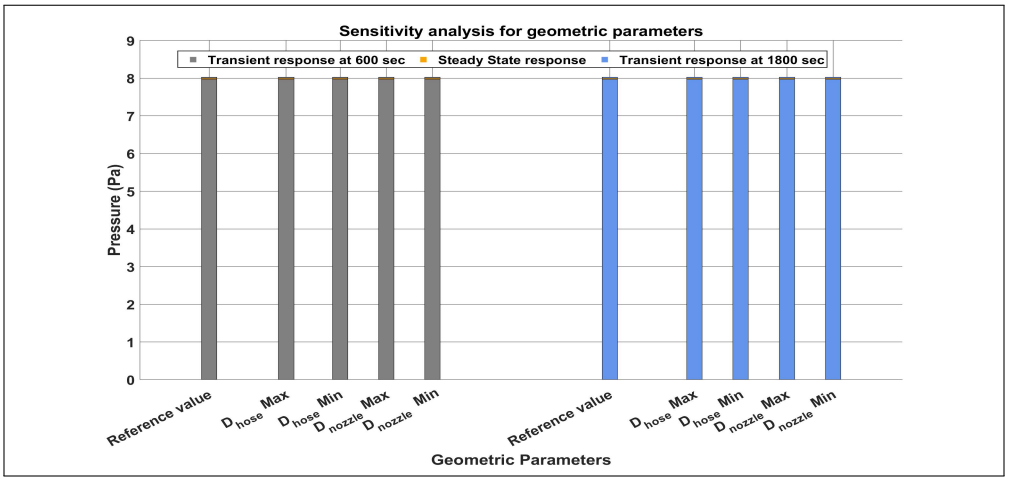

Figure D.3: Sensitivity analysis: Pressure for geometric parameters